A 2,205-year record of tropical cyclone strikes near Yucatán, Mexico, from mud layers in a stalagmite

Author: James Pyburn

Boston College

The Graduate School of Arts and Sciences

Department of Geology and Geophysics

A 2,205 YEAR RECORD OF TROPICAL CYCLONE STRIKES NEAR YUCATAN, MEXICO, FROM MUD LAYERS IN A STALAGMITE

a thesis

by

JAMES PYBURN

submitted in partial fulfillment of the requirements

for the degree of

Masters of Science

A 2,205-year record of tropical cyclone strikes near Yucatán, Mexico, from mud layers in a stalagmite.

James Pyburn

Abstract:

Tropical cyclones (TCs), known as hurricanes in the Atlantic and Typhoons in the Pacific, are among the most destructive and deadly natural disasters that occur on Earth. Attempts to understand how TCs relate to the global climate system, and future risk assessments are dependent upon having records of TC activity that pre-date the modern meteorological records, which are commonly not older than 130 years (Nott, 2003). Paleotempestology is a sub-discipline of paleoclimatology that attempts to extend the TC record beyond the meteorological record through the use of proxies. Presented here is the establishment of a paleotempestology proxy based on clastic mud being suspended in the water column by floods caused by TCs and deposited in stalagmite CH-1, collected in June of 2007 from Cenote Chaltun-Ha, a low-lying cave from the Yucatán Peninsula. CH-1 was dated by a combination of ^{210}Pb, U/Th, and layer counting techniques, creating an age model for its entire length. The years with mud layers were compared to the historical TC record from 1852-2006. Nineteen mud layers were identified for this time period. All of the mud layers deposited in years with at least one TC passing within 330 km of Cenote Chaltun-Ha.

A total of 265 mud layers were identified in CH-1 dating from 198 BC to 2006 AD. Relatively high TC frequency, ~16 mud layers/century, was recorded in CH-1 from 198 BC to ~1233 AD. This period was followed by eight centuries of relatively low TC frequency, ~7 mud layers/century. The low frequency period hit a low point in the 1600s with 4 mud layers. Since the 1600s the TC frequency recorded in CH-1 has been on the rise, indicating possible periods of higher than present TC frequency in the future for the Yucatán region. This trend of high TC frequency followed by a sudden drop and subsequent increase is also reported in published sand overwash deposit research.

$\delta^{18}O$ and $\delta^{13}C$ values collected from CH-1 provide insight into the timing of regional droughts. A low $\delta^{18}O$ value from 1815 provides evidence that "The Year Without a Summer" caused by the 1815 eruption of the Tambora volcano in Indonesia had a climatic effect on the Yucatán. A land-use signal related to the agricultural production boom of *Agave Fourcroydes,* a succulent plant known as Henequen, in the early 20th century was also detected in $\delta^{13}C$ values.

Acknowledgments:

I would first like to thank Dr. Amy Frappier for being my advisor and friend. The advice I received goes beyond the limits of science and into many other aspects of my life, and the adventures we shared, from field trips to baby stories, will be with me for years to come.

Secondly, I would like to thank my very supportive wife and forgiving daughter. Without their understanding and support I would never have been able to spend 10 hours writing in the middle of the summer when we could have been playing at the beach or the pool together.

I also need to thank Dr. Yvette Kuiper and Dr. Noah Snyder for sufficiently grilling me during my oral exams, providing useful comments on this thesis, and for providing great scientific support throughout this project.

Many thanks go to Dr. Eugene Perry, Dr. Bruce Dahlin, Dr. Tim Beach, and Dr. Cliff Brown for the incredible learning experience that was my fieldwork in the Yucatán. These men helped enrich my field experience in ways I could never have previously imagined. I would also like to give my gratitude to Maria Crosby, Meaghan Baldwin, Ryan Cumpston, and Alex Johnston for begin great companions and fellow field warriors.

I would also like to thank Dr. Ken Galli for all his help in the lab and with vehicles and with procuring items ranging from sonicating baths to AA batteries and the list goes on.

I received much technical help from the following people: Dr. Scott Carpenter, Dr. Reide Corbett, Dr. Xianfeng Wang, Dr. Dorinda Ostermann, Dr. Scot Birdwhistell, Dr. Steven Pike, Dr. Brian Frappier, Alan Vachon, and Gregory Cane.

I would like to mention all the grad-students who were at Boston College during my time there. They provided much technical help, as well as much-needed breaks from the technical work.

I would like to thank Margaret McCarthy for all her administrative help and her smiling face that was always willing to have a little chat with me.

And lastly, I would like to thank the faculty of the department of Geology and Geophysics at Boston College.

This work was carried out with the aid of a grant from the Inter-American Institute for Global Change Research (IAI) ***CRN*** *11 #2050 which is supported by the US National Science Foundation (Grant GEO-0452325).*

Table of Contents: **Page**

Table of figures and tables **Page**

1. Introduction

Paleotempestology, "the study of prehistoric tempests or storms," (Nott, 2003) is a field of research that is currently growing thanks to new techniques for identifying large storm events in climate records ranging from lake cores to historical documents. There is also a growing need to understand the implications of anthropogenic climate change on tropical cyclone (TC) activity (Nott, 2003). The establishment of multiple proxies is vital to refine the understanding of trends in TC frequency, intensity, and variability of landfall locations. Increasing the proxies available will improve the resolution of the paleo-TC record owing to the differences in sensitivity and location of the various proxies. Peleotempestologists and paleoclimatologists can make more informed predictions for the future with improved understanding of the TC/climate relationship from the past. The construction of climate models capable of predicting the impacts of climate change on the frequency or intensity of TCs will also benefit from a higher resolution paleo-TC record for calibration.

Currently established paleotempestology proxies include sand over wash deposits in coastal lagoons, negative $\delta^{18}O$ anomalies recorded in corals, stalagmites and tree-rings, historical documentation from shipping logs and personal journals, and beach ridges

(Nott, 2003). Each of these proxies is useful in different locations, and all are necessary to create a complete picture of the variations in the timing, distribution, and frequency of TCs beyond the historical record.

The goal of this project was to establish a paleotempestology proxy in a stalagmite sample collected from a cave, in the Mexican state of Yucatán, approximately 45 km southeast of Merida. The caves in the Yucatán peninsula are locally known as cenotes, and they have pools of water in the deepest part, which is the local water table.

Previously, negative $\delta^{18}O$ value anomalies in stalagmites have been correlated with TC occurrences (Frappier, 2007; Lawrence and Gedzelman, 1996; Nott, 2003). However, the acquisition of a high-resolution $\delta^{18}O$ value dataset is labor intensive, expensive, and time consuming, and the data is reliant on mass-spectrometry for precise, accurate, and reliable results.

The work presented here has two main goals: 1) to establish the effectiveness of a relatively cheap and quick TC proxy based on mud layers deposited during cyclogenic cave flooding. This method relies on lab work only for the establishment of an age model, and 2) to investigate the TC history of the Yucatán peninsula.

The proxy developed in this study is based on a stratigraphic anomaly in the growth of stalagmites from the Yucatán peninsula, or any other low-lying, heavily karstified region. Sedimentation in cave settings is dominated by precipitation of secondary calcite minerals, known as speleothems, which grow on the cave ceilings, floors and walls. Mud layers are not common in speleothems used for paleoclimate

studies, but have been reported as flood records in at least two caves from temperate zones (Dorale et al., 2005; Niggemann et al., 2003).

The hypothesis this study attempted to validate was based on the following assumptions:

1. When a TC passes over the Yucatán peninsula, the regional water table rises due to the high permeability of the karst aquifer.
2. This rise in water table suspends clastic material (mud, calcite rafts, bat guano or feces) that is then deposited onto cave surfaces including stalagmites as the water recedes.
3. As the cave resumes its normal condition, active cave formations continue to grow, incorporating the clastic material into the calcite as a mud layer. The action from the drip water pushes the mud to the side of stalagmites, creating lobes on the periphery. Calcite deposited from cyclogenic drip water containing a negative $\delta^{18}O$ value anomaly is the first calcite deposited after the mud layer.

   Thus, my hypothesis is that:

   (1) Secondary cave calcite from Chaltun-Ha should faithfully record a mud layer in the annual layer for any year in which there is a TC that raises the water table enough to flood the cave, and

   (2) The $\delta^{18}O$ values from calcite immediately post-dating the mud layers should confirm that the flooding was cyclogenic by virtue of their anomalously low measured values.

Further goals of the research presented are: 1) construction of a general paleoclimate record, including drought and TC events; 2) to report a possible land-use proxy recorded by $\delta^{13}C$ values in a stalagmite based on the Henequen boom from the early 20th century; 3) to make recommendations for future work related to the interpretation of climate in the past from mud layers in stalagmites.

The main steps involved in the establishment of the mud layer proxy presented here were: (1) collect a stalagmite, CH-1, from a low-lying region that is likely sensitive to flooding, and section and polish it to investigate the stratigraphy; (2) collect high-resolution $\delta^{13}C$ and $\delta^{18}O$ values to test if the stable isotopes of carbon and oxygen record shifts in climate in CH-1. Also to attempt to use negative $\delta^{18}O$ value anomalies in the calcite as secondary lines of evidence to confirm the cyclogenic nature of the mud layers; (3) use radiometric isotopes ^{210}Pb and U/Th to verify the presence of annual carbonate layers in CH-1 and subsequently to establish an integrated age model for its entire length, allowing for the dating of any depth within CH-1; (4) identify the stratigraphic location and ages of all identifiable mud layers and compare them to historical TC records. The result of this study is a new paleotempestology proxy that will serve as a cheap and time-efficient tool for the study of the relationships between climate and TC activity.

2. Background:

To test whether stalagmites from low-lying tropical regions faithfully record TCs through the existence of mud layers in their calcite stratigraphy, some assumptions of how paleoclimate proxies are developed must first be considered. Consideration must also be given to caves as chemical and clastic depositional environments to understand the interplay between calcite and mud deposition. A regional climatological, hydrological, and geological background is also provided below to gain an understanding of why the mud layer proxy works.

a. *Proxies*

In order to understand quantitative changes in the climate system that occurred prior to the existence of an observational record, we need to compare modern changes observed in the instrumental climate records, such as rainfall amounts and temperatures measured with thermometers, to paleoclimatic records based on proxies. Proxies are historical or natural archives of climatic variation. Natural proxy records exist in climate archives such as ice cores, tree rings, lake and ocean sediment cores, corals, and speleothems (Mann, 2007). Such natural proxies record climatic variations in many forms at resolutions ranging from sub-annual to millennial.

The establishment of paleoclimate proxies relies on the geologic principle of uniformitarianism (Hutton, 1788). Proxies must first be tested to see if they record climatic information that can be correlated to direct instrumental records like temperature or rainfall amount before any conclusions about pre-historic climates can be made. Once the proxy is calibrated, independently validated, and duplicated on the modern record, the

law of uniformitarianism can be applied, assuming that the processes in the past that are being investigated occurred under similar conditions as the modern (Jones and Mann, 2004; Mann, 2007).

b. *Cave sediments*

i. *Speleothems*

Speleothems are non-organic, micro-crystalline carbonate minerals that form in caves of karstified aquifers (Fairchild et al., 2006). Speleothems grow in many morphologies, including soda straws and stalactites that grow down from the ceiling, and stalagmites and flowstones that grow up from the cave floor. Stalagmites are the preferred speleothem for paleoclimatic research due to their relatively straight-forward stratigraphy, allowing for simple age model development (Fairchild et al., 2006). Caves develop in karst, a mass of rock with so many cavities that overland flow (rivers etc.) is nearly non-existent (Fairchild et al., 2006), as a result of underground drainage of meteoric water. As meteoric water percolates through soil, it gets saturated with CO_2 from plant respiration, creating carbonic acid. The acidic water has an increased ability to dissolve carbonates (Gonzalez and Lohmann, 1988). The aggressive water percolates through pre-existing networks of fissures and pores, widening the voids created. The chemical weathering of carbonates charges the meteoric water with ions, principally Ca^{2+}

and CO_3^{2-} in limestone terranes. Once a void is opened, precipitation of stalagmites can begin.

The air inside of caves has pCO_2 levels lower than the drip water by at least an order of magnitude, driving the degassing of the CO_2 from the water which commonly deposits its Ca^{2+} and CO_3^{2-} ions as calcite (Dreybrodt, 1980; Hendy, 1971; McDermott, 2004). Speleothems can have growth rates of 0.01-1.5 mm/yr, affecting the level of detail that can be resolved in speleothems as paleoclimate records (Frappier et al., 2007; McDermott, 2004; Spotl and Mattey, 2006). Vertical extension rates or growth rates are dependent on the amount of meteoric water introduced into the cave, the diffusion of Ca^{2+} and CO_3^{2-} ions in the solution, the thickness of the water lens on the top of the active stalagmite, and the diffusion of CO_2 in the solution. The limiting factor for rate of deposition is the concentration of Ca^{2+} ions in the water lens (Dreybrodt, 1980) and pCO^2 difference between the drip water and cave air (Fairchild et al., 2006). An in-depth discussion on the deposition of stalagmites can be found elsewhere (Dreybrodt, 1980; Fairchild et al., 2006; Gonzalez and Lohmann, 1988; Hendy, 1971; McDermott, 2004; White, 2007).

ii. *Clastic sediments in caves*

Although caves are known for ornamentation by chemical speleothems, clastics also occur as important cave facies. Mud and other clastic sediments in caves can be autochthonous or allochthonous. Autochthonous sediments come from weathering of the country rock, mechanical weathering or breakdown of the cave, and guano.

Transportation of sediment primarily occurs in channels, and can be bed load or suspended load (White, 2007). Allochthonous sediments can be entrance talus, infiltrates, stream transported sediments, debris flow, and aeolian deposits (White, 2007).

c. *Emplacement of clastic sediments in stalagmites by flooding*

A rapid rise in the groundwater level can occur on a regional scale due to the caverns and passageways within karst. This creates the potential for flooding in the caves and cenotes of the Yucatán (Marin, 1990; Perry et al., 1995; Pope et al., 2001). Examples are given below.

Dorale et al. (2005) use a stalagmite record of flooding from the past 8000 years in Crevice cave from the Midwest US to make links between the El Niño-Southern Oscillation (ENSO) and historical flooding in the Midwest. The flooding created a flux of suspended sediment that was deposited as clastic layers incorporated into the calcite of a continuously growing stalagmite (Dorale et al., 2005). Niggemann et al. (2003) also report mud layers interpreted to be deposited post flooding in 3 stalagmites from B7 cave in western Germany. The mud layers were used as time events and were used to correlate the ages of the three stalagmites collected from the same elevation and cave gallery.

Cave flooding from TCs has rarely been studied, but one example exists from Cave Springs Cave in Virginia. Cave Springs Cave contains 610 m of stream channel

and therefore differs from typical Yucatán Ring of Cenotes caves, which are typically more like sinkholes. This study documented the flooding and solution weathering that occurred in this cave due to Hurricane Camille, 1969, which dropped 63-71 cm of rain at several locations in Virginia. Flooding in Cave Springs Cave exceeded 3 m (Doehring, 1971).

The regional water table in Northern Yucatán rose by at least 1 m immediately after Hurricane Gilbert in September of 1988, and overland flow persisted for more than 10 days (Dr. Eugene Perry, personal communication, 2009). A study of the freshwater-saltwater interface in the karst aquifer of Northern Yucatán in response to Hurricane Isidore in 2002 revealed that the primary flow direction in response to such a rapid recharge of water is vertical (Escolero et al., 2007). Another interesting feature was what Escolero et al. (2007) described as a 'piston' effect, whereby the water table level raised and fell regularly. After the initial rise of the water table following Isidore, the water table bounced up and down with peaks arriving every 5 days. These results were the same in two wells from different locations, and the peaks occurred at the same time in both, indicating that flow in the case of rapid recharge is preferentially vertical (Escolero et al., 2007). The study was conducted 27 days after hurricane Isidore and the water level was still at least 43.3 cm above the ambient water level, dropping by approximately 25 mm/day.

Together, these studies illustrate that in regions with the right environmental conditions, like low-lying karst in a tropical or sub-tropical setting, floods in caves could record TCs by depositing mud inside actively growing cave formations.

d. *Stable isotopes in speleothems*

The effectiveness of $\delta^{18}O$ and $\delta^{13}C$ values from speleothems as paleoclimatology records is aided by a few conditions found in most caves. First, the air temperature in caves (deeper than ~ -15 m or so) is typically constant at the average annual air temperature ± 1° C at the location of the cave (Fairchild et al., 2006; McDermott, 2004). Second, the cave atmosphere typically has humidity levels from 95-99%, reducing evaporation of drip-water which might cause kinetic isotope fractionation (Hendy, 1971; McDermott, 2004). The $\delta^{18}O$ values of the calcite deposited under these equilibrium conditions depends on the $\delta^{18}O$ values of the drip-water and the temperature dependent fractionation of drip-water and deposited calcite (Lachniet, 2009; McDermott, 2004). A full review of the $\delta^{18}O$ values of meteoric water can be found in Dansgaard (1964) and Lachniet (2009).

Variations in $\delta^{18}O$ and $\delta^{13}C$ values with time in speleothems are related (Fairchild et al., 2006; Frappier et al., 2007; Spotl and Mattey, 2006; Webster et al., 2007). However, the mechanism behind this relationship is not well understood. One hypothesis is that the covariance is due to kinetic effects such as evaporation or rapid degassing (Mickler et al., 2004; Mickler et al., 2006), while another hypothesis that this effect is due to changes in soil ecosystems following climatic shifts (Frappier et al., 2002a; Rousseau et al., 2005).

One method to test if calcite was deposited in isotopic equilibrium is to perform what is called a 'Hendy' test. This consists of measuring several discrete $\delta^{18}O$ and $\delta^{13}C$

values from a single layer perpendicular to the growth axis. The criteria to pass the Hendy test are; (1) $\delta^{18}O$ values remain constant along a single growth layer; (2) there is no correlating increase of $\delta^{18}O$ and $\delta^{13}C$ values (Hendy, 1971). Although this method has been under scrutiny because of sampling difficulties and inconclusive results (Dorale and Liu, 2009; Drysdale et al., 2004; Linge et al., 2001; Mickler et al., 2006), it remains the only way to rule out equilibrium conditions. The test is very conservative, and stalagmites that fail the Hendy test may actually have been deposited in stable isotope equilibrium (Dorale and Liu, 2009). The best known method to test whether deposition of $\delta^{18}O$ and $\delta^{13}C$ values occurred under equilibrium conditions remains reproducibility of the data (Dorale and Liu, 2009).

Paleoclimate studies using stalagmite records of $\delta^{18}O$ and $\delta^{13}C$ values can be found in Dorale et al. (1992), Frappier et al. (2007), Goede (1994), Lauritzen (1993), Nott et al. (2007), and Webster et al. (2007).

e. *Tropical Cyclones*

A TC is defined as a "cyclone that originates over tropical oceans and is driven principally by heat transfer from the ocean." TCs have various names around the world including tropical storms, hurricanes and typhoons (Emanuel, 2003). Hurricanes are Atlantic TCs with wind speeds exceeding 33 m/s (Emanuel, 2003). Hurricanes can be classified on the Saffir-Simpson scale of intensity by wind speed. (Figure 1).

Type	Category	Pressure (mb)	Winds (knots)	Winds (mph)	Surge (ft)
Depression	TD	-----	< 34	< 39	
Tropical Storm	TS	-----	34-63	39-73	
Hurricane	1	> 980	64-82	74-95	4-5
Hurricane	2	965-980	83-95	96-110	6-8
Hurricane	3	945-965	96-112	111-130	9-12
Hurricane	4	920-945	113-135	131-155	13-18
Hurricane	5	< 920	>135	>155	>18

Figure 1. Saffir-Simpson Scale, whereby TC intensities are classified.

TCs are among the most deadly and costly natural disasters in the world (Emanuel, 2003). Single TCs have caused over 80 billion dollars of damage, and been responsible for nearly 500,000 deaths (Emanuel, 2003; McCloskey and Keller, 2006). Understanding variability in the frequency and intensity of TCs is important for development of coastal human settlements and evaluating the need for better warning systems and evacuation infrastructure (Nott et al., 2007), as well as evaluating the correlation between climate change and TC activity.

Modern hurricane detection and surveillance began in the 1940s with hurricane hunter reconnaissance aircraft, then expanded in the 1960s with the first orbital satellites monitoring the oceans, and by the 1970s nearly all TCs were recorded by satellite observations (Emanuel, 2003). Prior to the late 20th century, storm records come from documentation of storms that made landfall on populated areas or interrupted shipping lanes (Garcia-Herrera et al., 2005).

TCs generally form over tropical waters with surface temperatures exceeding 26°C (Emanuel, 2003; Palmén, 1948), and they always form from a previous atmospheric

disturbance (Emanuel, 2003; Riehl, 1948). Another important factor in the formation of TCs is an environment of minimal vertical shear, allowing the formation of clouds to heights of 15 km (Emanuel, 2003; Gray, 1968). TCs seldom form closer to the equator than 5° latitude where vorticity is low, and generally move westward and poleward at speeds ~2-10 m/s. If they survive long enough, TCs will often "recurve" and begin moving to the east when they travel to the extra-tropical regions. TCs in the Atlantic develop mostly during the months of June to November with a peak in development in September (Emanuel, 2003). An average of 5 hurricanes formed in the North Atlantic each season from 1886-1996. (Elsner and Kara, 1999).

i. *Stable Isotopes in TCs*

Rain from hurricanes has low $\delta^{18}O$ values compared to normal rain storms by ~6‰ (Figure 2)(Lawrence and Gedzelman, 1996). The hatched design in figure 2 is all rain events from June-September from 1985 to 1992, collected about 50 kilometers southeast of Houston, Texas. The black set is a collection of precipitation samples from a hurricane and four tropical storms. This figure shows how the oxygen isotope values from hurricane rain is very low and similar to the sea surface vapor, unlike the isotopically heavier precipitation from summer storms (Lawrence and Gedzelman, 1996).

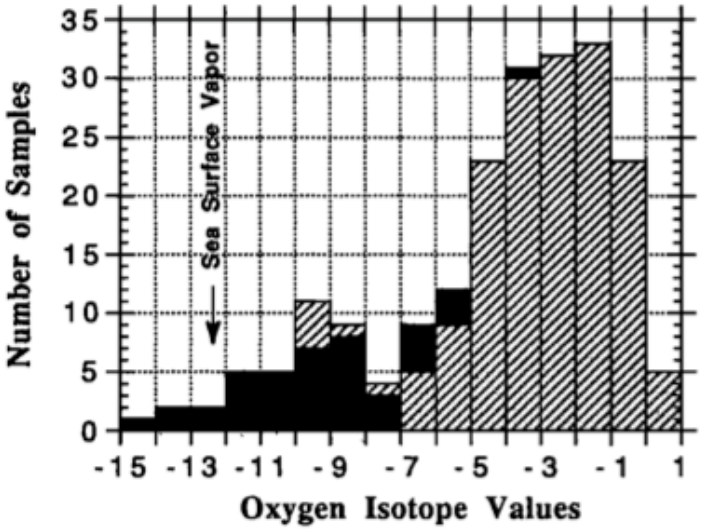

Figure 2. $\delta^{18}O$ distribution from two precipitation datasets.

A number of processes contribute to this effect. The primary cause is the height of the clouds in a hurricane, which can reach up to 15 km in altitude (Lawrence and Gedzelman, 1996). The atmosphere at 15 km is very cold, which reduces the amount of water the air can hold, and extensive isotopic differentiation can occur at cold condensation temperatures (Dansgaard, 1964; Lawrence and Gedzelman, 1996). The condensed water in a TC thus starts on its path to the surface of the Earth with a lower $\delta^{18}O$ value than it would have had it originated in a lower, warmer cloud top. As the water droplets fall through the air, isotope exchange occurs which causes the water to lose the light $H_2{}^{16}O$, and take in heavy $H_2{}^{18}O$ molecules from the vapor, removing heavy isotopes from the clouds early in the storms lifecycle. This has the effect of lowering the $\delta^{18}O$ values of the remaining vapor, causing the raindrops to form with progressively lower $\delta^{18}O$ values over time. This is known as the "Amount Effect" (Dansgaard, 1964).

In frontal storms, the air below the cloud generally has low humidity, causing the droplet to partially evaporate and allowing isotope fractionation to occur, leaving the water droplet enriched in the heavy isotope. However, high humidity below the cloud deck exists in hurricanes preventing evaporative fractionation of the water droplets as they fall to the Earth. All of these processes work together to maintain the very negative isotopic values the water had after its initial condensation from the tops of the high clouds (Lawrence and Gedzelman, 1996).

The rainwater from hurricanes has progressively lower $\delta^{18}O$ values toward the eyewall cloud of the hurricane (Lawrence and Gedzelman, 1996), and more intense TCs generally also have lower $\delta^{18}O$ value anomalies (Lawrence and Gedzelman, 1996). This is partially due to the increasing elevation of the cloud tops toward the eyewall centers of hurricanes, lowering the temperature of the air the vapor is condensing out of. This could also be due to the recycling of light vapor rained out on the leading edge of the storm and evaporated back into the TC (Lawrence and Gedzelman, 1996). The $\delta^{18}O$ values of the rain get significantly lower when the storm makes landfall, due to the lack of seawater evaporation supplying new $H_2{}^{18}O$ to the vapor mass (Dansgaard, 1964; Lawrence and Gedzelman, 1996).

During TCs, rapidly ascending air masses cause deep cooling in the vapor, massive rainout, low fractions of remaining vapor, and isotopically light precipitation. Temperature affects the $\delta^{18}O$ values because the fractionation between vapor and condensate increases with decreasing temperature, so that when rain is removed, the $\delta^{18}O$ values of the remaining vapor will decrease more dramatically (Dansgaard, 1964). The

combination of these processes accounts for ~6‰ lower $\delta^{18}O$ values in TCs than other summer rainwater, at least as observed in Texas (Frappier et al., 2007; Lawrence and Gedzelman, 1996), providing an isotopic tracer in the ground water which percolates into the cave environment.

Starting with ocean water in the bottom right of figure 3, fractionation lowers the $\delta^{18}O$ of the vapor coming off of the ocean surface. Rayleigh distillation of the rising vapor continues to decrease the $\delta^{18}O$ values in the vapor. The cloud tops of a hurricane can reach 15 km, providing very efficient cold condensation, allowing extensive isotopic fractionation between the condensed water and vapor. Isotope exchange occurs on the droplet's path to Earth, effectively stripping the vapor cloud of heavy water molecules early in the storms lifecycle. The atmosphere below the clouds has near 100% humidity, preventing any fractionation due to evaporation, and the droplet lands on the Earth's surface with approximately the same $\delta^{18}O$ value it had in the high cloud tops (Lawrence and Gedzelman, 1996). Gedzelman et al. (2003) suggest that isotope ratios drop to low levels within 2 days of the beginning of organized circulation, long before the storm reaches hurricane intensity or begins to drop rain with isotopic anomalies over land where it can be recorded by precipitating calcite in a stalagmite.

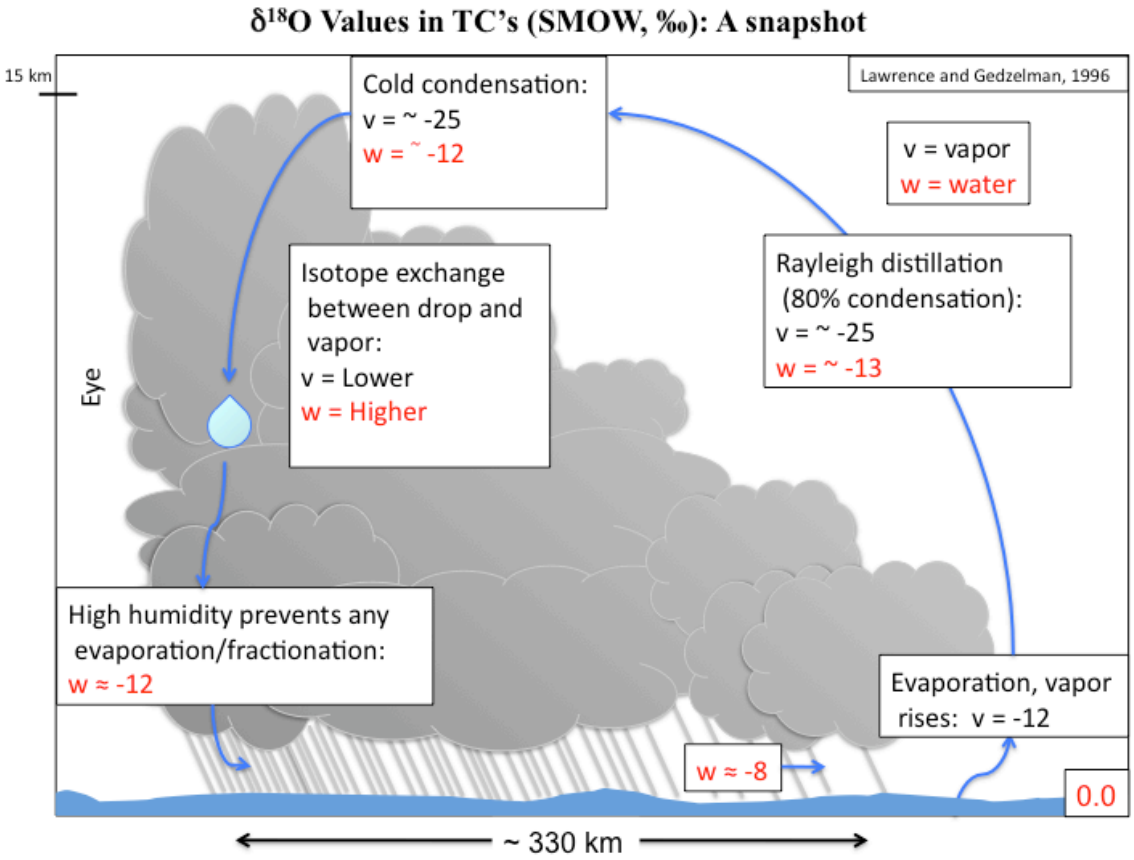

Figure 3. Water $\delta^{18}O$ value evolution in a TC.

TCs provide a short-lived but voluminous burst of low $\delta^{18}O$ value water in streams and groundwater that can act as a natural isotopic tracer spike. The low $\delta^{18}O$ values associated with TCs are present in the surface water for up to a few weeks (Lawrence, 1998). Between storm events, the isotopic value of the water entering the cave returns to normal summer levels (Lawrence, 1998). If the cave system is in equilibrium, the $\delta^{18}O$ values of the calcite in speleothems should reflect the isotopic value of the water it was precipitated from (Hendy, 1971) and hence $\delta^{18}O$ values from stalagmite calcite should display a short-lived negative spike correlating to the timing of the TC passing within ~330 km of the cave site.

Frappier et al. (2007) observed this phenomenon in stalagmite ATM-7, from Actun Tunichil Muknal cave in central Belize, and correlated the negative $\delta^{18}O$ value anomalies to known storm events. ATM-7 accurately recorded ten TCs that made landfall within 300 km of its collection location between 1975 and 2000. The size of measured $\delta^{18}O$ value excursions showed a positive correlation to storm intensity, but without substantial relation with the distance of the storm track from the cave (Frappier et al., 2007; Nott et al., 2007).

Doing this type of study is costly and time consuming, and dependent upon finding a stalagmite that was deposited under equilibrium conditions with a fast enough growth rate to resolve TC rain $\delta^{18}O$ value anomalies. It is also possible that every study of this type would require calibrating the $\delta^{18}O$ values and their anomalies with the modern TC records collected from satellite data before any studies done on previous time periods could begin. For all of these reasons, a TC proxy that is relatively quick, cheap, and easy is highly desirable.

Improving the understanding of climate-TC interactions is an important goal of the paleotempestology community, and requires proxy records with diverse record lengths and spatial distribution to assess any correlation between changing climate and TC intensity or frequency (Frappier et al., 2008). The need to develop more TC proxies stems from the different time scales, resolutions, potential locations, and TC parameters that existing proxies are able to detect. Numerous types of proxies are required for a more complete view of how all these parameters have changed through time.

ii. *Paleotempestology*

This young science uses various tools to identify TCs in different geo- and biological proxy records. Sedimentological records of the extreme winds and storm surge exist in the form of washover deposits, which are sand layers up to tens of centimeters thick, deposited in back barrier lagoons and swamps where fine grained sediments are usually deposited (Nott, 2003). This technique has been shown to work in the Caribbean, the Gulf of Mexico and the southeastern and eastern US (Donnelly et al., 2001a; Donnelly et al., 2004; Donnelly et al., 2001b; Frappier et al., 2008; Liu and Fearn, 1993, 2000; McCloskey and Keller, 2006).

Other methods of storm identification include coral rubble ridges, historical documentation, and stable isotope records (Nott, 2003). Coral rubble ridges occur in areas with coral reefs near the shore. The high energy TC event transports pieces of the reefs either onshore or offshore.

A currently used cheap and quick proxy exists in the form of historical documentation. Journals of individuals and institutions have been documented to record very well dated TC activity, but are limited to locations where records were kept and preserved (Frappier et al., 2008; Garcia-Herrera et al., 2005; Liu et al., 2001)

Stable oxygen isotopes have been shown to record hurricanes in tree cellulose in the southeast United States (Miller et al., 2006). The $\delta^{18}O$ values of tree cellulose largely reflects the isotopic composition of its source water (Saurer et al., 1997), recording negative anomalies created by TCs.

f. *Field site*

The karst geomorphology and sub-tropical location of the Yucatán Peninsula make it an ideal site to look for hurricane records in stalagmites. The Yucatán Peninsula is a carbonate platform separating the Caribbean Sea and the Gulf of Mexico at ~21° N latitude (Figure 4). It is the surface expression of the Yucatán Platform made of transitional to continental crust and covered by up to 6 km of Late Jurassic through Paleogene carbonates, mostly limestone and evaporites (Rosenfeld, 2001). Soil cover in the Mexican state of Quintana Roo to the north east of the state of Yucatán is 20 cm thick (Vargas and Allen, 2008), and is very thin or absent throughout much of the peninsula (Perry et al., 2009). This karst landscape is very porous and riddled with caves and sinkhole cenotes. There is little relief, with a large area <30 m above sea level, and normally no overland water flow across the northern peninsula. Figure 5 shows the TC activity within 370 km of Cenote Chaltun-Ha by decade.

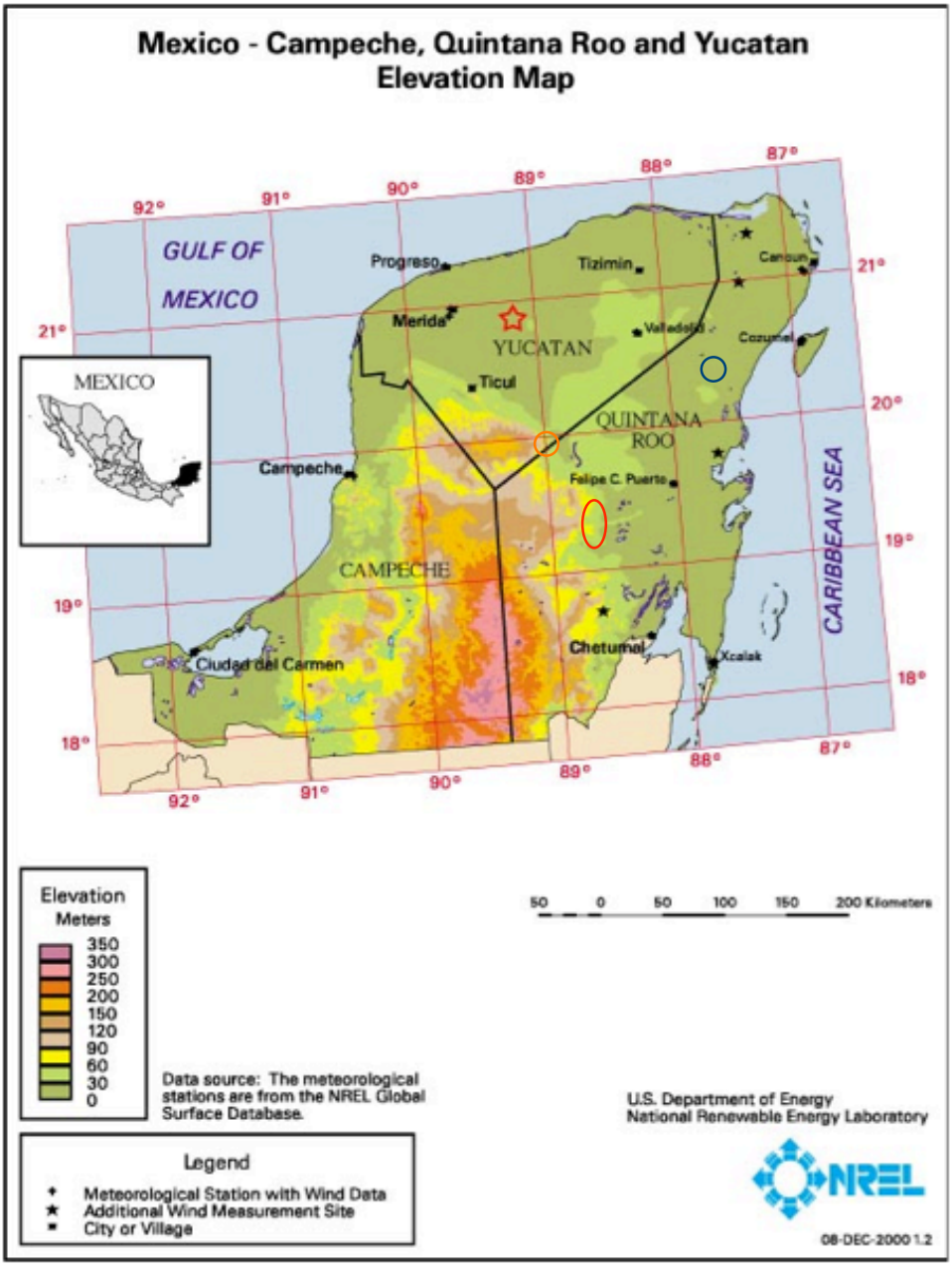

Figure 4. Elevation map of the Yucatán Peninsula. Red star indicates the location of Cenote Chaltun-Ha, collection location of CH-1. The red oval is the location of Lake Chichancanab, the blue circle is the location of Lake Punta Laguna, and the orange circle is Chen Kulu cave in Mayapan.

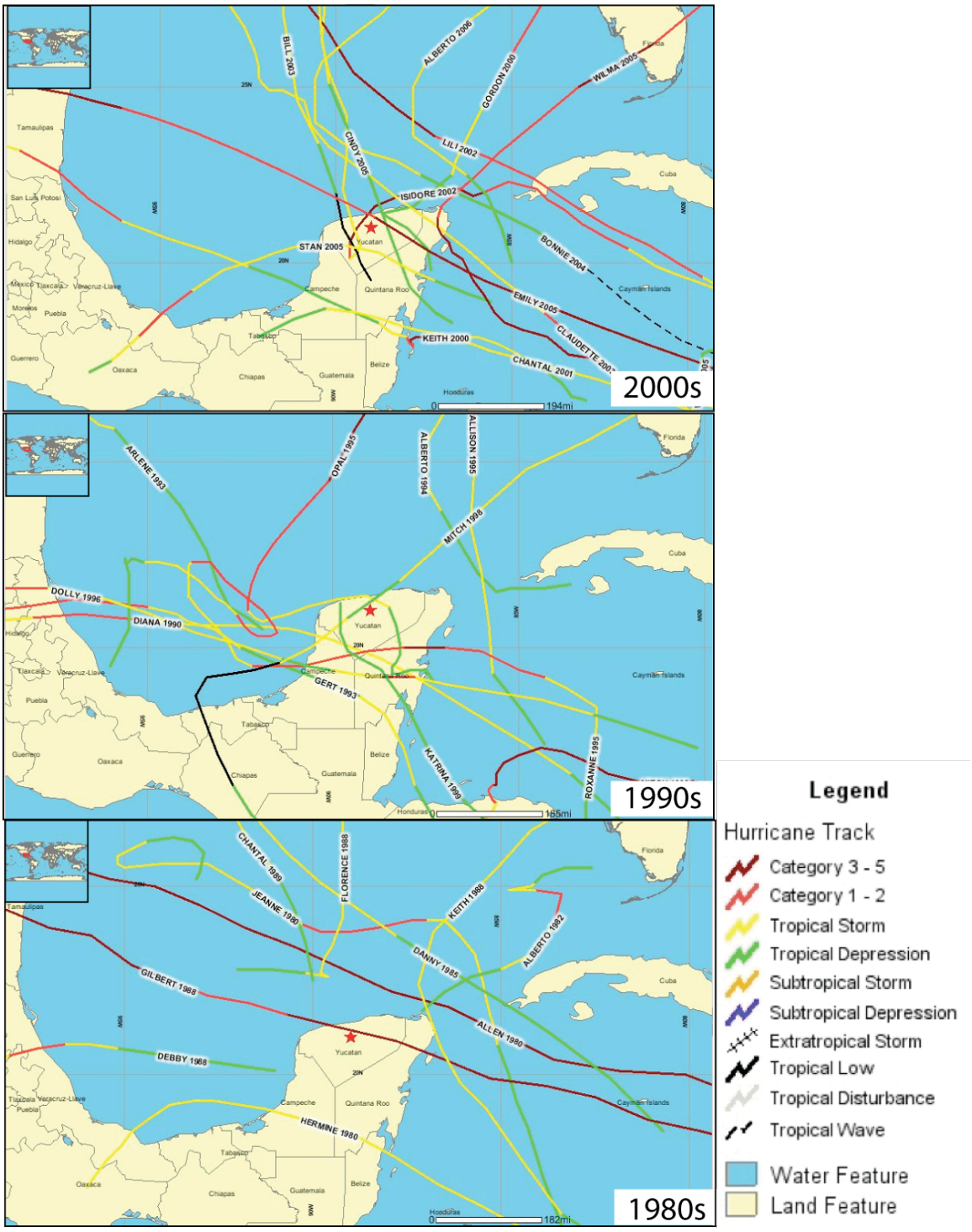
2000s
BILL 2003
ALBERTO 2006
GORDON 2000
WILMA 2005
CINDY 2005
LILI 2002
ISIDORE 2002
STAN 2005
BONNIE 2004
EMILY 2005
KEITH 2000
CHANTAL 2001
194mi
1990s
ARLENE 1993
OPAL 1995
ALBERTO 1994
ALLISON 1995
MITCH 1998
DOLLY 1996
DIANA 1990
GERT 1993
KATRINA 1999
ROXANNE 1995
185mi
1980s
CHANTAL 1989
FLORENCE 1988
JEANNE 1980
KEITH 1988
DANNY 1985
ALBERTO 1982
GILBERT 1988
ALLEN 1980
DEBBY 1988
HERMINE 1980
182mi
Legend
Hurricane Track
Category 3 - 5
Category 1 - 2
Tropical Storm
Tropical Depression
Subtropical Storm
Subtropical Depression
Extratropical Storm
Tropical Low
Tropical Disturbance
Tropical Wave
Water Feature
Land Feature

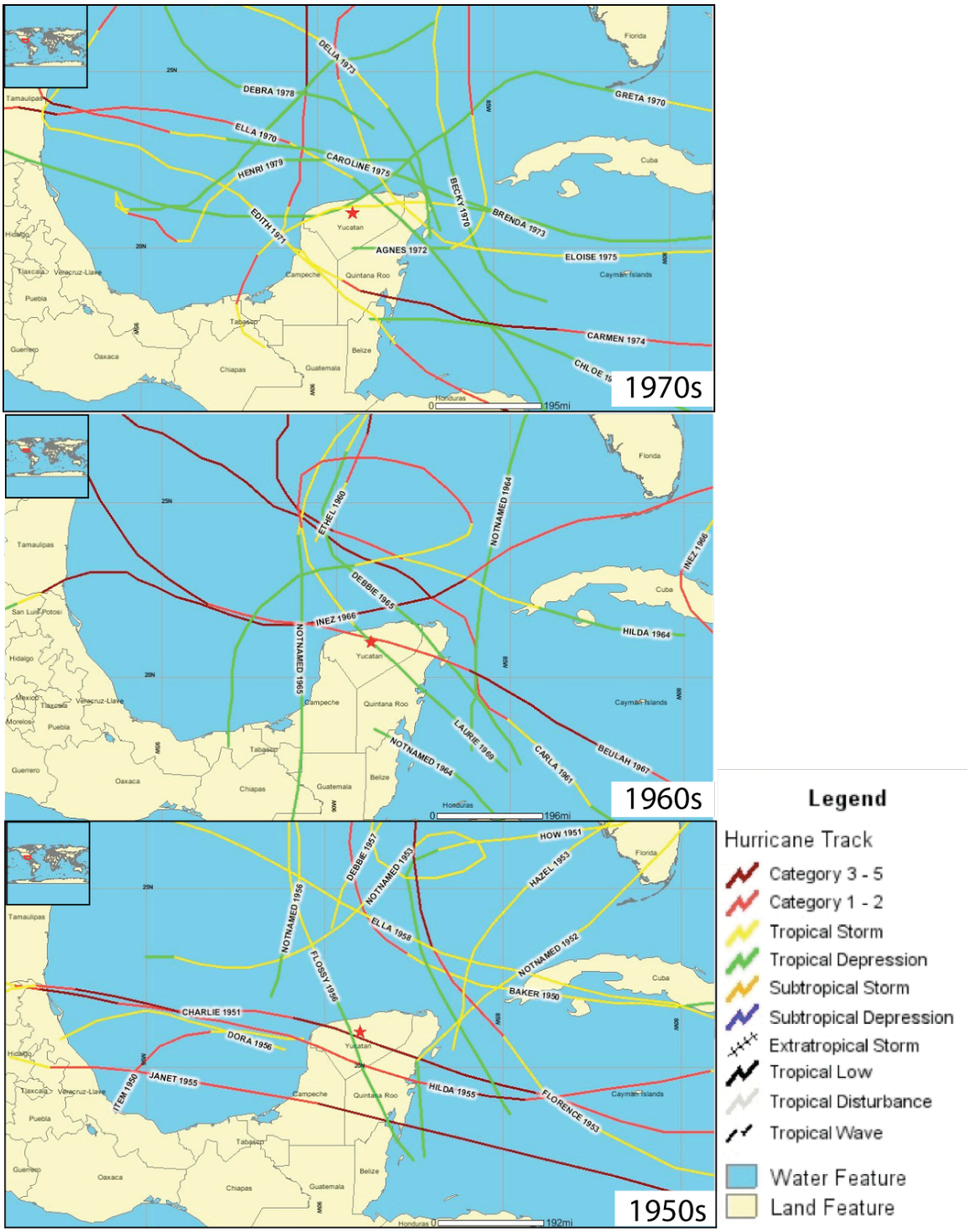

Figure 5. Best track data from NOAA breaking down the TC activity within 370 km of Cenote Chaltun-Ha by decade.

i. *Caves of the Yucatán*

The caves in this karst region are extensive. Some are very deep, some are very long, and many are interconnected by corridors that can lie above or below the water table. The aquifer below the Yucatán has a low hydraulic gradient of 7-10 mm/km, suggesting very high permeability in the region (Steinich and Marin, 1996). This implies that even if a TC track did not go directly over a cave, the water table should respond on a regional scale. Indeed, the low elevation means that the caves in the region are in close proximity to the groundwater table. The water table is ~15 m below the surface at the study site.

The extensive karst development and interconnected nature of the cave systems in the Yucatán means that there should be a large amount of clastic influx into the cave (Bosch and White, 2007). The main movement of clastic sediments through karst aquifers is episodic, with most of the transport occurring when pulses of storm water pass through the system (Bosch and White, 2007).

An important feature in the region is the Ring of Cenotes. This is a semi-circular ring of sinkholes in northwestern Yucatán that is the surficial expression of the Chicxulub crater formed by the bolide impact implicated in the extinction of the dinosaurs at the Cretaceous/Tertiary boundary (Pope et al., 1991).

The climate of the Yucatán varies from north to south. The location of the Yucatán Peninsula near the boundary of the tropics and subtropics means the northern part of the peninsula receives significantly less rain than the south (Figure 6). Figure 6 also shows the prevailing wind direction from east to west by the E-W rainfall gradient of

about 4 mm/km. Mean annual rainfall in the state of Yucatán from the years of 1941-2005 was 1091mm (Servicio Meteorologico Nacional, 2008). Rainfall in the region has two peaks, one in June, and a second in September coinciding with the peak in hurricane season (Figure 7). "Were it not for the hurricanes, the northern part of the peninsula would be dry like the arid parts of Mexico" (Me-Bar and Valdez, 2003; Vivó Escoto, 1964).

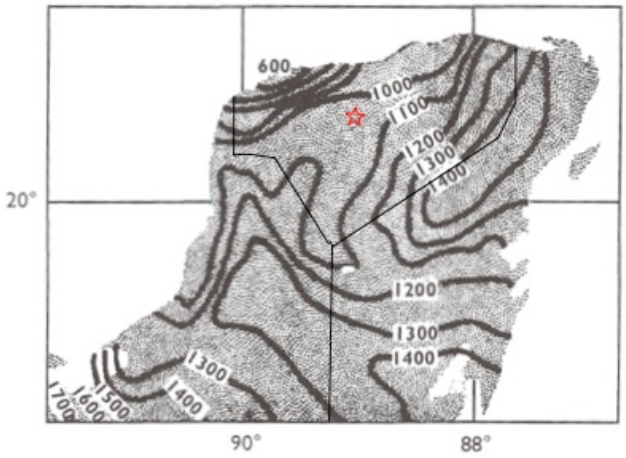

Figure 6. Average annual rainfall for the Yucatan Peninsula in mm (Gill, 2000). Red star is the location of Cenote Chaltun-Ha.

ii. *Paleoclimatology of the Yucatán*

Speleothem paleoclimate studies from the Caribbean region include a study revealing monsoonal variability in Costa Rica (Lachniet et al., 2004), as well as a stalagmite study relating high $\delta^{18}O$ values to droughts around the time of the collapse of the Mayan civilization (Webster et al., 2007). Other paleoclimate records from the Yucatán Peninsula primarily consist of lake sediment cores from Lake Chichancanab in the state of Yucatán, and other Cenotes in the region as well as the Cariaco basin off the

Venezuela coast to the south of the Yucatán (Curtis et al., 1996; Haug et al., 2001; Hodell et al., 2005b; Hodell et al., 1995). These studies have primarily focused on droughts over the last several millennia and how the droughts relate to the Mayan civilization. All of these studies suggest that the water table in the Yucatán peninsula may have enough variability in its recharge to be sensitive to TCs.

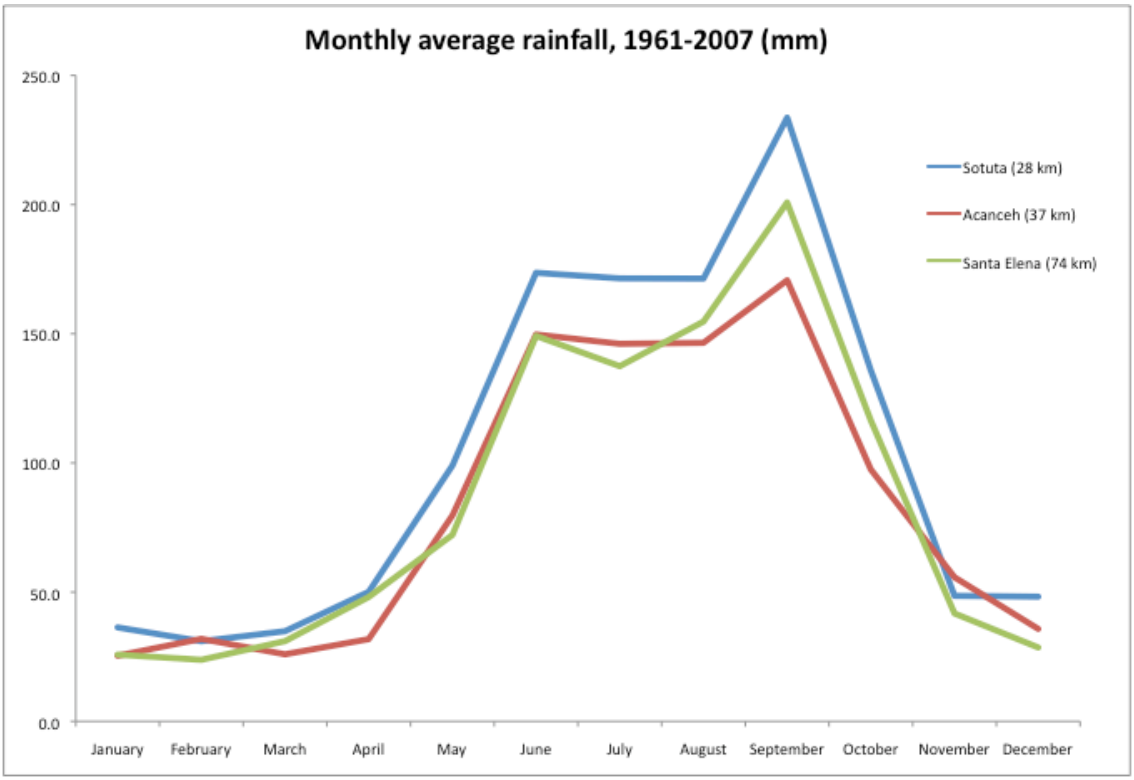

Figure 7. Monthly average rainfall from 1961-2007 for 3 towns averaging 46 km from Chaltun-Ha. The peak coincides with the peak of hurricane season in September.

g. *Conceptual model for mud-layer proxy*

From personal accounts of locals, we believe that many Yucatán caves and cenotes flood for several days after a TC event (personal communication, Dr. Cliff

Brown; Cornelio and Francisco de Huhí, 2007; Dr. Eugene Perry, Feb. 1st 2009). Dr. Amy Frappier has also observed on a 2003 field trip that after the hurricane floodwater recedes, a layer of mud, calcite rafts, and surface organic debris is deposited over the entire flooded portion of the cave, and the active drips clean mud off the tops of growing speleothems, pushing clastics to the edges of the stalagmite. Presumably, calcite deposition resumes, and incorporates the mud layers into the stalagmite (Figure 8). The first calcite layers deposited after the mud layer are hypothesized to contain the anomalous $\delta^{18}O$ values associated with cyclogenic waters. Dirty layers have been observed in sectioned stalagmites from this region (Figure 9-10). These mud layers are visual evidence of flood events corresponding to TCs that caused heavy rains in Yucatán.

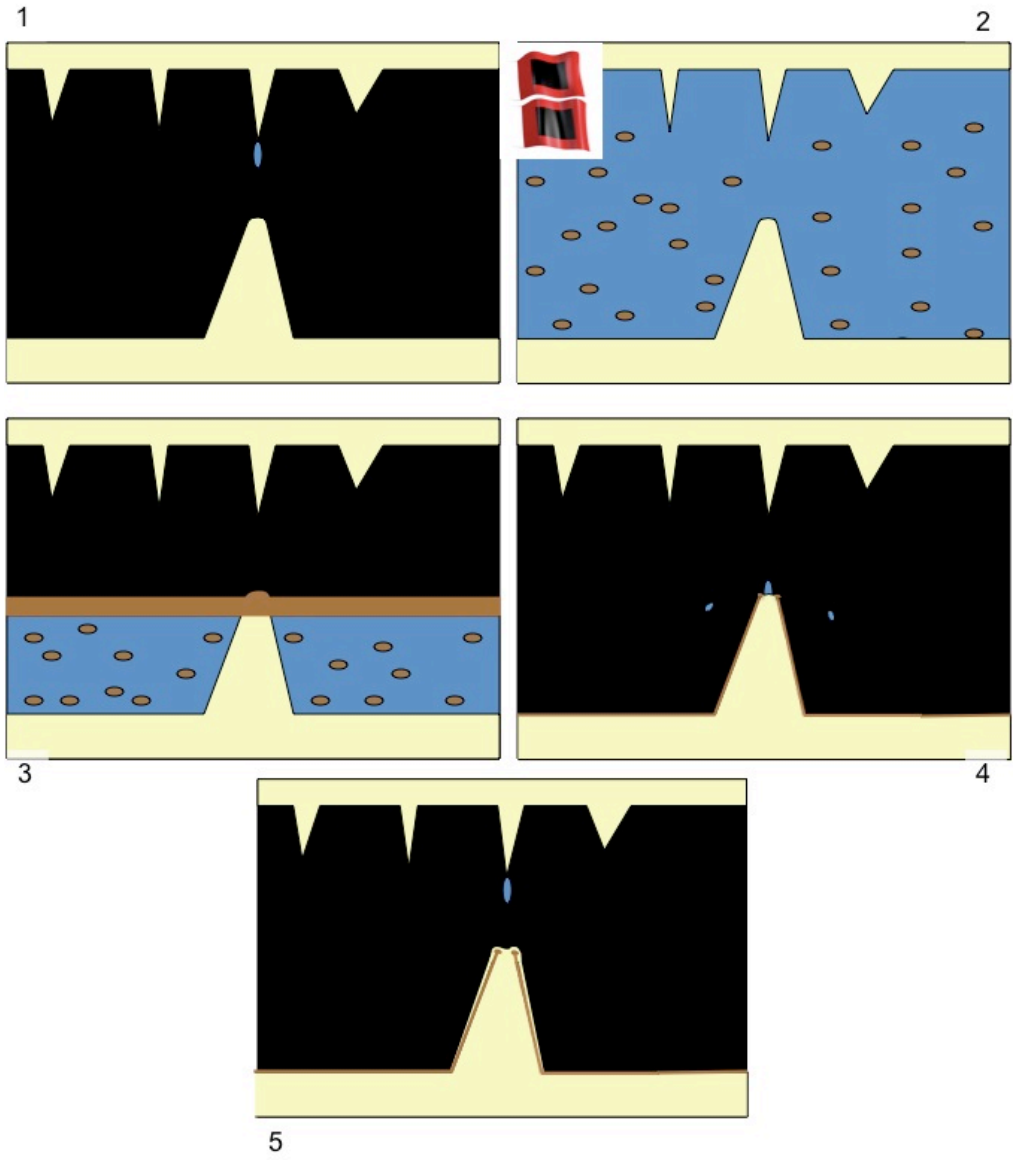

Figure 8. Conceptual model for the deposition of flood generated mud layers in stalagmites. 1. Air filled cave, calcite deposition. 2. TC Passes (denoted by the two red flags used by the US Coast Guard to indicate a hurricane warning is in effect) causing regional flooding in caves. 3. As the water recedes mud is deposited on surfaces, including stalagmites. 4. Air filled state resumes. Drip water sourced deposition of calcite continues. Some mud is removed by drips. 5. Calcite deposition continues, incorporating the mud.

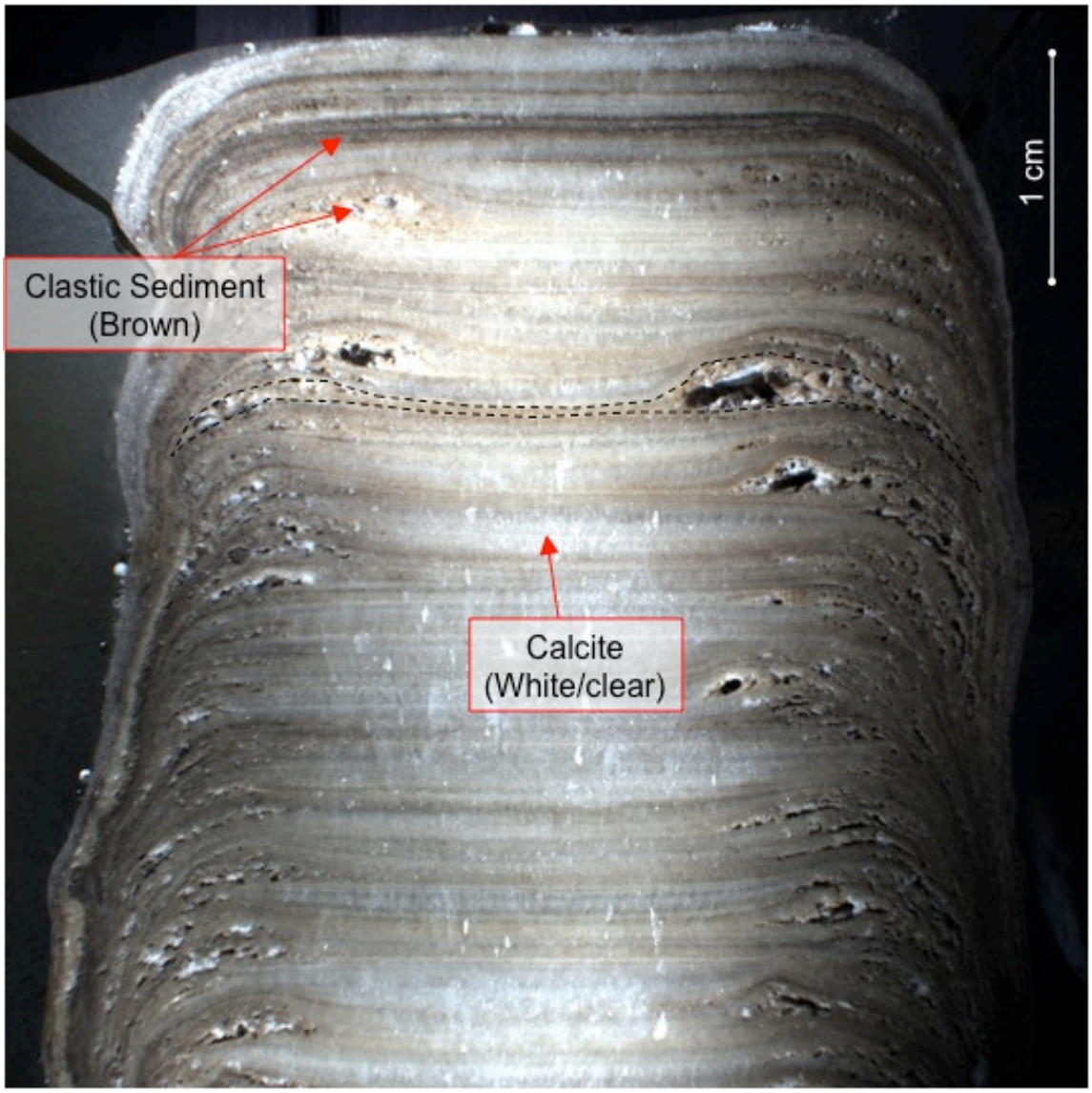

Figure 9. Cross-section picture of CH-1 showing layers of calcite deposition and dark layers of clastic sedimentation. Dashed outline shows a continuous dark layer thickening toward the edges.

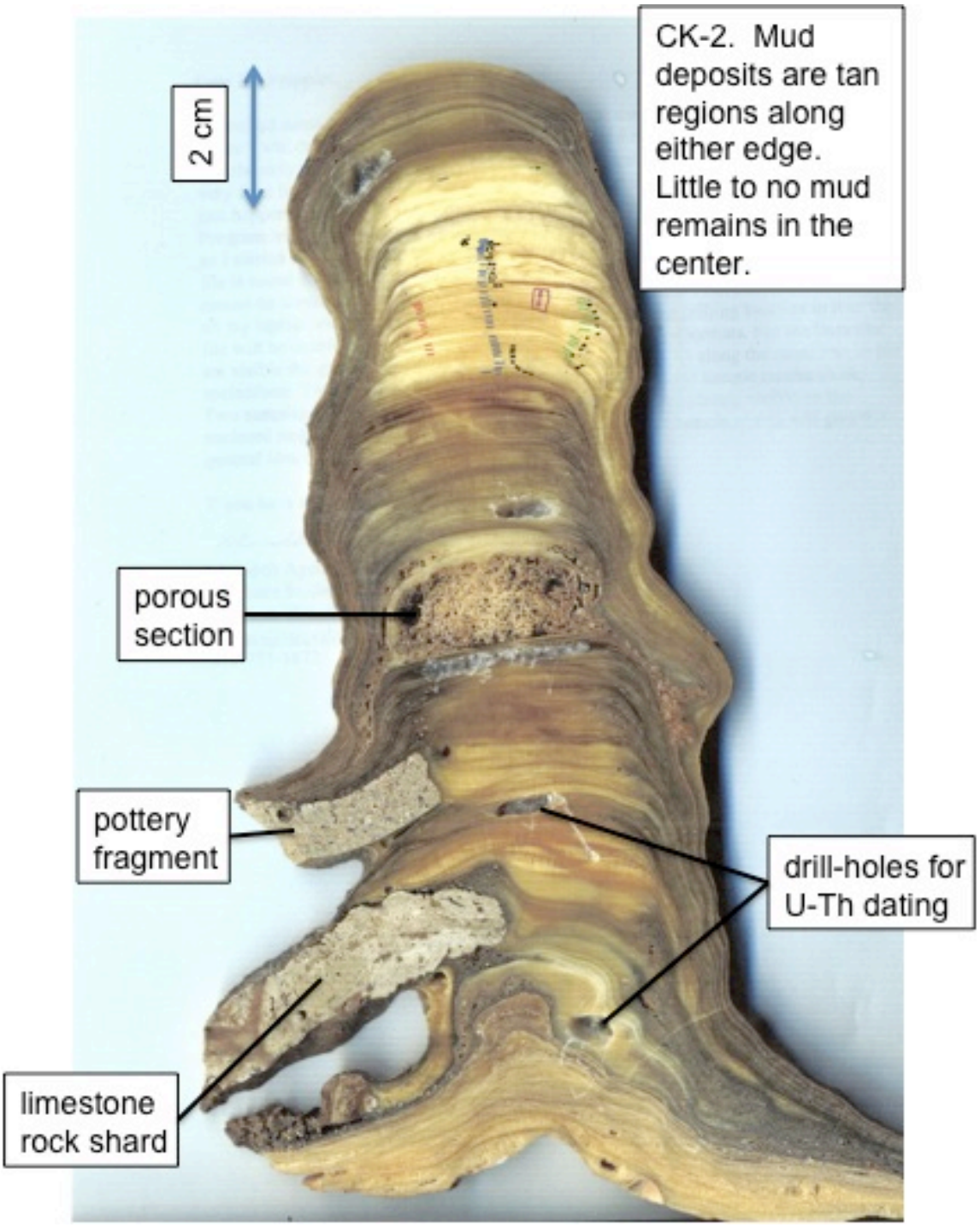

Figure 10. Stalagmite CK-2 from Chen Kulu cave in Mayapan, Yucatán Mexico showing intra-calcite mud layers.

3. Methods

To test my hypothesis stated above I began by carefully selecting a storm-sensitive stalagmite, CH-1, and vertically sectioned and polished it. Various methods for inspecting the stratigraphy were then used including white light and fluorescent light microscopy and layer counting. In combination with the layer counting, I used two different radiogenic isotopes to develop an age/depth model. I also gathered calcite powders along the growth axis. Light stable isotope mass spectrometry of the calcite samples yielded a high and a low-resolution $\delta^{18}O$ and $\delta^{13}C$ dataset. I then analyzed the results visually and statistically for a hurricane signal, and compared the results to mud layers and to the historical hurricane record, as well as other climate and paleoclimate data from the region to assess the confidence that CH-1 has recorded climate signals faithfully during its growth.

a. *Field Methods*

The sample selection method for this research was based on the method presented in Frappier (2008), and discussions with Jeff Dorale suggesting suspended mud may be captured in stalagmites recording floods (personal communication, 2006-2007). For this study I carefully chose a stalagmite, CH-1, from Cenote Chaltun-Ha (Figure 11). Chaltun-Ha is a part of the Ring of Cenotes, and is located outside Rancho Chaltun-Ha in the Mexican state of Yucatán. Rancho Chaltun-Ha is a modern hacienda with cattle fencing and grazing, high-power electrical lines, and land in various stages of

development and agricultural usage. The site shares many characteristics with most caves in the region: for example, it has standing water in the lowest part of the cave, the air-filled passages of the cave are shallow, and it consists of one large room. The cavern is about 18 m wide with a short side passage in the deepest air-filled part of the cave. Chaltun-Ha lies in an area that should be sensitive to flooding from TCs because of its low elevation and close connection to the water table (Marin, 1990).

CH-1 was collected from beyond the twilight zone in the side passage, approximately 7 m below the ground level and 4.4 m above the water table. The top of CH-1 was approximately 1 m below the soda straw that was the source of the water drip, meaning there was approximately 6 m of soil and epikarst above the soda straw, with likely at least 5.8 m of epikarst in this zone. This should allow for short residence times and limited mixing of the ground water that eventually drips onto CH-1, meaning the $\delta^{18}O$ and $\delta^{13}C$ values will be less muted by homogenization and the TC signature should be significantly below the background $\delta^{18}O$ value of -2 to -3.9 ‰. The high evaporation rate in the region should also help increase the isotopic contrast between cyclogenic water and the background meteoric water. The relatively high $\delta^{18}O$ values from the meteoric water in the Yucatán should increase the contrast between background and anomalous $\delta^{18}O$ values.

Figure 11. Exterior of CH-1, collected from Chaltun-Ha on July 27th, 2007.

The geometry of the cave near the water table is like a wedge (see sketch map, Figure 12), i.e., the roof and floor of the cave slope towards the opening. This means the section of the cave that CH-1 was collected from had less void volume for flood water to fill than a pit or rectangular geometry, allowing flood waters to rise high enough to cover CH-1 with mud. The distance from the cave entrance to the standing water was 32.5 m, at a 10º incline.

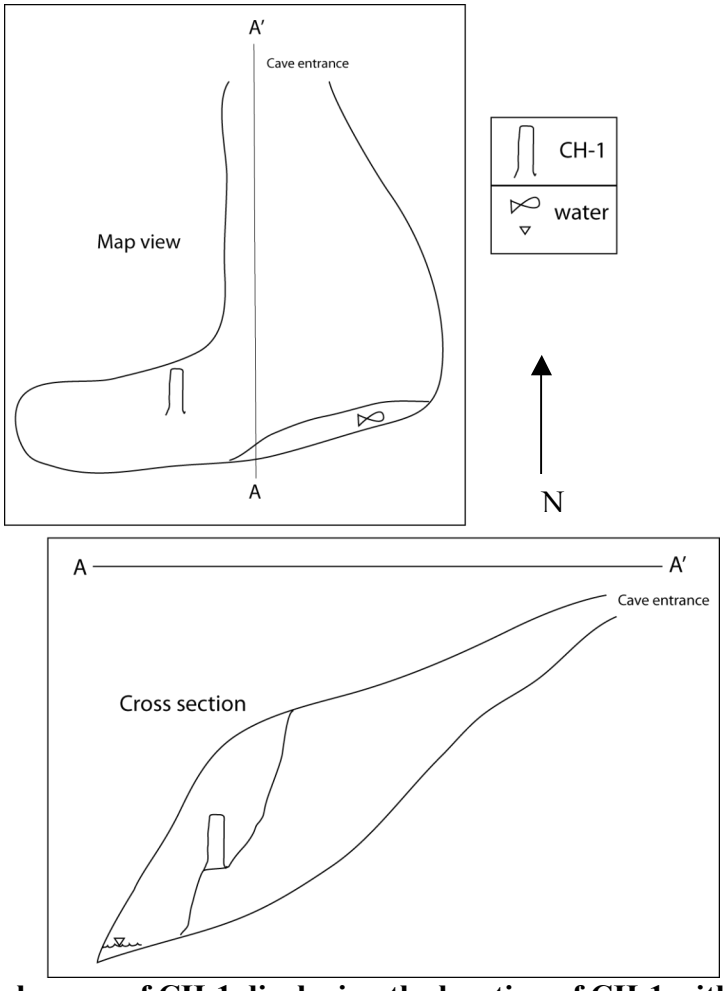

Figure 12. Sketch maps of CH-1 displaying the location of CH-1 within Cenote Chaltun-Ha and the general shape and layout of the cave. These sketch maps are not to scale.

We followed the selection method of Frappier (2008a) in the following manner: the stalagmite must be actively growing, so it would have a better chance of recording TCs from the last 30-50 years. During this period, satellites have accurately recorded TCs, providing a complete historical TC record (Landsea et al., 2000; Landsea et al., 2008) ideal for comparison to the CH-1 stratigraphic record. The stalagmite had to be symmetric and have a flat or round top, indicating regular growth. Asymmetrical stalagmites may indicate air motion or unstable drip locations, enhancing kinetic effects that mask the climate signal of interest. The desired length should be 10 cm to 1 m long to assure enough of a record of growth to capture at least the last 30-50 years. CH-1 is 18.5 cm long. The selection method was modified for this study to find a stalagmite that was sensitive to flooding. Caves that flood are generally avoided for stalagmite studies because abrasion and corrosion from floodwaters can erode previously deposited calcite (Frappier, 2008a)

Chaltun-Ha has an entrance elevation of 37 m above sea level. A local informed us in 2007 that Chaltun-Ha was flooded for at least 2 days after a recent hurricane. During collection in 2007, Chaltun-Ha had mud deposits over much of the floor and formations, including wet mud deposits a few cm thick next to CH-1, indicating recent flooding. CH-1 was growing in a small niche high on the side passage wall. At collection, it was covered in dirt over its entire exterior, except for the drip center, which was clean and showed clear calcite growth (Figure 11).

The water table in Chaltun-Ha at the time of collection was 4.4 m below stalagmite CH-1. Thus any included mud layers identified in the stalagmite presumably

record water table elevations at least 4.4 m above the ambient level. Calcite rafts were observed floating on the water and on the wet mud banks around the pool. We observed fish swimming in the pool, suggesting this pool was indeed a persistent feature connected to the local ground water system. Environmental measurements were taken with a Kestrel weather meter device at 4:40 PM inside Cenote Chaltun-Ha. The temperature was 32.1°C, with humidity at least 78.7%.

Potential problems with CH-1 include the fact that it was collected from a shallow cave near the entrance. Temperature, humidity, and pCO^2 levels are typically more variable close to cave entrances (Baldini et al., 2008) Furthermore, shallow caves provide less potential storage in the vadose zone and can have seasonal growth discontinuities. The easy access to the study site allows opportunity for human and animal disturbance as well. The only way to test if any of these factors were problems in CH-1 would be to collect another stalagmite either from Chaltun-Ha, or a nearby cave.

b. *Sample Preparation Methods*

CH-1 was encased in epoxy in a custom crafted cardboard box and longitudinally sectioned with an orientation that would section the main growth shaft and the secondary shaft in the same plane. The sample was cut into two central slabs using a diamond bit band saw blade at the machine shop at Boston College with the help of Alan Vachon. CH-1 was then polished using 3M Wetordry polishing paper starting with 400 grit, and fining to 2000 grit. The high-polish was then achieved using pool table felt and aluminum and tin oxide polishing powders up to 4000 grit at Boston College in the 2007-

2008 academic year. It was then placed in a 22 qt Fisher Scientific mechanical ultrasonic cleaner in heated de-ionized water for six hours to clean all the grit, felt, and carbonate powder from the pores and cavities on the sample (Frappier, 2007). The photography for the analysis was taken with the CM-2 microsampling system with stalagmite option, epifluorescence imaging, transmitted light base, and horizontal drill micromilling assembly at Boston College, as well as high-resolution scans. Layer counting, described in more detail below, was performed on high-resolution digital photographs in plain white light and fluorescent light. Layer counting and stratigraphic mapping were completed using the software packages Adobe Illustrator and Image J 64. Fluorescent light had more distinct variation, and therefore was the preferred light for layer counting.

c. *Dating*

Reliable radiometric dating is required in order to obtain absolute ages for the deposition history of CH-1, and to test for cyclicity in the fine growth laminae – specifically for the presence of annual banding.

i. *Radiometric isotope dating*

1. *^{210}Pb*

I used α-detection of the short-lived radionuclide ^{210}Pb (half-life 22.1 yr.) to date CH-1 (Baskaran and Iliffe, 1993; Frappier et al., 2002b; Frappier et al., 2007). The ^{210}Pb isotope is part of the ^{238}U decay series, and is produced at a constant rate by its immediate precursor, ^{222}Rn (half-life 3.8 d) (Appleby and Oldfield, 1978; Baskaran and Iliffe, 1993).

There is a high concentration of Rn atoms in their aqueous phase in ground water, which then percolates into the cave system. The Rn atoms are present in the secondary calcite that precipitates and then decays into ^{210}Pb. This is known as excess ^{210}Pb. The ^{210}Pb isotope is not soluble in natural waters, and accumulates in the crystal lattice of cave formations including stalagmites (Baskaran and Iliffe, 1993). The incorporated ^{210}Pb decays *in situ* in speleothems and other environmental archives such as lake cores. The ^{210}Pb dating method has an effective age range of 100-150 years (Baskaran and Iliffe, 1993).

To determine the age of a stalagmite's layer using excess ^{210}Pb requires determining the growth rate from the equation:

$$^{210}Pb(x) = {}^{210}Pb_s e^{(-\lambda/s)d}$$

where $^{210}Pb_s$ and $^{210}Pb(x)$ are the activities of excess ^{210}Pb in the most recent layer(s) and at any other layer (x), λ is the decay constant (0.0311 yr^{-1}), d is the distance between the two layers, and s is the growth rate in mm/yr (Baskaran and Iliffe, 1993). Assumptions include: a constant ^{210}Pb flux, an actively growing stalagmite over the time measured, and no supported ^{210}Pb is measured. Supported ^{210}Pb is derived from ^{222}Rn decay within the stalagmite growth column (Appleby and Oldfield, 1983; Baskaran and Iliffe, 1993). For alpha detection, an additional assumption is that ^{210}Pb is in secular equilibrium with ^{210}Po. Secular equilibrium is the state after which the daughter isotope is only present because of the decay of the parent. This is because the daughter has a half-life that is significantly shorter than the parent isotope. This means that any measurement of the daughter's activity is equivalent to the activity of the parent's. The ^{210}Po isotope is part

of the decay chain from ^{210}Pb to ^{206}Pb, and it has a half-life of 138.4 days. Its daughter is the stable ^{206}Pb isotope. The alpha emission energy of ^{210}Po is 5.307 MeV, which is higher and easier to detect than the ^{210}Pb decay energy of 3.792 MeV (Nittrouer et al., 1979). For this reason, ^{210}Po is actually detected in this process.

Ten approximately 0.1 g samples were drilled along stratigraphic layers out of the unpolished back of the main CH-1 slab and analyzed for ^{210}Pb activity. Dr. D. Reide Corbett performed the α–decay detection in the geochemical and environmental radioactivity detection lab at East Carolina University in March 2009 after finding no detectable ^{210}Pb activity via γ-detection. Total ^{210}Pb activities were measured by alpha spectroscopy following the methodology of Nittrouer et al. (1979). Samples were spiked with a known activity of ^{209}Po yield tracer, and partially digested with 8N HNO_3 by microwave heating. The ^{210}Po and ^{209}Po isotopes from the solution were then electrodeposited onto nickel planchets in a dilute acid solution (Flynn, 1968, modified). Samples were α-counted individually in an Ortec Octete detector, and activities were calculated based on the gross counts of ^{209}Po and ^{210}Po. The supported activity was found as the average ^{210}Pb activity at the base of the stalagmite. Excess activities were calculated by subtracting the supported activity from the total measured activity for each sample. Accumulation rates reported here were determined using the constant flux:constant supply (CF:CS) model (Appleby and Oldfield, 1992).

2. *U/Th*

Most contemporary calcite stalagmite studies obtain age control using the potentially high-precision U/Th dating method (Edwards et al., 1987). However, dating of so-called 'dirty stalagmites' is often thwarted by the high initial Th load of included mud (Schwarcz and Latham, 1989). Also, many speleothems from the Yucatan peninsula have proved difficult to date with high precision due to low uranium concentrations. Despite these twin potential problems, U/Th dating was attempted on the cleanest layers of the CH-1 stalagmite where mud layers were least common in the attempt to obtain age information for the calcite deposited prior to the range of ^{210}Pb dating. Using both U/Th and ^{210}Pb allowed for the dating of the top and bottom of CH-1, as well as adding duplication and confidence to two analytical techniques which each had their set of difficulties and uncertainties in this specific sample.

Four samples were collected from the lower portion of CH-1 for U/Th analysis by drilling along stratigraphic layers with the no visible mud layers (Figure 13)(Edwards et al., 1987). The analysis was performed under the direction of Xianfeng Wang at the Minnesota Isotope Lab in the Department of Geology and Geophysics, University of Minnesota, following the methods of Edwards et al. (1987) and Shen et al. (2002).

Uncertainties specific to CH-1 for both methods exist. For ^{210}Pb the slow growth rate made it difficult to get more than two samples with any measurable ^{210}Pb activity. Another difficulty was the layer thicknesses. CH-1's layers are so thin that it would be impossible to obtain sufficient material by sampling a single layer, thus reducing the potential precision due to the spread of ages captured by each sample. On the other hand,

the small diameter of the stalagmite resulted in layer geometries that also prevented the collection of large mass samples, limiting analytical precision (Dorale and Liu, 2009). I attempted to drill sample powders for dating that followed the layer geometry, following the recommendations of Dorale and Liu (2009).

Figure 13. Scan of the polished slab of CH-1 showing the 4 locations of U/Th dates.

The mud layers make U/Th dating of the calcite difficult because the mud introduces excess Th. Detritus in calcite is commonly enriched in ^{230}Th, and can contain variable amounts of ^{230}Th, ^{234}U, and ^{238}U (Bischoff and Fitzpatrick, 1991; Labonne et al., 2002; Schwarcz and Latham, 1989). The best solution to this problem that was available for CH-1 was to try to sample only layers that were made of calcite that appeared to be free from detrital mud.

ii. *Stratigraphy: Calcite Coupled Laminae and Interbedded Clastic Muds*

Layer counting is a visual stratigraphic technique for recognizing annual laminae (analogous to varves or tree-rings) based on the variations in calcite deposition between the wet and dry seasons, which are very pronounced in the Yucatán Peninsula (Figure 14). As shown in Figure 14, the Yucatán Peninsula has multiple Koppen climates. In the Koppen scheme, Aw climates have a pronounced dry season with one or more months in which precipitation is less than 60 mm. Aw_0 is the driest of the Aw climates, with annual rainfall of 1000-1100 mm, and BS receives 250-500 mm annual rainfall. Typically, in such seasonal climates, stalagmites develop annual layers (Baker et al., 2008). Each year two layers are deposited: one layer of opaque calcite, sometimes called white porous calcite (WPC), coupled with a clear layer of dark compact calcite (DCC) (Kendall and Broughton, 1978). The differences in color are due to the different morphologies of the calcite crystals deposited under different hydrological regimes (Baker et al., 2008). Each calcite couplet should thus represent one hydrological year. In addition to visible couplets, annual variations in fluorescent humic acids flushed into the cave system by

rainwater can be seen and measured using a mercury light source to excite the intrinsic fluorescence of these organic substances (Sharp, 2007). Brighter excitation seen in the calcite of stalagmites is normally due to higher rainfall, and darker, less fluorescent material is deposited during the dry season.

Figure 14. Climates of the Yucatán Peninsula classified by the Koppen system. The red star is the study site (after Gill, 2000).

A series of high-resolution images of the polished surface of CH-1 was collected using the CM-2 epifluorescence microscopy module with a broadband fluorescence excitation lamp and a Chroma 49000 series CFP filter at 6x magnification. Each photograph was ~1.5 cm x 1.5 cm.

Using these epi-fluorescence images, a total of 56 mud layers within the top 30.11 mm of the stalagmite growth axis were identified and their depths below the growth surface were measured. The age model developed was used to assign ages to the mud layers based on their depths. Using Image J64, four adjacent gray scale measurements were taken along transects drawn perpendicular to the laminae in the center of CH-1 and parallel to the growth axis. These grayscale transects were averaged and plotted as a function of depth below the growth surface. A 3-point (3-pixel) running mean was then applied to remove high frequency noise, revealing cycles of grayscale brightness that reflect fluorescence intensity. The cycles resulting from variations in fluorescence were assumed to represent one hydrological year, and the peaks were manually counted.

In order to account for the flood-deposited mud layers that also generated low-fluorescence layers, I systematically removed the clastic layers from the counts of annual laminae in the following manner: Mud layers that had measurable thicknesses observed in plain and fluorescent light that were present across the entire width of the CH-1 cross-section were assumed to cause a false cycle. Each fluorescence cycle whose depth matched the depth of a mud layer was subtracted from the final cycle count. This procedure resulted in an adjusted count of the number of cycles (interpreted as hydrological years) in the top 30.11 mm of CH-1. Furthermore, by subtracting the adjusted number of cycles stratigraphically above each mud layer from 2007.5, the time of stalagmite collection, it was possible to determine the calendar year of each mud layer's deposition. Using these layer-counting-derived dates for each mud layer, I

calculated growth rates for each section between the first 56 mud layers. The growth rates across this section were then compared to the growth rates attained from the ^{210}Pb dating. A similar exercise was performed between the two U/Th samples in the lower section of CH-1.

The mud layers in the remainder of CH-1 were identified with lower resolution images. Mud layers that were only present on the periphery of CH-1 were tallied, and assigned a location as precisely as possible by interpolating the layer into the center of CH-1 for dating purposes.

iii. *Age model formulation*

To build an integrated age-depth model for the entire length of CH-1, I have used the radiogenic dating ages to determine absolute rates of growth, and compared growth rates derived from radiometric and fluorescent layer counting techniques to test the validity of the assumption that the observed fluorescent couplets are deposited annually. Figure 15 shows the different sections of CH-1's age model, with the dating techniques used appropriately labeled. The growth rate for Section 1, the uppermost section, was developed using the layer counting technique, which was supported by the ^{210}Pb growth rate. Using the couplet thickness measurements and the adjusted layer counting ages, I have determined an average rate of growth for each of the sections between the first 56 mud layers in the top 30.11 mm of CH-1. The remainder of the age-depth model was based on the U/Th dates and/or layer counting. The second section of CH-1 had a growth rate determined from the difference in the ages from the bottom of section 1 and the age

from U/Th sample 3. Section 2 was the longest section, ~110 mm, and high-resolution imagery of this section has not yet been collected, making it impossible to count layers. The third section was bounded on two sides by U/Th dates, and there was good imagery of the section, allowing for layer counting to verify the growth rate. With this age model I am able to estimate the age of any layer within CH-1 based on its depth. The precision of my age-depth model varies from $\leq \pm 2$ years in Section 1 to as low as $\pm$ 160 years in Section 2.

d. *Stable isotope data collection*

i. *Stable Isotope Ratio Mass Spectrometry*

The stable isotope ratios of gas samples are measured on an isotope ratio mass spectrometer (IRMS), which consists of an inlet system, ion source, flight tube, an ion collector, and a recording system (Sharp, 2007). Two gasses are measured in dual inlet analysis mode. One is the unknown sample and the other a reference sample to compare the measurements and to allow for the comparison of the results to those from any other lab. The gasses are alternately induced into the machine's ion source rapidly to reduce noise caused by measuring the two gasses at different times. The gasses are ionized and focused into a beam that is accelerated down the flight tube and through a magnetic field. The charged particles are deflected at different angles due to their differing masses. After coming out of the flight tube they are collected in an array of Faraday cups where the current that is created is amplified and recorded. The mass of each ion collected is

Figure 15. Showing the dating method used for the three sections of CH-1

measured by the amount of deflection each ion experiences in the magnet. The machine which records the results automatically yields isotopic ratios and delta values (Hendy, 1971)

ii. *Calcite Stable Isotope Sampling and Microsampling*

Three sampling resolutions were collected for the stable isotope analyses reported here (Figure 16). The oval highlights the first ~10 samples of the 1 mm discrete sample holes, the red rectangle the 0.2 mm continuous milling trough, and the blue square the trough of the first 2 mm of the 0.02 mm continuous microsampling. The troughs are difficult to see in this scan of CH-1.

An initial low-resolution sampling line with a resolution of 1.0 mm was performed using a micomill to drill at discrete points along the drip-center through the length of CH-1's main growth axis as well as the secondary growth axis (oval in Figure 16). This low-resolution dataset was collected with the smallest drill bit available, before any knowledge of CH-1's growth rate. Each discrete point from the low-resolution dataset represents ~0.5 mm of calcite material analyzed at once, representing ~12.5 years. The 12.5 year/sample ratio represents a climate signal that is recording trends on a slightly longer than decadal scale, and was used for millennial scale climatic interpretations. A milling trough with 0.2 mm vertical resolution was performed in the top 8.1 mm along the growth axis, but the data was not used in this study (red rectangle in Figure 16). Finally, a micromilling trough with 0.02 mm (20 μm) vertical resolution was performed in the top 15.1 mm of CH-1 along the growth axis (blue square in Figure 16).

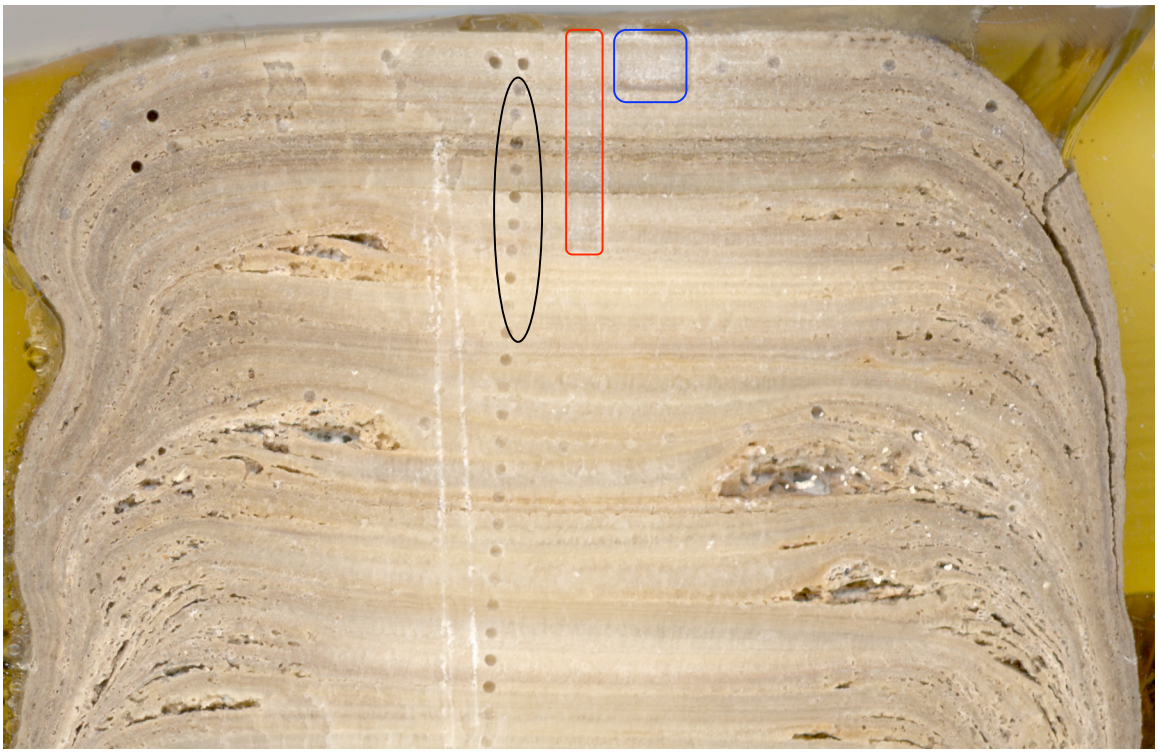

Figure 16. Illustrating the three sampling resolutions used for calcite powder collection.

The low-resolution (1 mm) and medium-resolution (0.2 mm) sampling and $\delta^{18}O$ and $\delta^{13}C$ analysis were both performed at the WHOI Micropaleontology Mass Spec Facility in Woods Hole, MA. Using a Finnigan-MAT 253 gas isotope ratio mass spectrometer (IRMS), 15-70 µg of powdered carbonate were analyzed for $\delta^{18}O$ and $\delta^{13}C$ values. The first 1.98 mm of microsampling and stable isotope analyses were both performed at the WHOI Micropaleontology Mass Spec Facility in Woods Hole, MA. CH-1 was milled along the growth axis at 20 µm intervals, at a trough depth of 140 µm.

The top 15.1 mm of CH-1 were micro-milled at the EAGLES isotope lab in Devlin 301 at Boston College. Powdered carbonate samples of 50-100 µg of carbonate were analyzed for $\delta^{18}O$ and $\delta^{13}C$ values using a ThermoFinnigan MAT 253 Dual Inlet

System at the KPESIL - W. M. Keck Paleoenvironmental and Environmental Stable Isotope Laboratory at the University of Kansas. Microsamples were shipped via FedEx in specially built containers created by the KPESIL personnel.

iii. *Hendy tests*

Three individual 'Hendy' test analyses were performed at WHOI (Garcia-Herrera et al., 2005). Between seven and ten discretely drilled samples were collected from each of three different growth layers in order to compare $\delta^{18}O$ and $\delta^{13}C$ values from the extreme edges and the central part of CH-1. The Hendy tests were performed on three layers within the top two cm of CH-1. 'Hendy 1' and 'Hendy 2' (0.1 cm and 0.45 cm from the top respectively) (Figure 17) were chosen because they had relatively flat, and regular geometries, and because they were relatively thick, making it possible to sample a consistent time line across the stalagmite surface. These layers presumably make it possible to test for the presence of equilibrium conditions during 'normal' deposition. 'Hendy 3' (1.5 cm from the top) was chosen because of the mud lobes on the perimeter of the deposition surface, creating a 'pooled' geometry and a thicker layer. The third layer was chosen to test for equilibrium deposition in the small pools that were created atop the stalagmite by mud deposited by flooding of Chaltun-Ha (Figure 17).

e. *Data analysis*

Initial analysis of the $\delta^{18}O$ and $\delta^{13}C$ values entailed basic descriptive statistics of mean, standard deviation, maximum, and minimum. This was followed by overlaying

graphs of the $\delta^{18}O$ and $\delta^{13}C$ values vs. depth onto CH-1 photographs in the locations from which the data was collected and visually inspecting the relation of the data to the stratigraphy of CH-1. This was followed by a comparison of $\delta^{18}O$ and $\delta^{13}C$ values to local weather data consisting of rainfall, evaporation, and maximum and minimum temperatures from 4 locations averaging 47 km from Cenote Chaltun-Ha, as well as the Southern Oscillation Index (SOI), average meteoric water isotope values (waterisotopes.org) and other speleothem paleoclimate records from the region to test reproducibility of the climatic signal. A TC prediction model was developed based on the high-resolution $\delta^{18}O$ and $\delta^{13}C$ datasets in the software package SPSS using a binary logistic regression.

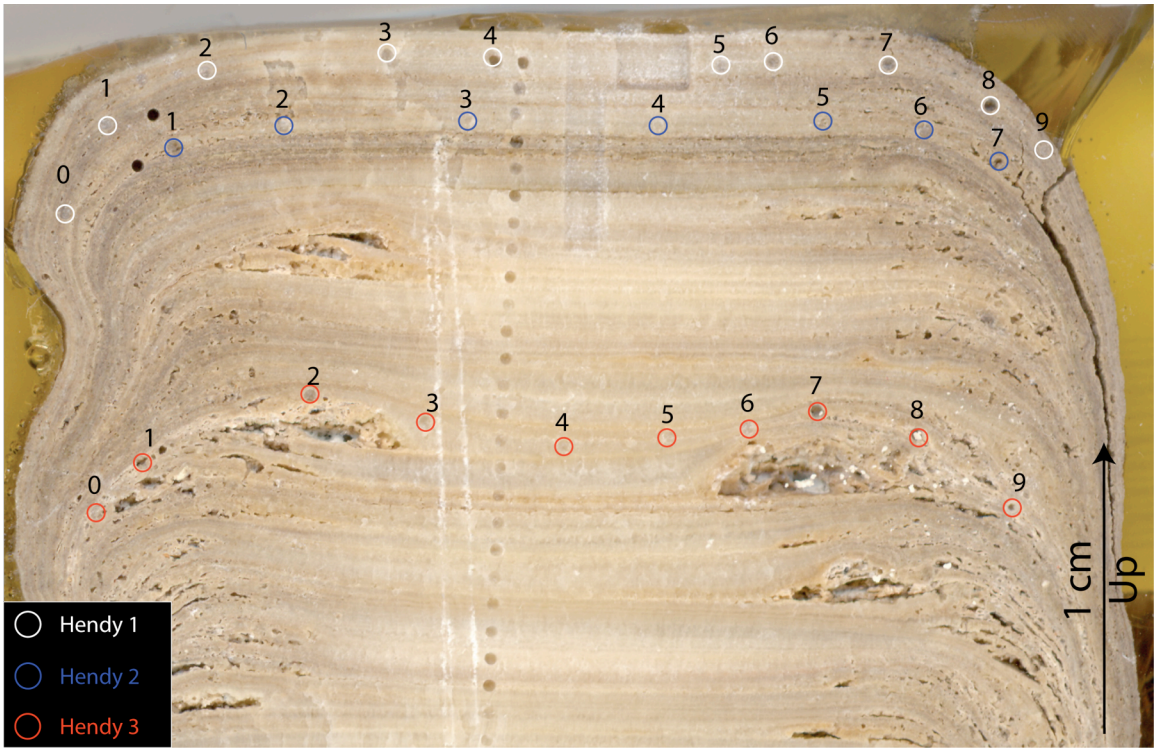

Figure 17. Locations of samples drilled for the 3 Hendy tests.

i. *TC prediction model calibration*

A probability function to predict TCs based on high-resolution $\delta^{18}O$ and $\delta^{13}C$ values was developed in an attempt to quantify the likelihood that any given sample represented a TC event. The four-term probability function had $\delta^{18}O$ and $\delta^{13}C$ and $\delta^{18}O_d$ as coefficients, and a constant. The $\delta^{18}O_d$ coefficient was defined as the difference between adjacent $\delta^{18}O$ values (Frappier et al., 2007).

To develop this probability function, the high-resolution $\delta^{18}O$ and $\delta^{13}C$ values were visually inspected for short-lived, negative excursions in the $\delta^{18}O$ values that were not present in the $\delta^{13}C$ values. These excursions were assumed to be TCs. The storms identified visually were then correlated to historical TC strikes and were then used to define the coefficients for the four-term binary logistical regression model developed by Frappier et al. (2007). Within the 5 excursions identified as cyclogenic since 1900 (Figure 18), the data point with the lowest $\delta^{18}O$ value was coded as a 1, while all other data points in the data set were coded as 0. The probability function was then applied to the remaining $\delta^{18}O$ and $\delta^{13}C$ values.

ii. *Weather data analysis*

Historical TC data was collected primarily from NOAA's Coastal Services Center database (NOAA, 2009). The search performed was by the latitude and longitude of Cenote Chaltun-Ha, lat: 21, long: -89, TC categories including tropical storm, tropical depression, and hurricanes category 1-5 within a distance of 200 nautical miles, or 230.1 miles from the Cenote Chaltun-Ha, from years 1851-2007. The best track data was used

to measure how close the eye of each TC passed to Cenote Chaltun-Ha, and the highest category of each storm as it passed was used to determine intensity.

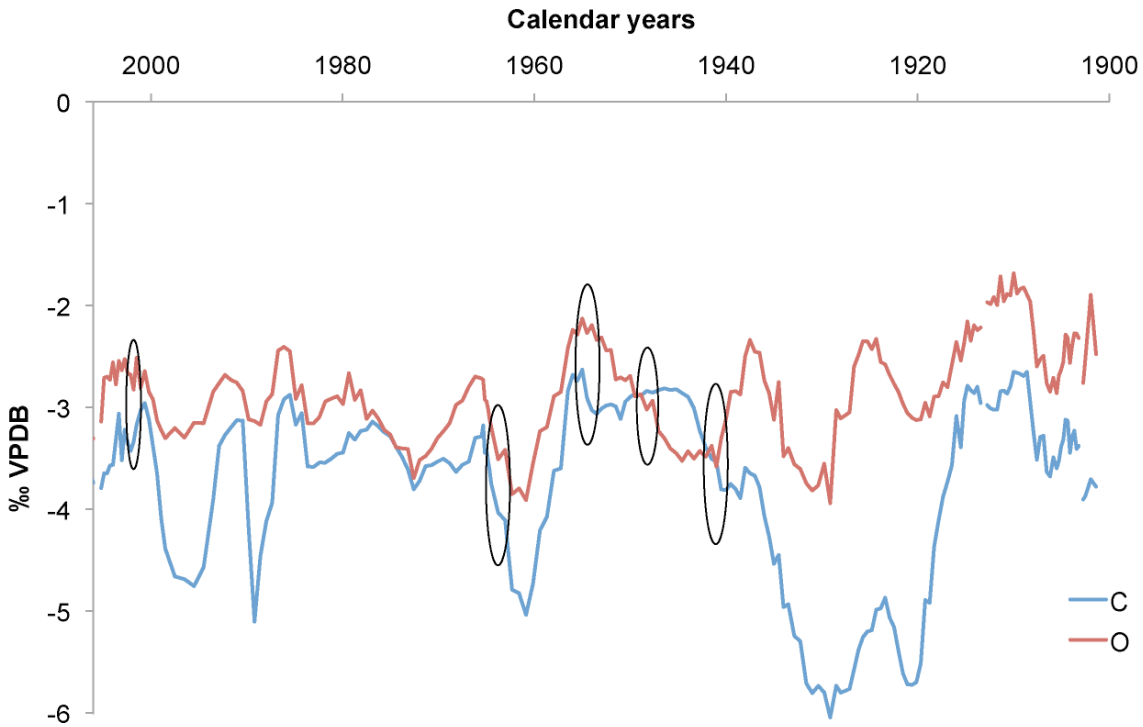

Figure 18. The locations of the five visual excursions in $\delta^{18}O$ values are circled.

Historical TC records for the Caribbean region from earlier than 1851 are sparse, but some records exist in the form of Spanish shipping documentary records. Of the 70 TCs documented to have occurred between 1520 and 1895, 5 were very likely to have crossed the Yucatán peninsula and so were considered in the analysis of the efficacy of the proxy.

The $\delta^{18}O$ and $\delta^{13}C$ values were compared to the Southern Oscillation Index (SOI) to look for a correlation between local climate and the El Nino-Southern Oscillation from

1876 to 2007. The SOI data was collected from the Australian Government Bureau of Meteorology SOI Archives (Australian Government, 2009).

Weather data from many stations across the peninsula dating from the mid 1960s to 2007 was obtained from the Comisión Nacional Del Agua de México, courtesy of Dr. Bruce Dahlin. Weather data from four meteorological stations were used to gain some insight to the recent climate history for the region (Figure 19). This weather data were then compared to the SOI and the stable isotope record, as well as comparing the stable isotopes and the SOI.

The weather data from the 4 stations shown in Figure 19 were averaged yearly starting in 1961 in Sotuta, 1969 in Santa Elena, and 1978 in Acanceh and Holca through 2006, the last year with complete data. Yearly temperature, rainfall, and water budget (rainfall-evaporation) measurements provided recent climate trends and instrumental data to compare to the $\delta^{18}O$ and $\delta^{13}C$ values collected from CH-1.

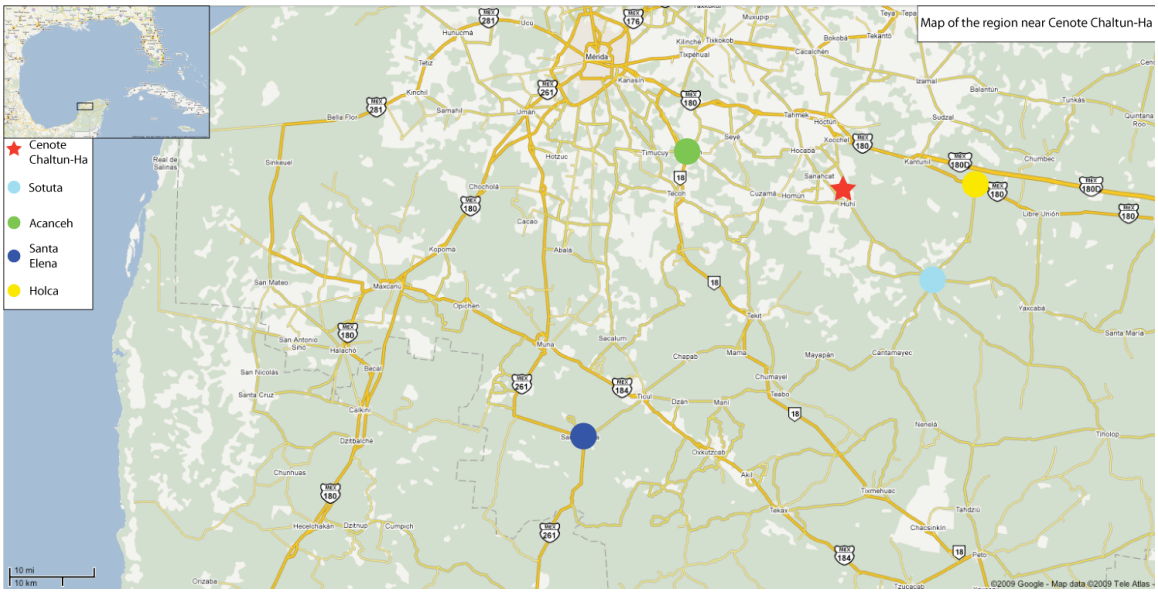

Figure 19. Locations of the four meteorological stations where weather data was used to assess the local climate of Rancho Chaltun-Ha.

Monthly rainfall averages from the four stations were analyzed for each of the five years that had a mud layer spanning the years 1960-2007. The average monthly rainfall for all the years combined was then removed from these monthly averages to find monthly anomalies. This exercise was an attempt to determine what kind of anomalous influx of water would be required to produce a flood recorded by a mud layer in CH-1. The same method was applied to three years with historical TCs that were not represented by a visible mud layer within CH-1. Precipitation data for the days the historical TC passed through Chaltun-Ha's region were also analyzed in an attempt to quantify the conditions required to deposit a mud layer in CH-1.

4. Results

The stratigraphy of CH-1 contains many clues to its deposition history providing insights to the mud layer deposition, climatology, and growth rate of CH-1. Annual calcite couplets combined with ^{210}Pb and U/Th data combine to create an age model that is of critical importance to understanding the timing of mud layer deposition, as well as constraining any climatic interpretations based on the $\delta^{18}O$ and $\delta^{13}C$ values. Integrating the depositional history of CH-1 with the age model, climatic interpretations, and historical TC record allows for the testing of the mud layers as a viable paleotempestology proxy.

a. *Age Model*

Layer counting, ^{210}Pb, and U/Th dating techniques were integrated to test for the presence of annual laminae, test for growth hiatuses, and to develop the age/depth model used to assign ages to mud layers throughout the main growth shaft of CH-1.

i. *Radiometric dating*

1. *^{210}Pb α-detection*

Of the ten samples of CH-1 analyzed for ^{210}Pb activity, two had detectable activities above error (Table 1). Using the depths of the deepest sample with activity (age must be less than 100 yr) and the shallowest sample without activity, the growth rate was bracketed (Table 2).

The ^{210}Pb dating method revealed an average growth rate of 0.04 ± 0.004 mm/yr in the top 6.4 mm of CH-1. The limits of detection of ^{210}Pb activity is up to 100-150 years based on the 22.2-year half-life (Baskaran and Iliffe, 1993). The cessation of ^{210}Pb activity should thus mark the spot in CH-1 that is 100-150 years old. The exact depth at which ^{210}Pb activity ceased cannot be known from discrete sampling. However, three possible locations of the cessation of ^{210}Pb were assumed; immediately after sample 2, half way between sample 2 and 3, and immediately prior to sample 3. The extremes in possible ^{210}Pb activity detection of 100 or 150 years were then applied to each of the locations where activity is assumed to cease, predicting a range of growth rates that provided some confidence in the measured growth rate of 0.04 mm/yr (table 2).

number	sample top distance from top (mm)	sample midpoint distance from top (mm)	sample bottom distance from top (mm)	Excess Pb-210 (dpm/g)		
1 (activity present)	0	0.5	1	1.92	+/-	0.26
2 (activity present)	2.2	2.7	3.2	0.18	+/-	0.14
3 (no activity present)	5.8	6.3	6.8	0.02	+/-	0.10
4	10.5	11	11.5	0.06	+/-	0.13
5	21.6	22.1	22.6	-0.01	+/-	0.12
6	40.6	41.1	41.6	0.04	+/-	0.12
7	62.3	62.8	63.3	0.02	+/-	0.14
8	95.1	95.6	96.1	-0.06	+/-	0.09
9	140.8	141.3	141.8	0.03	+/-	0.10
10	170.6	171.1	171.6	-0.11	+/-	0.09

Table 1: Excess ^{210}Pb activities in CH-1 sub-samples measured by α-detection.

Growth rates in mm/yr:

post #2 cutoff	Distance from top 2.7 mm
100 years 0.027 mm/yr	**150 years** 0.018 mm/yr
mid-point cutoff	**Distance from top 4.5 mm**
100 years 0.045 mm/yr	**150 years** 0.03 mm/yr
pre #3 cutoff	**Distance from top 6.3 mm**
100 years 0.063 mm/yr	**150 years** 0.042 mm/yr

Table 2: Range of growth rates based on the different ranges of depths for onset of detectable 210-Pb activity in CH-1 and effective detection age (100 and 150) of ^{210}Pb activity cessation.

2. *U/Th*

The U/Th dating from the purest, mud-free calcite layers available (Figure 20) yielded the dates in Table 3. Sample 1 had excess ^{232}Th making the resulting age older than the rest of the other samples, and was therefore discarded.

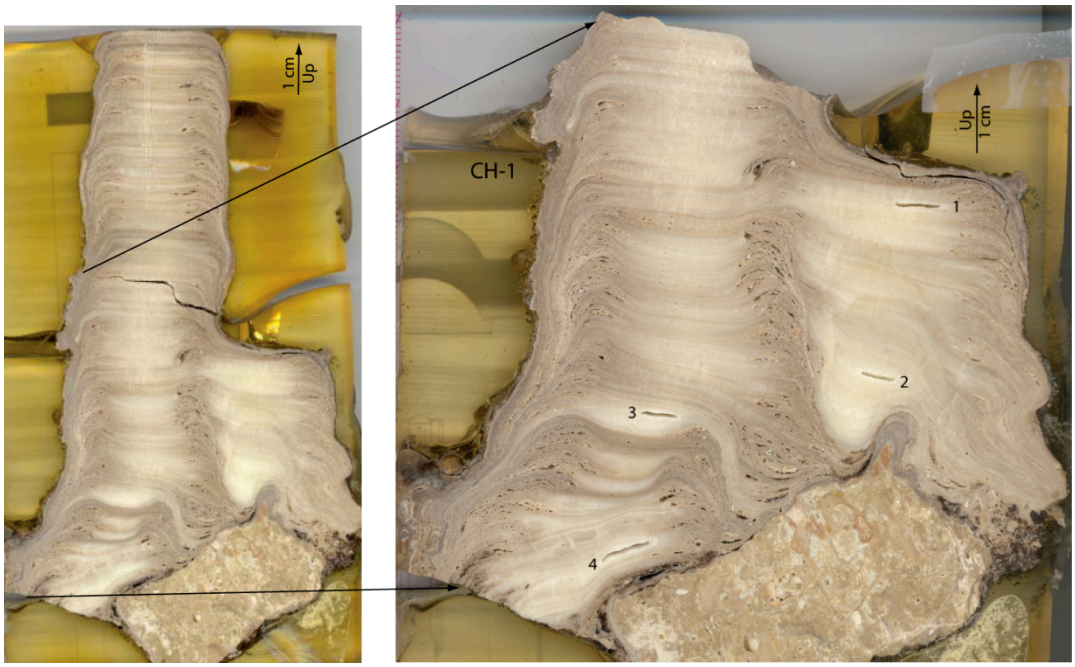

Figure 20. Location of the 4 U/Th data points.

^{230}Th dating results. The error is 2σ error.

Samp Numb	^{238}U ppb	^{232}Th ppt	^{230}Th / ^{232}Th x10^{-6}	δ^{234}U* measured	^{230}Th / ^{238}U activity	^{230}Th Age uncorrected	^{230}Th Age corrected	δ^{234}U$_{Initial}$* corrected	^{230}Th Age corrected
CH1-1	234.7 ±0.6	3214 ±65	28 ±2	-39.4 ±1.5	0.0229 ±0.0012	2636 ±138	**2221 ±325**	-40 ±2	**2163 ±325**
CH1-2	134.6 ±0.4	644 ±14	53 ±7	-36.1 ±1.8	0.0153 ±0.0021	1746 ±236	**1602 ±257**	-36 ±2	**1544 ±257**
CH1-3	215.4 ±0.5	718 ±15	86 ±7	-41.9 ±1.3	0.0174 ±0.0013	2003 ±146	**1902 ±163**	-42 ±1	**1844 ±163**
CH1-4	142.8 ±0.4	551 ±12	92 ±6	-29.2 ±1.8	0.0215 ±0.0013	2447 ±147	**2331 ±168**	-29 ±2	**2273 ±168**

*δ^{234}U = ([^{234}U/^{238}U]$_{activity}$ − 1)x1000. ** δ^{234}U$_{initial}$ was calculated based on ^{230}Th age (T), i.e., δ^{234}U$_{initial}$ = δ^{234}U$_{measured}$ x e$^{\lambda_{234}xT}$.
Corrected ^{230}Th ages assume the initial ^{230}Th/^{232}Th atomic ratio of 4.4 ±2.2 x10^{-6}. Those are the values for a material at secular equilibrium, with the bulk earth ^{232}Th/^{238}U value of 3.8. The errors are arbitrarily assumed to be 50%.
***B.P. stands for "Before Present" where the "Present" is defined as the year 1950 A.D.

Table 3. Summarizing the U/Th data.

ii. *Layer counting*

The top 30.1 mm of CH-1 contained 794 gray-scale cycles representing fluorescent band pairs. Six mud layers were identified as causing false bumps, and were subtracted from the final count, yielding a total of 788 ± 1.7 years in the top 30.1 mm. This resulted in an average growth rate of 0.038 ± 0.0003 mm/year (Figure 21). The red

ovals in Figure 21 show sections that where mud layers were obvious, and thick enough to create a false cycle. There were a total of 6 of these in the top 30.11 mm of CH-1, however, most were not as obvious as these three at this scale. The count for this section was 393 cycles, interpreted as 393 years.

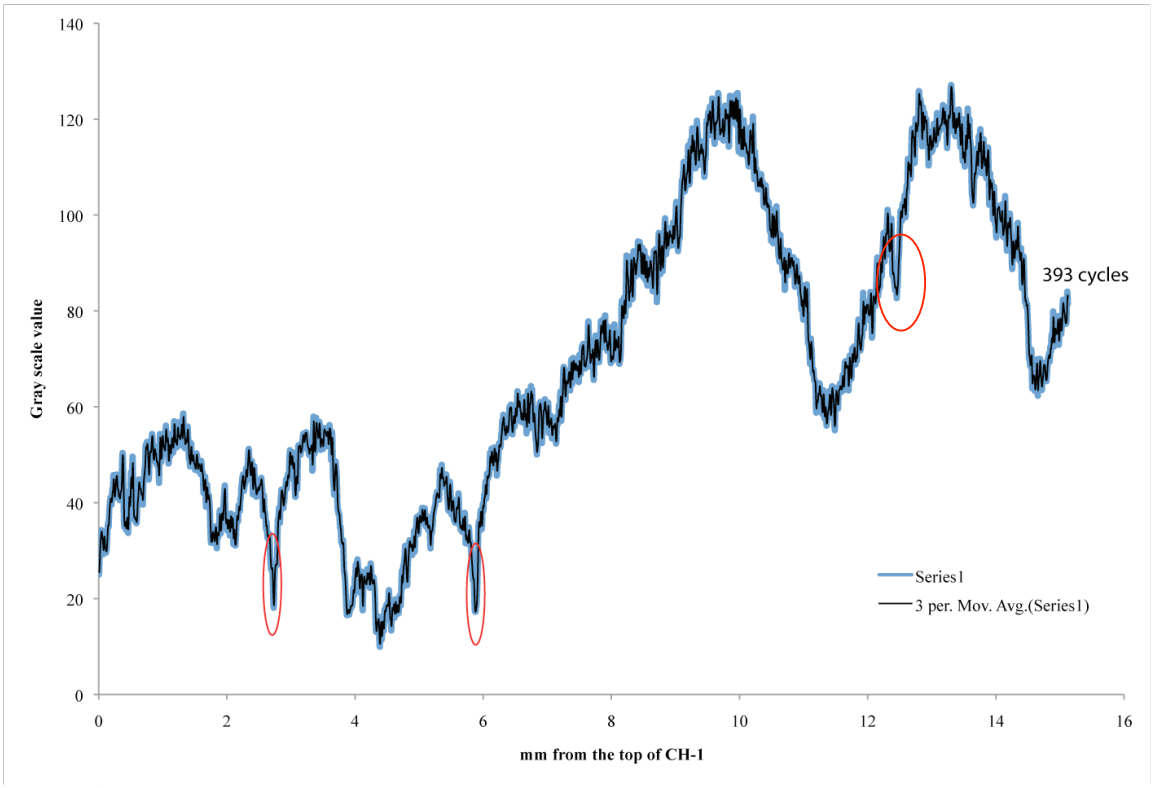

Figure 21. Chart of the average of four adjacent gray scale measurements in blue, and the three-period moving average used to count cycles in black.

iii. *Integrated age model*

The integrated age model can be seen in Table 4 and Figure 22.

Section:	Depths:	Ages:	Method:	Growth rate (mm/yr):
1	0-30.1 mm	2007 AD - 1222 AD	counting/210Pb	0.038 ± 0.0003
2	30.1-140.9 mm	1222 AD - 163 AD	U/Th	0.098 ± 0.024
3	140.9-163.66 mm	163 AD - 266 BC	U/Th	0.053 ± 0.2
All Axis 1	0-163.66 mm	2007 AD - 266 BC	U/Th	0.07 ± 0.044

Table 4. The age model for CH-1.

Figure 22. Integrated age model for CH-1 showing the U/Th dates. The bar along the side shows the growth rates for the different sections of CH-1 derived from ^{210}Pb data and cycle counting.

Combining the layer counting and radiogenic growth rates provided an age model for the length of the axis 1 of CH-1 (Table 4). Comparing the cycle counting and ^{210}Pb growth rates leads to the conclusion that it is most parsimonious to call the fluorescence cycles annual layers (Table 5). This also gave an indication that CH-1 was growing continuously during this interval. The top 30.11 mm had a growth rate of 0.038 mm/yr, and was based on ^{210}Pb activity, supported by the cycle counting exercise, and because it was supported by two methods provided the highest confidence of any section in the age model. The layer counting also provides the highest accuracy, providing yearly resolution and raising the confidence in the comparisons to instrumental TC and climate records for the top, youngest section.

Method	Growth rate (mm/yr)
Cycle counting (0 - 30.11 mm, 794 gray-scale cycles, 788 ± 1.7 years)	0.038 ± 0.0003
^{210}Pb (0 - 3.2 mm)	0.04 ± 0.004

Table 5. Comparison of age determination methods from the top 30.11 mm.

The next section was 109.15 mm long, and was the fastest growing section, with a growth rate of 0.098 ± 0.024 mm/yr. The top of the section was dated with layer counting grounded in the ^{210}Pb-dated section at the top of CH-1. The bottom was U/Th sample 3. It was the longest section and had the fewest controls on ages, increasing the uncertainty of the dates.

The lowermost section, the bottom 22.8 mm, is bracketed by U/Th dates 3 and 4. The difference between samples 3 and 4 from U/Th dates was 429 ± 168 years. The growth rate for this section was within a range of growth rates of 0.227 mm/yr and 0.043 mm/yr. The high range for this section was due to the shifting location of the growth center, complicating the measuring of distance between the samples. Notice the steeper angle in the calcite layers between U/Th samples two and three in Figure 22. The vertical distance used for the final age model was measured on the left sides of both sample holes due to the proximity to the center of the growth axis, which yielded a growth rate of 0.053 ± 0.2 mm/yr. Fluorescent layer counting as described above supported this growth rate. The layer counting in this section resulted in 470 years, easily within error of the U/Th dates.

The average growth rate for the entire length of the axis 1 of CH-1 was 0.070 mm/yr. Axis 2, discussed further below, only had one data point, so any growth rate estimates would be very poorly constrained and was left for future work.

b. *Stratigraphy*

The calcite in CH-1 has a compact microcrystalline texture, and is composed of sub-mm scale laminae interbedded with thin sub-mm scale gray/brown mud laminae. The calcite varies in color from white to transparent.

The top 101.8 mm of stratigraphy of CH-1 is fairly uniform except for the mud layers and lobes, and is about 40 mm in diameter (Figure 22). Below the top 101.8 mm of normal growth, a second growth axis is present parallel to the main growth. The

primary growth axis is still about 40 mm in diameter here, and is easily defined by the mud lobes. The secondary axis is also about 40 mm wide. CH-1 clearly had a time early on when a second drip was present approximately 40 mm from the main stalactite source, providing the $CaCO_3$ saturated water required to grow the secondary axis. For reasons I can only guess, the secondary axis stopped growing. This secondary growth axis stopped growing after the deposition of a mud lobe in the primary axis at 101.8 mm depth.

Mud layers were identified using the fluorescent images of CH-1 captured using the CM-2 microscope at the EAGLES isotope lab at Boston College. The mud layers do not fluoresce, making them easy to identify visually from microscope imaging performed on a highly polished cross-section with a fluorescence filter cube (Figure 23). The mud layers in the top 6 mm were mostly of uniform thickness across the growth layers and were visible across the entire width of the CH-1 polished cross-section. Six of these were of measurable thicknesses ranging from 0.03 mm to 0.11 mm. Below 6 mm, the mud layers tended to be very thin in the middle of CH-1, and much thicker on the sides forming lobes of varying sizes, making them much more evident on the periphery of CH-1. Some mud layers were completely absent from the center of CH-1. These "pinch-out" mud layers required correlation between the periphery and center of CH-1 in order to pinpoint their correct depth along the central growth axis. This was performed using visual comparisons, primarily interpolation following variations in the brightness of the luminescence from the sides to measure the depth of these layers (Figure 23). Growth axis 1 had 265 mud layers identified in it. Mud layers are also present in axis 2. The mud

still collects at the edge of the side growth, but only begins to create lobes and pooled deposition geometries at the top of axis 2.

In Figure 23, A is uniform thickness mud layers. B is mud layers that are easily visible on the periphery of CH-1 but that are absent from the growth center. C is mud lobes exemplifying varying thicknesses of mud layers in sections of CH-1. It is also evident that deposition of mud lobes is accompanied by a marked change in lamina morphology from thin continuous layers to deposition of thicker layers within a small central pool or drip cup. The two lobes labeled C illustrate how the lobes are often deposited on alternating sides of CH-1.

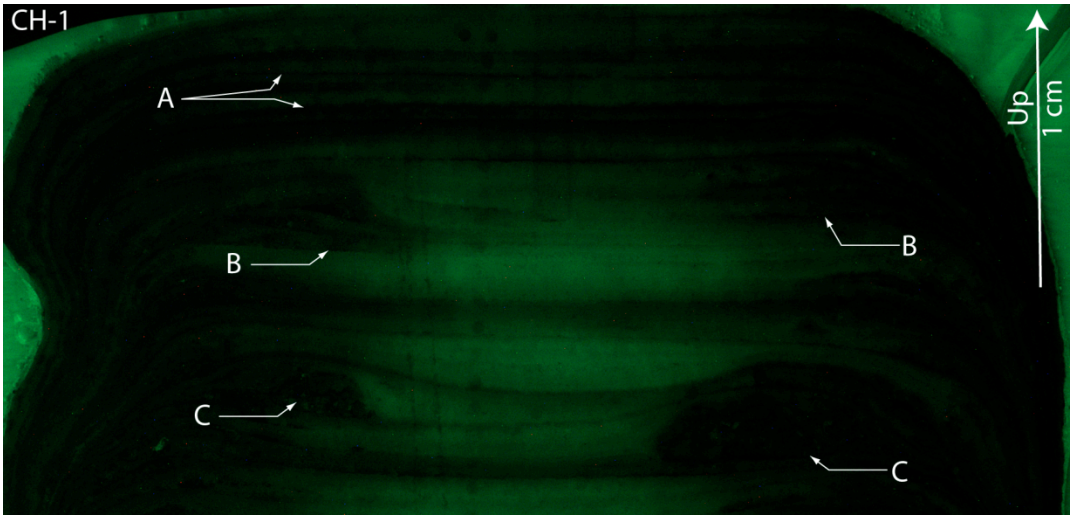

Figure 23. Top two centimeters of CH-1 in fluorescent light, showing examples of three different mud-layer morphologies discussed in the text.

The layers I interpret as annual are too thin to be easily seen in plain white light with the naked eye in most portions of CH-1. Most of the visible stratigraphy is due to the mud layers that are sometimes visible across the entire growth surface as darker layers. The layers of calcite and mud are mostly flat in the main growth axis of CH-1, except where the mud creates lobes. These lobes are generally not symmetrical. When a

mud lobe is present in cross-section, it is normally only present of one side of CH-1. The mud lobes alternate from the left to the right side on almost every mud layer in some sections as seen in Figure 23. The lobes create a small-scale accommodation space for deposition of calcite between flooding events. Calcite layers deposited in these pools often display onlapping relationships (Figure 23), providing evidence for post-mud layer pooling of drip water on the top of CH-1. The mud lobes and pooled calcite geometries are present from 6 mm to 56.5 mm depth, and are then absent for the next 31.5 mm (to 88 mm depth) of axis 1. Mud lobes are also present for the lowermost 71.8 mm (to 159.8 mm depth)(Figure 24).

The means of the $\delta^{18}O$ and $\delta^{13}C$ values and white light gray scales of the axis1 and axis 2 are not equal, with 99.98% confidence using a two-tailed t-test, indicating different depositional conditions, such as different residence times for source water in the epikarst (Table 6). Measurements were taken from portions of the two axes that were presumed to have grown contemporaneously. The gray scale measurements were both 45 mm long in both axes. The t-tests allowed us to reject the null hypothesis that the two axes had the same gray scale values with greater than 99.998% confidence, and greater than 99.99% that the $\delta^{18}O$ and $\delta^{13}C$ values were not from the same population. This evidence, coupled with visual evidence of a former drip located above axis 2 in close proximity to the original soda straw feeding axis 1 from field-site pictures, and visual inspection of the contacts of the calcite from axis 1 and axis 2, led to the conclusion that the growth axes were from 2 different drip sources.

Figure 24. High-resolution scan of CH-1 in polished cross-section, showing the differences in stratigraphy. Sections labeled A are sections without mud lobes, and sections labeled B have mud lobes of varying sizes. C is axis 1, and D is axis 2.

	White light gray scale		$\delta^{18}O$ values		$\delta^{13}C$ values	
	Axis 1	Axis 2	Axis 1	Axis 2	Axis 1	Axis 2
Mean	198.13	213.98	-3.17	-3.70	-5.21	-7.02
Std Dev	19.959	13.319	0.810	0.883	0.478	1.495
n	1033	1033	46	33	46	33
Se	0.747		0.192		0.235	
Sp	16.967		0.841		1.031	
t	-21.243		2.730		7.666	
H_0: Mean of Axis 1 = Mean of Axis 2 H_1: Mean of Axis 1 ≠ Mean of Axis 2 α = 0.002			α = 0.01			
Critical value for a two-tailed t-test with v = ∞ at 0.002 significance level	3.0902		Critical value for a two-tailed t-test with v = 77 at 0.01 significance level	2.6387		

Table 6. Results from the comparison of the means of gray scale value in white light and $\delta^{18}O$ and $\delta^{13}C$ values from sections of axis 1 of CH-1 and axis 2.

c. *Stable Isotope Results*

i. *Hendy tests*

The Hendy test assumes that each sample collected was deposited simultaneously. Given the low growth rate of CH-1, sampling from the same layer was very difficult, if not impossible, therefore any failures of the Hendy test should be viewed with skepticism (Dorale and Liu, 2009). However, if the sample passes a Hendy test despite this violation of assumptions, we can infer that the stalagmite was indeed deposited in isotopic equilibrium. The locations of the three Hendy tests can be seen in (Figure 17). The second Hendy test, labeled Hendy 2, was discarded because the analysis was bad in three samples due to equipment malfunction, leaving only four good data points.

'Hendy 1' had $\delta^{18}O$ values increasing towards the edges of CH-1, correlating with weak enrichment of both $\delta^{18}O$ and $\delta^{13}C$ values (Figure 25, a & b). 'Hendy 3' displays a

'hump' of higher $\delta^{18}O$ between 5 and 10 mm from the apex, and a large positive spike of $\delta^{18}O$ values at the extreme edges of CH-1 (Figure 25, c). However, as can be seen in Figure 8, these anomalies in Hendy 3 are likely the result of the mud lobe/pooled geometry of the stratigraphic offsets. The $\delta^{18}O$ and $\delta^{13}C$ values are less correlated than in 'Hendy 1' (Figure 25, c & d). . Hendy 1a shows an increase of in $\delta^{18}O$ values of 0.388 ‰/cm from the apex, with an r^2 value of 0.736, which is within the bounds set for the Hendy test. Hendy 1b shows a relation of enrichment of both $\delta^{18}O$ and $\delta^{13}C$ values but does not surpass the threshold required to fail the Hendy test. Hendy 2c came from the layer with a pooled geometry, and the bumps in the curve occur at the beginning of mud mounds creating the pool. Hendy 2d appears to have correlating enrichment of $\delta^{18}O$ and $\delta^{13}C$ values, however the r^2 value of 0.2991 shows that it is not a strong correlation. Neither line had increases in $\delta^{18}O$ values greater than the 0.8‰ cut off to fail the test, therefore it was concluded that neither test provided evidence of kinetic fractionation effects in the $\delta^{18}O$ and $\delta^{13}C$ values in the calcite for the upper ~2.5 cm of CH-1.

ii. *Paleoclimate analysis*

$\delta^{18}O$ and $\delta^{13}C$ values are reported from two datasets, a high-resolution continuous micromilled record (0.02 mm or 0.5 year per sample) and a discrete drilled low-resolution record (1 mm or roughly 12.5 years per sample). A summary of the two datasets can be found in Table 7. The low-resolution dataset shows a good level of co-variation between the $\delta^{18}O$ and $\delta^{13}C$ values, consistent with observations from other

speleothems. Wetter conditions generally lead to lower $\delta^{18}O$ values due to the "amount effect."

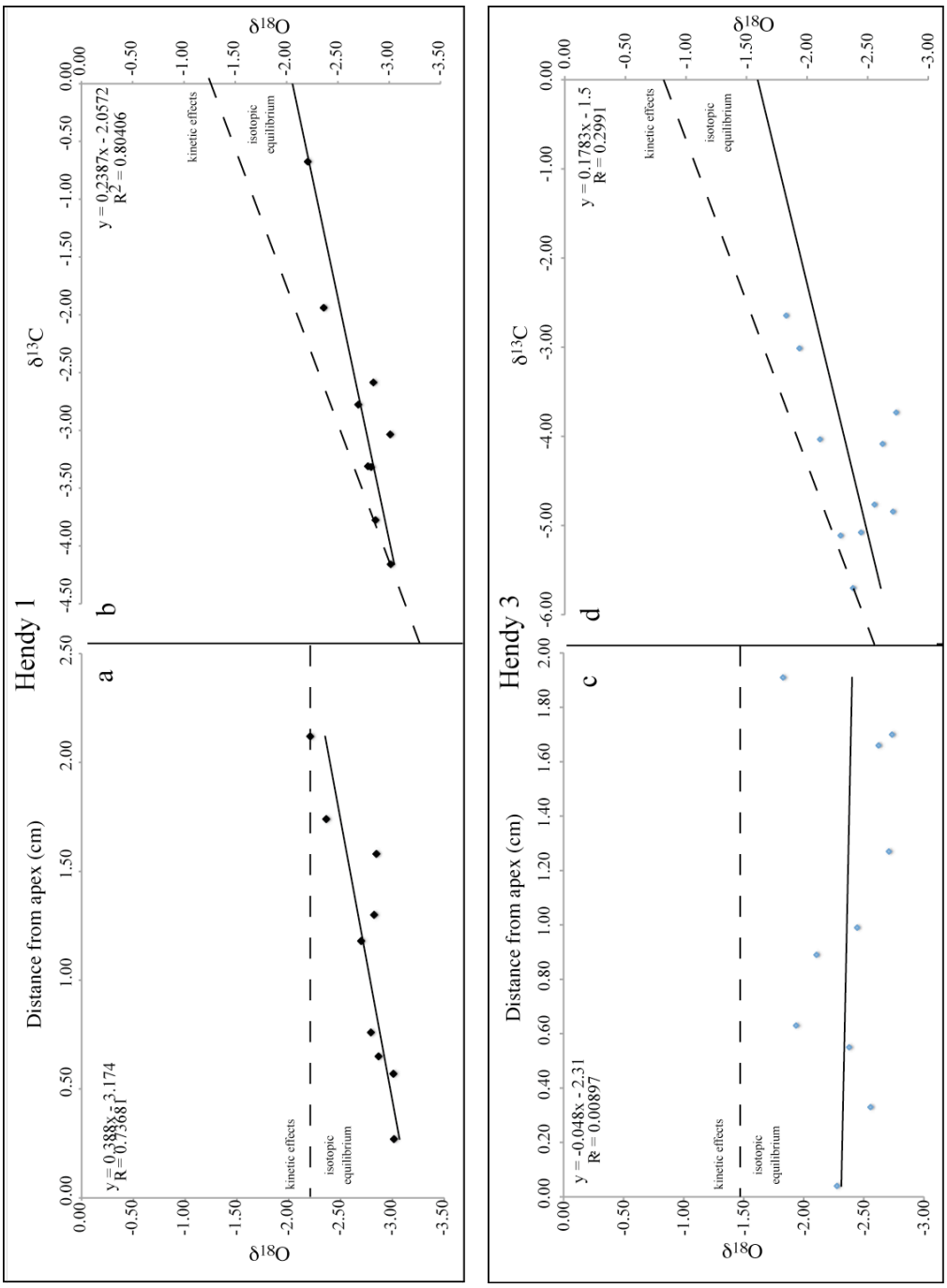

Figure 25. Hendy Test results for two layers at the top of CH-1. CH-1 passes the Hendy test on both of these lines.

	Low-res		High-res	
	$\delta^{13}C$	$\delta^{18}O$	$\delta^{13}C$	$\delta^{18}O$
Mean	-5.47	-3.19	-4.3	-2.8
Std dev	1.02	0.79	0.77	0.048
Max	-2.66	-1.41	-2.63	-1.17
Min	-9.11	-6.32	-6.09	-4.51
Covariance, C and O	0.449		0.142	
n	153		700	
Time covered	134 BC to 1976 AD		1640 to 2007	

Table 7. Summary of the two $\delta^{18}O$ and $\delta^{13}C$ value datasets in CH-1. Low-res dataset ends on the data point centered on 1976 due to the low sampling frequency; the top sample was collected 1.18 mm from the top of CH-1.

Wetter conditions also lead lower $\delta^{13}C$ values by increasing the ratio of C3 to C4 plants on the surface or increasing soil pCO^2 levels (Sharp, 2007). Photosynthesis in plants causes carbon isotope fractionation. Three different photosynthetic pathways are common in plants. The C3 pathway is common in plants from temperate zones that thrive with high atmospheric CO_2 levels. The C4 and CAM plants are generally from more arid environments. An example of a C3 plant is most trees, a C4 plant is maize, and most succulents are CAM plants. There is a 13‰ difference in $\delta^{13}C$ values from C3 and C4 plants, with C3 plants generally around -26‰ vs. PDB and C4 plants around -13‰ vs. PDB. CAM plants have similar $\delta^{13}C$ values to C4 (Sharp, 2007). Higher $\delta^{18}O$ values are due to either drier conditions or higher rates of evaporation, which can in turn cause the vegetation to shift more towards C4 and CAM plant resulting in higher $\delta^{13}C$ values in soils and therefore stalagmites (Sharp, 2007).

The trend of the low-resolution stable isotope record is increasing overall for both $\delta^{18}O$ and $\delta^{13}C$ values, but between the years of 134 BC until 1222 AD, the slope on the trend line for the $\delta^{18}O$ values has a slope of 0.0004 rising from -3.5708‰ to -3.0284‰, for an increase of 0.5424‰. From 1222 to 1976, the trend line has a slope of 0.0017, rising from -3.5642‰ to -2.2825‰, for a rise of 1.2818‰, indicating acceleration of a long-term drying period in the region (Figure 26).

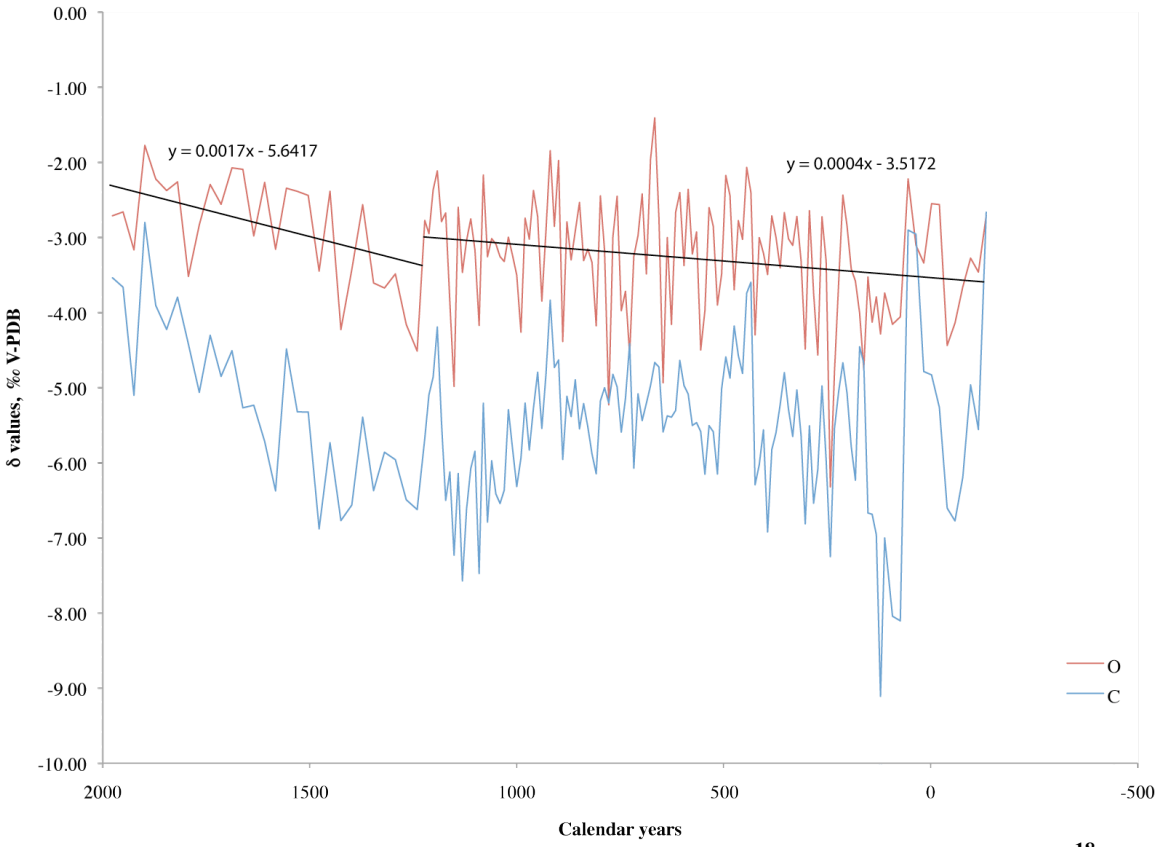

Figure 26. Time series showing the general co-variation of the low-resolution $\delta^{18}O$ and $\delta^{13}C$ values.

The entire CH-1 low-resolution stable isotope record is characterized by highs and lows in rapid succession. Given Northern Yucatán's historical susceptibility to

droughts, it stands to reason that these peaks in $\delta^{18}O$ values are likely indicative of droughts. From 134 BC to 1976 AD, there are about 27 peaks, which may have been decadal periods characterized by drought. The highest $\delta^{18}O$ value from the record comes from the year 666, and is 1.78‰ higher than the mean (Figure 26).

Comparison of the local precipitation weather data from 1961 to the high-resolution $\delta^{18}O$ and $\delta^{13}C$ values reveals an interesting trend (Figure 27). Precipitation is increasing at a rate of 0.85 mm/yr, while $\delta^{18}O$ values are increasing at a rate of 0.0091 ‰/yr, contradictory to what a simplistic application of the "amount effect" would predict for a period of increased rainfall (Figure 27). Possible explanations for this pattern will be addressed in the discussion section.

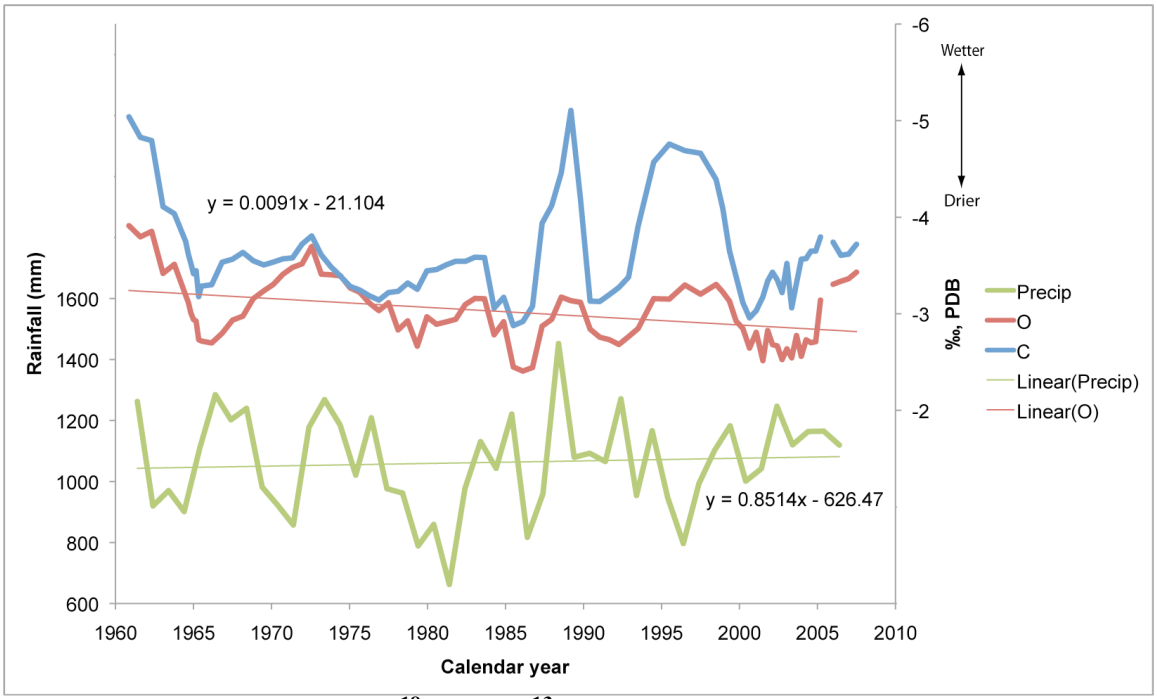

Figure 27. High-resolution $\delta^{18}O$ and $\delta^{13}C$ values in CH-1 compared to precipitation data showing surprising trends. Linear trends are shown for precipitation and $\delta^{18}O$ values.

An interesting feature appears in the CH-1 high-resolution $\delta^{13}C$ values beginning in 1915, and continuing through 2007. A very large and rapid drop in $\delta^{13}C$ values by ~2.7‰ occurs over 10 years, followed by a small recovery, and a subsequent drop to the lowest point in the high-resolution record of -6.05‰ in the year 1929 (Figure 28). The $\delta^{13}C$ values slowly recover to near the mean value followed by sudden drops at least three more times before 2007, although none of the subsequent drops in $\delta^{13}C$ values endure as long or are as extreme as the first drop. The variability in $\delta^{13}C$ values after 1915 is significantly higher, 0.79, than the rest of the record, 0.41.

iii. *Analysis of local weather data*

The local weather data revealed an increase in annual rainfall and water budget, and a decrease in monthly average temperature over the time period from the early 1960s to 2006 (Figure 29). All four weather stations analyzed show the same basic trends. The increase in rainfall was minimal, 0.85 mm/yr, but the water budget increase was 7.9 mm/yr due mainly to the lower temperatures reducing evaporation in the region.

The ENSO system, as measured by the Southern Oscillation Index (SOI), was compared to the $\delta^{13}C$ and $\delta^{18}O$ values from 1900-2007 to look for a poorly understood climate teleconnection found in stalagmite ATM-7 from Belize by Frappier et al. (Frappier et al., 2002a). Belize does not display any significant monthly weather anomalies related to El Niño, so it is puzzling that the $\delta^{13}C$ and $\delta^{18}O$ values would record these events. Evidence of the ENSO teleconnection was present in the $\delta^{13}C$ values of

CH-1 as well (Figure 30). However, ENSO may influence weather patterns in the Yucatán by making the wet season drier than normal (Giannini et al., 2000).

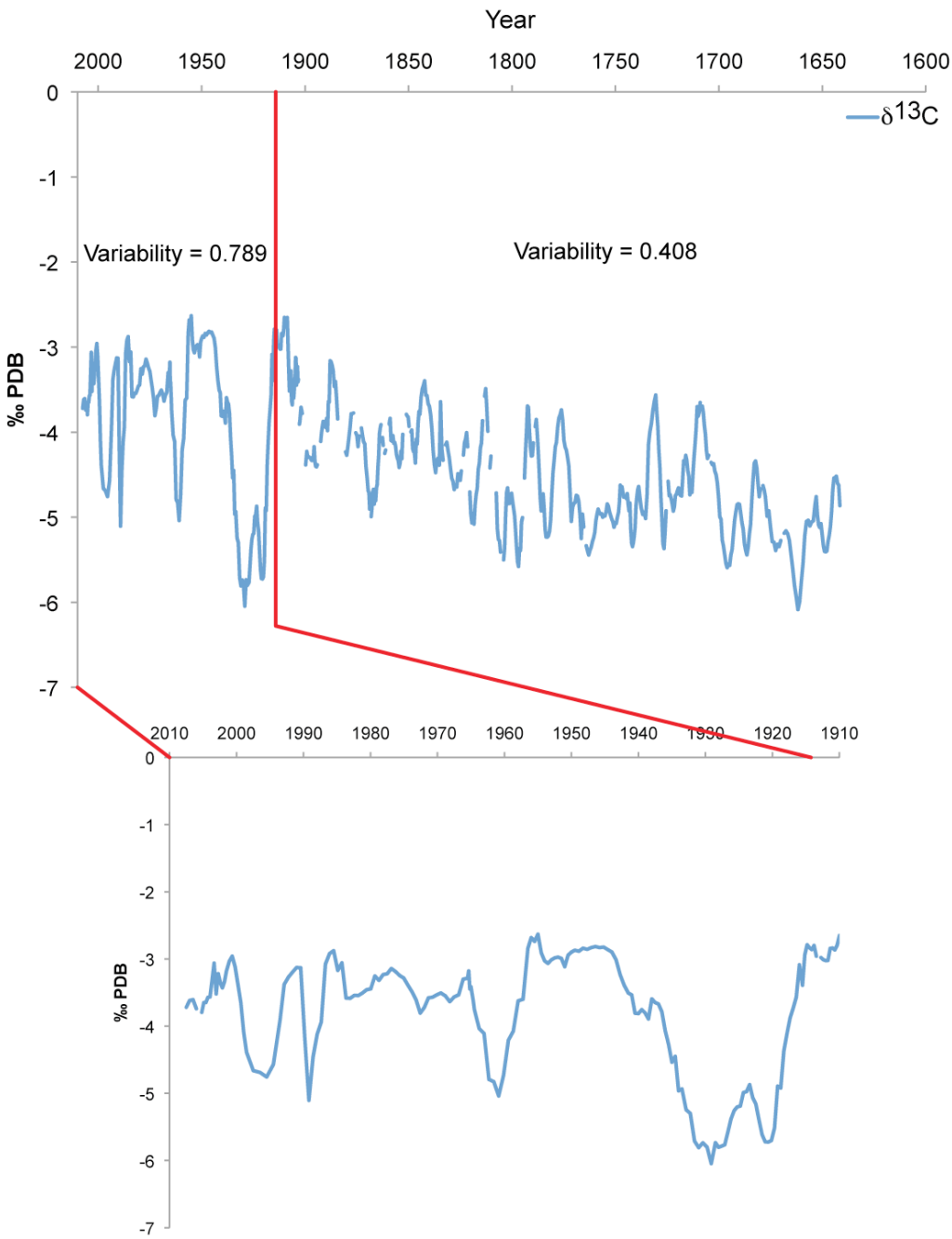

Figure 28. CH-1 high-resolution stable isotope record from 1639 to 2007. Note the increase in variability and shifts in $\delta^{13}C$ values extremes beginning in 1915.

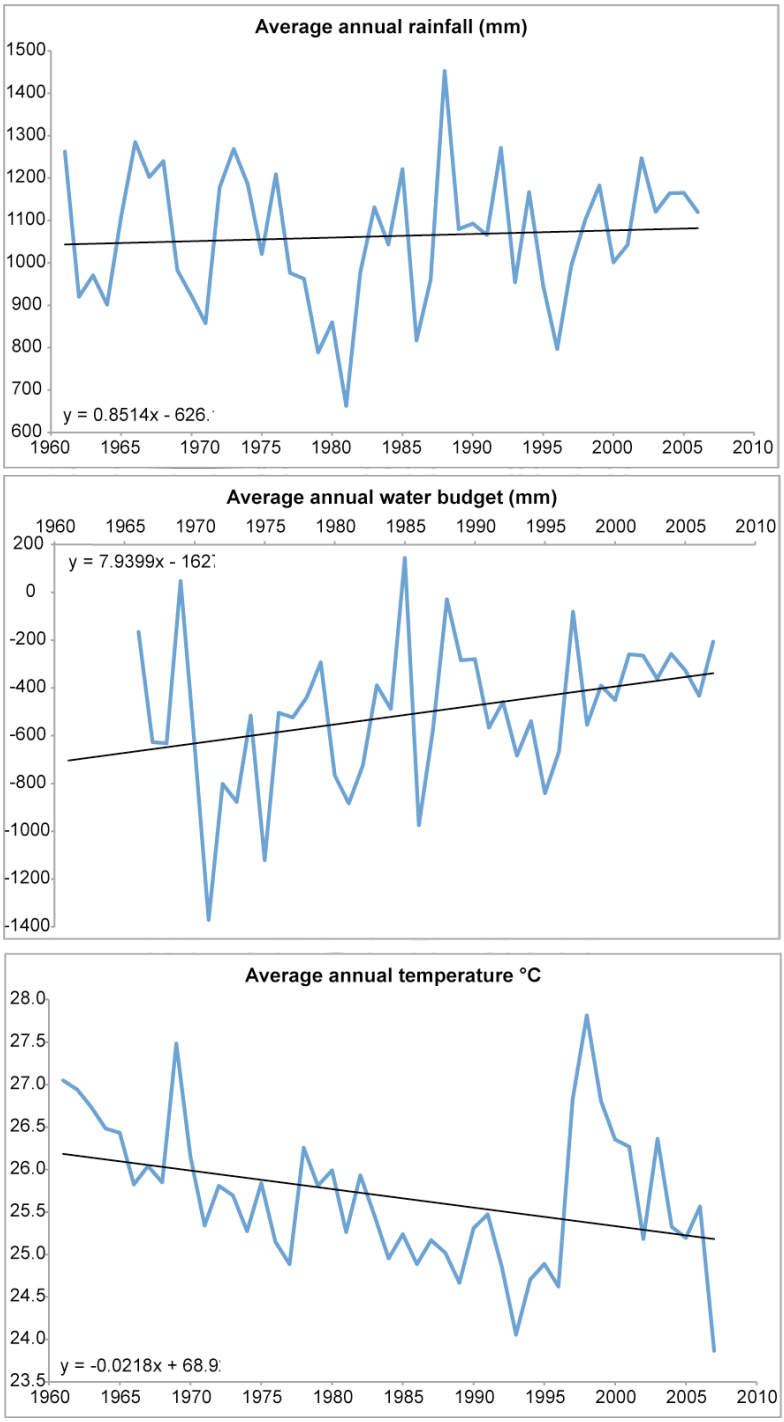

Figure 29. Trends in annual weather data averaged from four meteorological stations surrounding Cenote Chaltun-Ha.

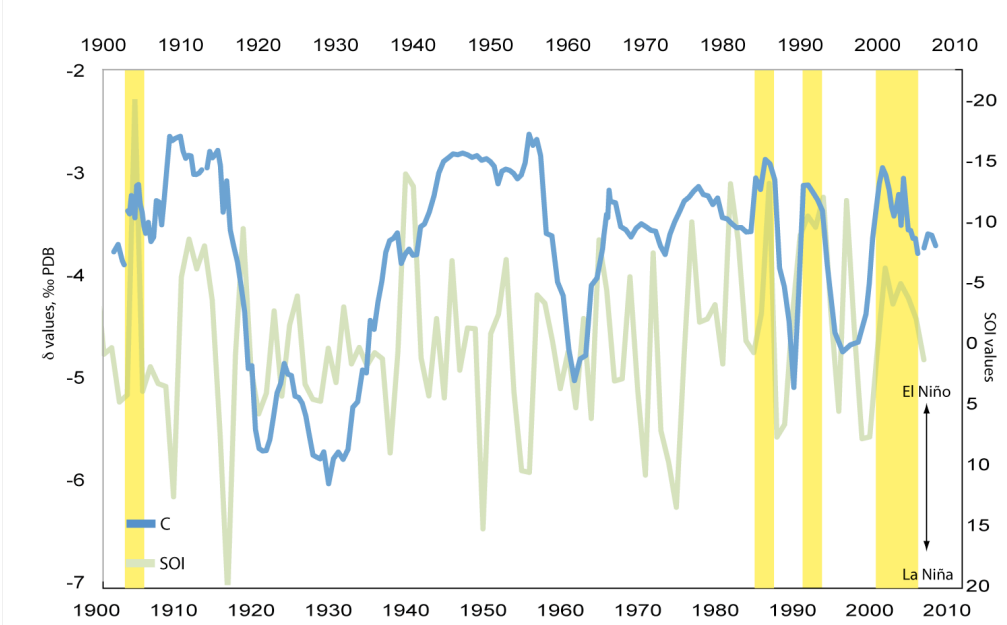

Figure 30. Yearly averaged SOI data plotted offset against the $\delta^{13}C$ values from CH-1. Yellow bars highlight areas of good agreement. The SOI record was offset 1 year, consistent with a proposed lag in response to ENSO in the Caribbean by Giannini et al. (2000) and observations from ATM-7 by Frappier et al. (2002a).

d. *Historical TC record*

i. *Historical TC analysis*

From 1852 to 2006, the Best Track Dataset shows 195 TCs whose eye passed within 370 km of Cenote Chaltun-Ha, for an average of 1.3 TCs/yr (NOAA, 2009). A TC was defined to have an intensity ranging from tropical depression (TD) up through category 5 hurricanes. An additional 5 TCs from Spanish documentary sources are assumed to have crossed the Yucatán peninsula due to the landfalls reported in Garcia-

Herrera, et al. (Garcia-Herrera et al., 2005) between the years of 1628 to 1751, for a total of 200 recorded TCs during the time period of the deposition of the top 30 mm of CH-1. There were 44 years within the Best Track dataset without a TC. The longest duration without a TC is 3 years. The longest duration between hurricanes (Cat 1-5) was 11 years, and the longest duration between major Hurricanes (Cat 3-5) was 20 years. The distribution of storm intensity can be seen in Figure 31.

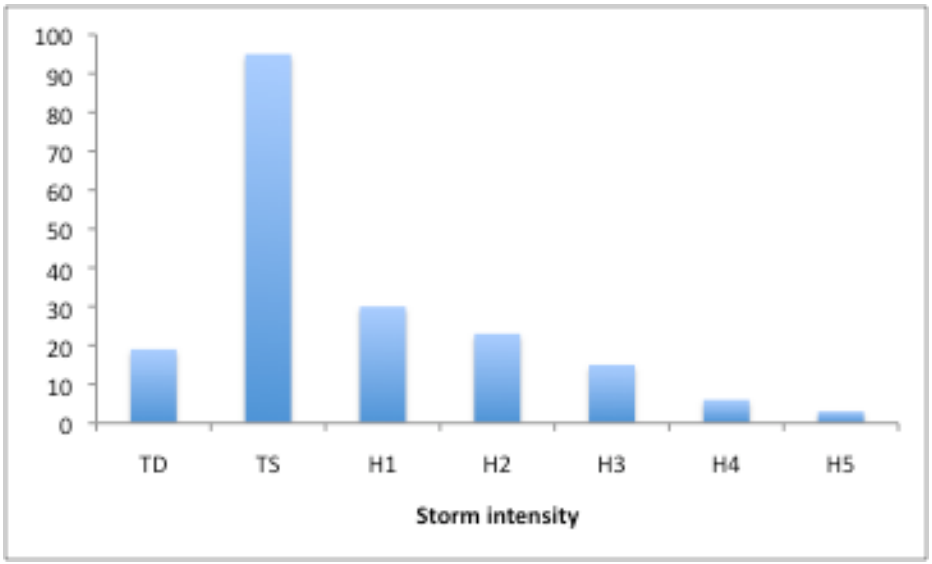

Figure 31. Histogram of storm intensity.

The strongest TC recorded was hurricane Allen in 1980, with a recorded wind speed of 165 knots. Allen was one of 3 category 5 hurricanes to strike the region. TCs with wind speeds as low as 25 knots also struck the region over this time. The closest storm track took tropical depression Laurie directly over Cenote Chaltun-Ha in 1969, while many storm tracks passed around 370 km from the cave site. A histogram of storms per month can be seen in Figure 32.

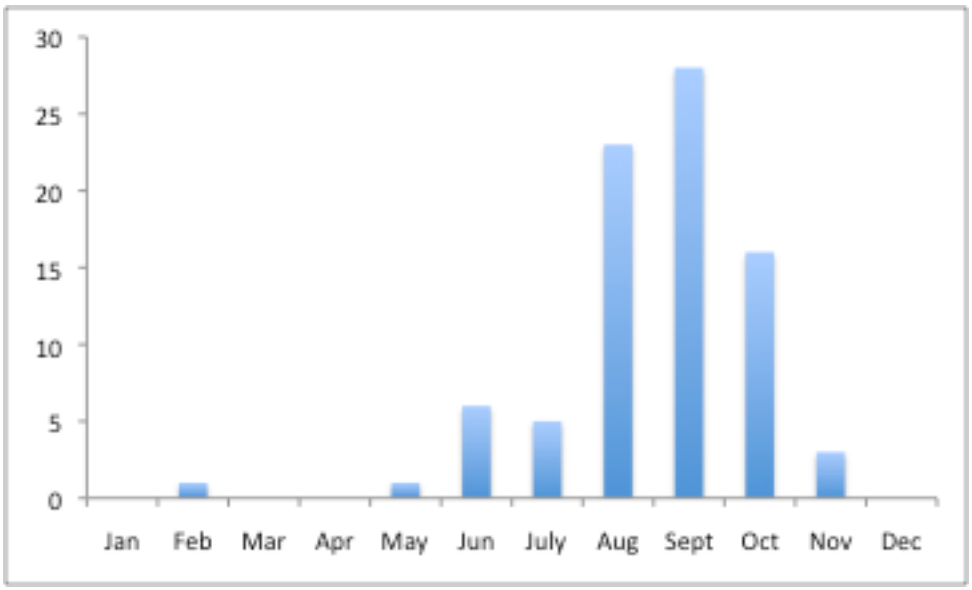

Figure 32. Histogram of TCs per month within 370 km of Cenote Chaltun-Ha, from 1852 to 2006.

e. *Mud layer stratigraphy*

A summary of the historical TCs recorded and their intensities, applicable mud layer thicknesses, and distances from Chaltun-Ha can be seen in Table 8. A total of 265 mud layers were observed within the main growth axis of CH-1. Of these, 19 occurred during the historical TC record (post 1852), all of which occurred in years with at least one TC, within the age-model error. Of the 111 years with at least one TC, 19 were recorded by mud layers, identifying 17% of the total years with TCs during this period. This left 92 years with at least one TC un-recorded by the mud layer proxy. The average distance from Cenote Chaltun-Ha to the closest point of the best track data for the 18 TCs that were recorded by mud layers was 188 km. The closest storm recorded passed directly over Cenote Chaltun-Ha, and the farthest storm that could be certain was being recorded (not concurrent with another closer storm in the same year) passed 331 km away

from the cave site. Though 7 of the 18 mud layers occurred in years with only one TC, the average number of TCs per year with a mud layer was 2.1.

year of mud layer	# of tcs same year	Name	Intensity	Distance (km)	Mud layer thickness (mm)
2005	4	Cindy	TD	45	
		Emily	H5	31	
		Stan	TS	67	
		Wilma	H5	197	
2001	1	Chantal	TS	262	0.03
1998	1	Mitch	TS	19	
1993	2	Gert	TS	238	
		Arlene	TD	312	
1969	1	Laurie	TD	0, 298	
1965	2	Debbie	TD	125	0.07
		N/A	TD	211	
1964	3	Hilda	H2	269	
		N/A	TD	314	
		N/A	TD	264	
1956	3	Dora	TS	225	
		Flossy	TD	26	
		N/A	TD	280	
1949	2	N/A	TS	301	
		N/A	TS	281	
1940	1	N/A	TS	147	0.05
1933	5	N/A	H2	16	
		N/A	TS	84	
		N/A	TS	89	
		N/A	TS	140	
		N/A	TS	224	
1928	1	N/A	TS	109	
1915	2	N/A	H3	302	0.1
		N/A	H4	331	
1905	2	N/A	TS	2	0.11
		N/A	TS	204	
1902	1	N/A	H2	186	
1894	2	N/A	H5	329	
		N/A	TS	310	
1887	4	N/A	TS	131	
		N/A	H2	153	
	0	N/A	H2	195	
		N/A	H2	286	
1868	1	N/A	H2	337	0.07
Average	2.0		ts (mode)	166	

Table 8. Summary of mud layers and the associated meteorological TC record.

Based on the high success rate of the mud layers indicating TCs in the historical record, analysis on the remaining mud layers in CH-1 was done assuming that each mud layer records a year with at least one TC that produced rainfall in the Yucatán. The mud layers were divided into centuries, and a histogram was plotted to analyze centennial trends in TC frequency, or at least frequency of TCs producing sufficient rains to flood and deposit mud layers. From the first century BC to the 12th century AD, there was an average of 14.7 mud layers per century. From the 13th century to the 20th century, there was an average of 7.1 mud layers (Figure 33). This sharp drop-off actually started in the mid-13th century. In the first 33 years of the 13th century there were 4 mud layers deposited (on par with the prevailing TC frequency), but during the remaining 67 years only 3 mud layers were deposited.

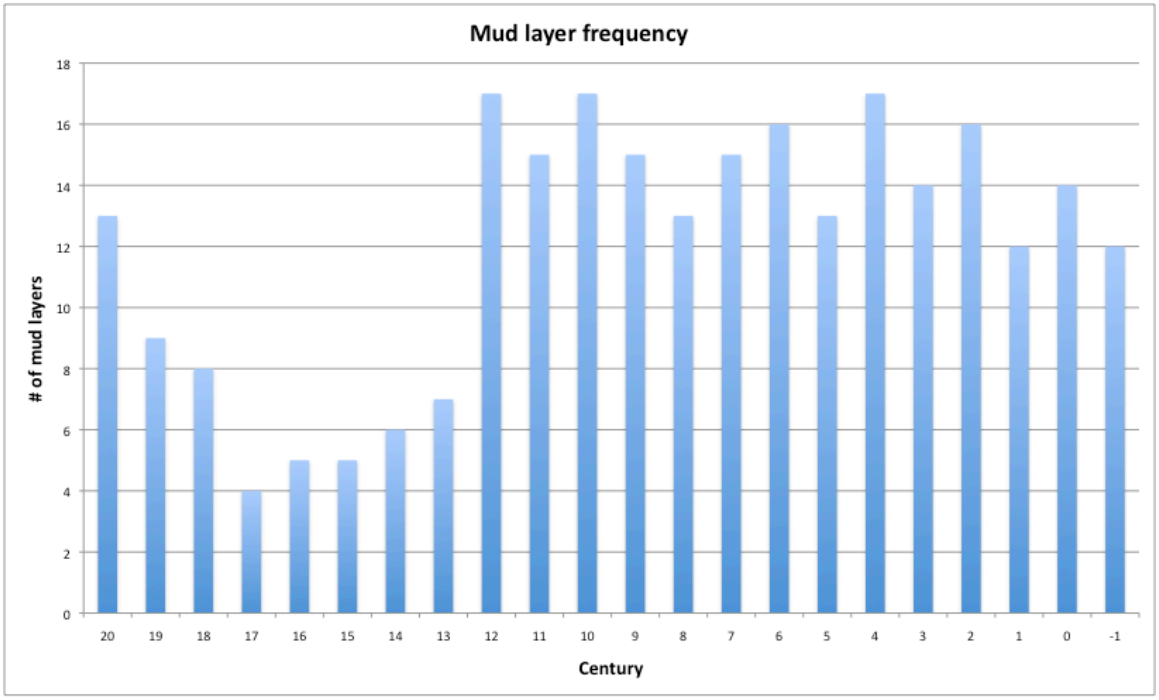

Figure 33. Histogram of CH-1mud layers by century.

The low frequency of mud layer deposition continued through the 17th century, followed by a positive trend in centennial mud layer frequency that began with the historical era, and continued through the present. There is a slight positive trend in the centennial mud layer frequency from 198 BC to 1200 AD of about 0.23 mud layers/century before the sharp drop in the 13th century. A summary of frequencies of years/mud layer can be seen in Table 9.

Time period	198 BC to 1233 AD	1234-1900	1901-2006
Mud layers	210	40	15
years	1431	666	105
mud/10 years	0.15	0.06	0.14

Table 9. Three periods of different centennial frequency of CH-1 mud layers, highlighting the 666 years with fewer mud layers deposited between 1234 and 1900.

5. Discussion

a. *Comparison to Previous work*

i. *TC identification probability function*

Frappier et al. (2007) present a 23 year stalagmite TC record from Belize that pioneered the method for cyclogenic $\delta^{18}O$ anomaly identification used in this study. A binary logistic regression probability function (1) correctly identified 8 of 10 TCs during the time, and incorrectly identified one low $\delta^{18}O$ excursion in the ATM-7 dataset of

nearly 1200 samples ($\delta^{18}O_d$ is defined as the difference of $\delta^{18}O$ values between adjacent samples).

$$\text{probability} = 0.51 * \delta^{13}C + 1.85 * \delta^{18}O - 11.01 * \delta^{18}O_d - 12.86 \quad (1)$$

Probabilitys greater than 0.05 were considered excursions recording TCs.

One question that remained from the work of Frappier et al. was of the reproducibility of the probability function. If the function could be shown to work repeatedly on multiple stalagmites from different regions, this would allow future workers to microsample a stalagmite during the time interval interesting to the study. If the model were not universally applicable, or at least applicable to stalagmites from the Caribbean or some other sub-region, researchers would have to calibrate the model with respect to the historical record each time a study following this method began on a new stalagmite, limiting the usefulness of this paleotempestology tool.

Applying the TC probability function from ATM-7 (1) to the high-resolution CH-1 stable isotope record only resulted in two instances of positive probabilities in the first 150 years of record, during which there were at least 195 historical TCs and 111 years with 1 or more TC events. The two data points with positive probabilities were from adjacent measurements from 1988, a year with 4 TC strikes on the Yucatán. This suggests that TC rainfall can in some extreme instances be identified in stalagmite records using storm excursion models developed for a different stalagmite, but without reliability. There are a few reasons that the ATM-7 model might be inappropriate for the

CH-1 dataset, including a lower growth rate to sample ratio and the difference in residence times for cyclogenic waters in different locations. However, given that the probability function from ATM-7 (1) missed ~190 TCs, a new probability function for identifying cyclogenic low $\delta^{18}O$ excursions was developed for CH-1 (2).

The function applied to CH-1 was:

$$\text{probability} = 1.887 * \delta^{13}C - 1.498 * \delta^{18}O + 1.077 * \delta^{18}O_d - 1.558 \quad (2)$$

This probability function was developed in the same way as (1). It was unable to predict any TCs in CH-1's high-resolution dataset, even those coded as storms. A potential reason for the lack of success for this method in CH-1 is the slow growth rate. Stalagmite ATM7 had a growth rate of ~1.1 mm/yr, allowing for weekly to monthly resolution of $\delta^{18}O$ and $\delta^{13}C$ calcite values (Frappier et al., 2007). If we assume a stable 1.1 mm/yr growth rate for an entire year, and a 3-9 month residence time of the $\delta^{18}O$ value anomaly, as reported in Frappier et al. (2002a; Frappier et al., 2008), there should be between 0.275 and 0.825 mm of calcite thickness deposited from cyclogenic water, easily resolvable at the 0.02 mm micro sampling interval used on ATM7, providing a high signal-to-noise ratio.

CH-1 had a growth rate of ~0.04 mm/yr for the time period of historical TC records. If I make the assumptions of stable 0.04 mm/yr growth rate, and a 3 week residence time for the cyclogenic water, the calcite containing the anomaly should be ~0.0023 mm thick, an order of magnitude below the 0.02 mm sampling rate used in CH-

1, providing a very low signal-to-noise ratio. Each high-resolution calcite sample represents the average of 6 months of $\delta^{18}O$ and $\delta^{13}C$ values. Some cyclogenic water may suppress the $\delta^{18}O$ value of drip water in Chaltun-Ha (Frappier, 2008b), but the inability to sample at a high enough resolution suggests that identifying individual storm events from the background isotopic variability is not expected to be possible.

However, there is reason to doubt that the main pulse of isotopically anomalous TC water feeding the drip for CH-1 could have a residence time exceeding 3 weeks in the epikarst, or could even drip onto CH-1. The epikarst above CH-1 is estimated to be 5.8 m thick, with only 0.2 m of soil, meaning that most water falling on the surface probably infiltrates into Cenote Chaltun-Ha quickly, reducing the likelihood that a $\delta^{18}O$ value anomaly would be detectable in calcite (Ayalon et al., 1998; Tooth and Fairchild, 2003).

Based on what Escolero et al. (2007) termed the 'piston' effect, whereby nearby groundwater levels rose and fell regularly for nearly a month in two wells after Hurricane Isidore in 2002, it may not even have been possible for calcite to resume deposition on CH-1 after a flood event for up to a month. Escolero et al. reported data from two wells near Merida (Figure 34). The water tables dropped at an average rate of 10.7 mm/day in one well, and 32.7 mm/day in the other well during the 41 days that followed Hurricane Isidore. This same response may be expected in general in the water table of a diffuse type of karst system like the Yucatán (Fiorillo, 2009). If CH-1 was still submerged after a TC, the cyclogenic drip water may fall into the flood, and never deposit the $\delta^{18}O$ value anomaly. If the water table did oscillate after a TC at Chaltun-Ha, mud from the original flooding event, as well as any calcite that may have been deposited from the drip during a

brief dry period, may be washed away. The final recession of water should deposit a mud layer recording the event, however the cyclogenic water responsible for depositing a negative $\delta^{18}O$ value anomaly would not likely deposit a measurable amount of calcite.

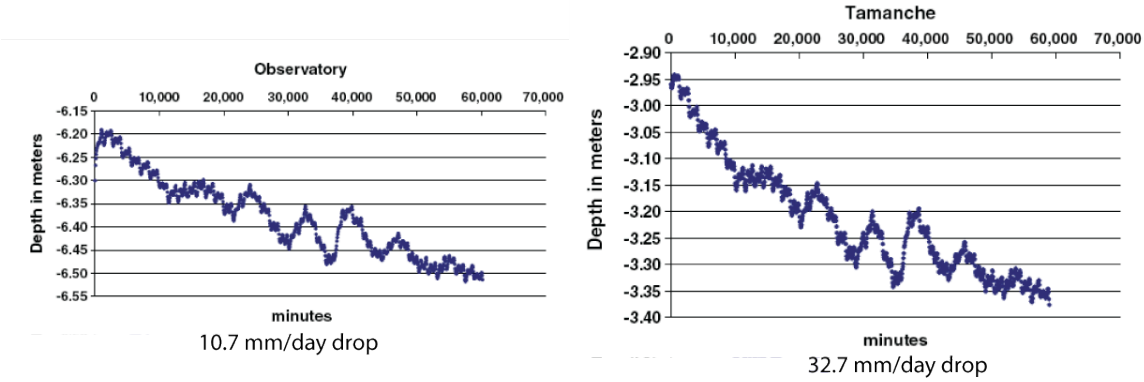

Figure 34. Data from two wells from Escolero et al. (2007) demonstrating the 'piston' effect of the ground water table in response to rapid recharge. The large peaks in groundwater elevation arrive at a frequency of 5 days.

If the rate at which the water table fell in Chaltun-Ha were assumed to be an average of the two wells measured, roughly 20 mm/day, a flood of 1 m above CH-1 would take 5 days to subside to the point that the top of the stalagmite was exposed to new drips and continued calcite growth. Chaltun-Ha has flooded to the opening of the cave from TCs based on personal accounts of locals. This means that CH-1 may have been submerged up to 3 or 4 m deep, requiring up to 20 days to recede below the level of CH-1 based on results from Escolero et al. (2007). This upper estimate seems a bit high, but even if CH-1 were covered for 5 days, this would likely prevent at least some cyclogenic calcite deposition and reduce the signal-to-noise ratio for the stable isotope proxy even further. If a storm were to have flooded Chaltun-Ha only high enough to deposit a mud layer on CH-1 before the waters receded, CH-1 is more likely to have

calcite deposition from cyclogenic water that may be detectable at the ~semi-annual sampling rate achieved in the high-resolution record presented here.

For these reasons I believe that the $\delta^{18}O$ value anomaly proxy is not successful for CH-1, and possibly would not be useful in other caves that flood. Future work may include an exercise to develop a probability function using more or different predictor values or another method of $\delta^{18}O$ value analysis altogether. However, it is likely that only even more detailed stable isotope sampling, for example via ion microprobe (Orland et al., 2009), could answer directly the question of whether the lack of a reliable stable isotope TC proxy in CH-1 is due primarily to depositional process or the low semi-annual sampling rate achieved in this study. In the future, the stable isotope TC proxy may be useful in stalagmites from caves that flood when the growth rate is very high, and/or when the cyclogenic water's residence time is longer, and/or when the flooding event is short-lived.

ii. *Paleotempestology of the Caribbean*

Other paleotempestology work done in the Caribbean and Gulf of Mexico use overwash deposits in coastal lakes as proxies for TC strikes. The records of Donnelly and Woodruff (2007), Liu and Fearn (2000) and Liu (2007) overlap the TC record from CH-1. Donnelly and Woodruff's study was from Puerto Rico and spans from 6000 yr BP. Liu and Fearn's study was from the panhandle of Florida, and covers 7000 yr BP, and Liu's study is a broader overview of paleotempestology.

Assumptions for this type of work include a relatively stable sea level, that the deposits are from oceanic sources, and not from fluvial sources, and that the barrier between the ocean and the lake has remained intact (Nott, 2003). Intensity of the TC responsible for modern overwash deposits is possible to calculate based on the height of the overwashed barrier (Woodruff et al., 2008), but the assumption that the barrier has remained the same altitude over time must be made, or a paleo-altitude study must be done (Nott, 2003).

Donnelly and Woodruff (2007) present a record of TC frequency variability on the millennial scale. The authors identify 4 periods ranging from ~ 100 years to over a thousand years of relative quiescence in TC strikes in Puerto Rico. Of these, two occur prior to CH-1's record. The other two occur from 1000 yr BP through ~250 yr BP (Figure 35). However, only one large sand layer interrupts this 750-year long period of TC quiescence. Puerto Rico then shows an increase in major TC strikes toward the present.

Liu and Fearn (2000) report a record of TC frequency similar to Donnelly and Woodruff's. Sand layer frequency in Western Lake, FL is fairly regular from ~3500 until ~1500 ^{14}C yr BP, with 11 sand layers during this time. There is only one sand layer after this interval, indicating a strong local storm strike ~450 ^{14}C yr BP (Figure 36).

Liu (2007) reports periods of 'hyperactivity' (3800-1000 ybp) and relative quiescence (5000-3800, 1000-0 ybp) of strong (category 3-5) TCs in the Caribbean basin. Liu suggests a possible mechanism for the variability in strong TCs is a southwest shift in

the Bermuda High, a persistent region of high pressure currently centered over Bermuda, channeling TCs toward the Gulf of Mexico (Liu, 2007).

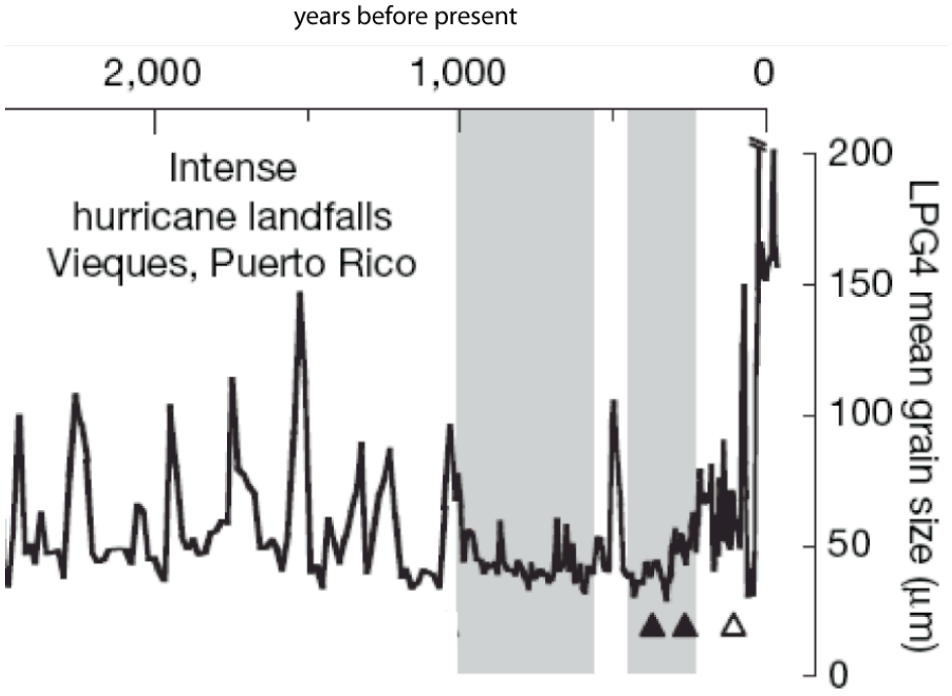

Figure 35. Modified from Donnelly and Woodruff (2007) showing grain size from Laguna Playa Grande, Vieques, Puerto Rico during the time of growth of CH-1. Large grains indicate TC overwash of clastic beach material into the lagoon. The authors highlight times with little TC activity in gray.

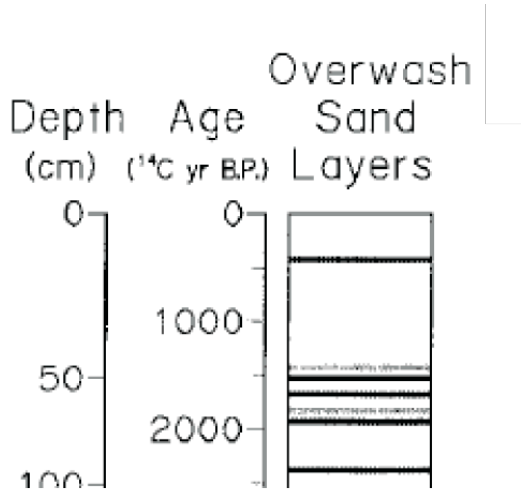

Figure 36. Modified from Liu and Fearn (2000) showing the same time scale as Figure 35 from Donnelly and Woodruff (2007). Both of these records show a similar period of low TC frequency after ~1000 ybp.

A pattern similar to that observed at Vieques is detected in CH-1's mud layers – namely high TC frequency from the mid 1700s through the present and low TC frequency during the 13th – 17th centuries (Figure 37). CH-1 is also in agreement with the Western Lake record, showing a period of high TC activity from ~2000 – 1400 ybp.

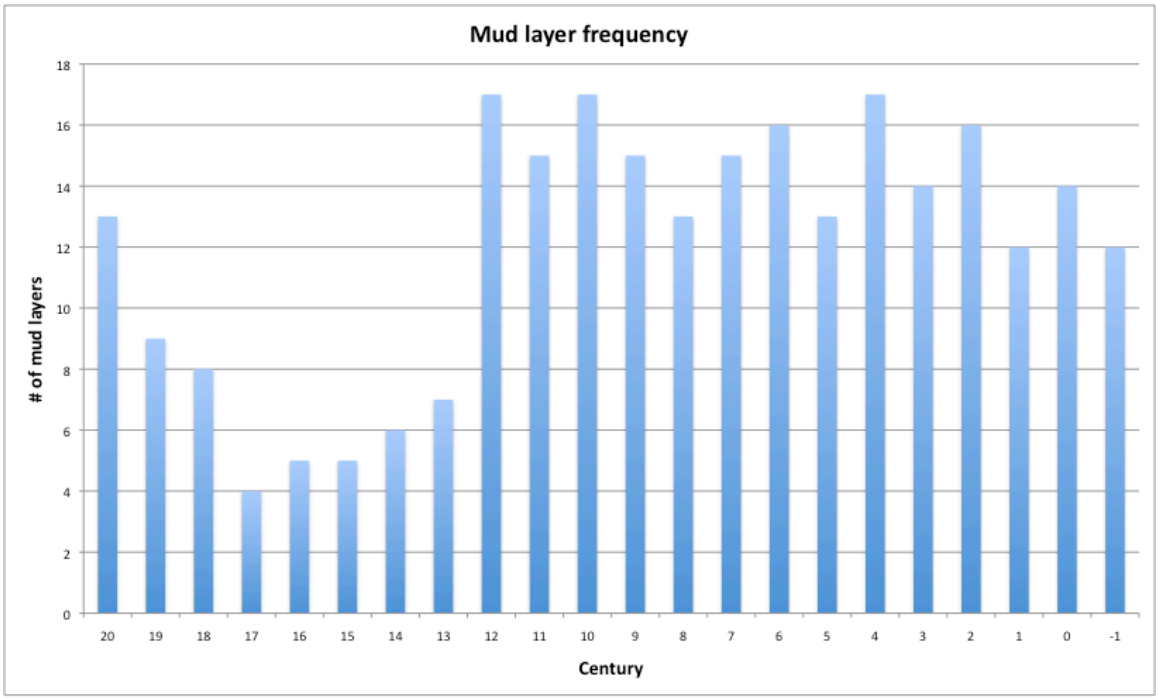

Figure 37. Mud layer frequency in CH-1 displaying a drop in TC activity in the Yucatán at around the same time as Donnelly and Woodruff, and Liu and Fearn.

One advantage to the mud-layer proxy record presented from CH-1 is resolution; assuming that each mud layer represents a year with at least one TC, a record of at least 265 individual TCs over ~2,000 years has been resolved in CH-1. The overwash method as reported by Liu and Fearn has resolved 12 sand deposits, presumably from TCs, over a

~3,500 year period. Donnelly and Woodruff present a record of ~20 sand deposits over ~5,500 years. All three records show the same trend in TC frequency, but the sensitivity of CH-1 is obviously higher, providing useful TC frequency information during the 13th to 20th centuries. Both proxy techniques generally cannot distinguish multiple storms occurring close together; but the CH-1 mud layer proxy can distinguish individual years with and without TC events in the capture area. One disadvantage compared to the coastal washover proxies is that CH-1 does not selectively record storms of high (local) intensity. So, while analysis of CH-1 can identify years with TCs near the Yucatan in the capture area, this record alone cannot tell us how the climatology of the most damaging major hurricanes have changed over time. Selection of a stalagmite in a flooding cave with higher elevations above the local water table could produce a record sensitive to larger rain producing TCs. More ideally, if two or more stalagmites were collected from the same cave at various elevations above the water table an analysis of the degree of sensitivity may be possible.

The trend in the past 3 centuries suggests that the low TC frequency observed for 5 centuries spanning 1233 to ~1700 is actually anomalous, and that a more typical number of years with TCs per century in this region is much higher than what has been recorded in the meteorological record for the last ~150 years. This has many implications for the people who live in the Caribbean nations, and along the Gulf Coast of Mexico and the United States. TC records like this and others can show trends in TC frequency that may be useful for local governments and developers in TC prone regions.

Nott (2007) report strong TC landfall variability on a centennial scale in northeastern Australia as well. Nott used a $\delta^{18}O$ proxy from a U-series dated stalagmite collected near Cairns, Australia with a TC record going back to 1200 AD. If TC landfall frequency is increasing worldwide, this could be dangerous for people living in any coastal location prone to TCs.

Questions that this raises include what is driving the sudden drop and subsequent rise in TC frequency in the Caribbean, is it really a change in TC frequency or just a shift in the track locations away from the Caribbean, and what does this mean for the future? This time period roughly corresponds to the Little Ice Age (1400-1700 C.E.); a cooling that primarily affected the extra tropical Northern Hemisphere (Mann et al., 2009). This suggests that a climatic teleconnection related to what has been considered a Northern Hemisphere cooling event may have been felt as close to the equator as the Yucatán.

Understanding this variability will require much more future work to understand if this trend is only seen in the Caribbean, or if it is Atlantic basin wide, or worldwide. Using paleotempestology proxies in various locations around the world will be one key to solving this question, which underlines the necessity to develop and establish various proxies that can be used in multiple environments.

iii. *Reproducibility of the climate signal*

Paleoclimate proxy records from other stalagmites and lake cores from the Yucatán region, including $\delta^{18}O$ and $\delta^{13}C$ values, were used to test for reproducibility of the climate signal in CH-1. Lake cores from Lake Chichancanab (Hodell et al., 2005a)

and Lake Punta Laguna (Curtis et al., 1996), and a stalagmite from Macal Chasm in Belize (Webster et al., 2007) were used as climate records to report $\delta^{18}O$ and $\delta^{13}C$ values from the last ~3500 years.

Webster et al. report a stalagmite climate record spanning similar ages as CH-1 from Macal Chasm in Belize. Macal Chasm receives ~1500 mm of rainfall/year, about 400 mm more than Cenote Chaltun-Ha. The $\delta^{18}O$ and $\delta^{13}C$ values from the low-resolution CH-1 dataset were compared to the $\delta^{18}O$ and $\delta^{13}C$ values published by Webster et al. (Figures 38 and 39). The two datasets are generally in good agreement. The similarities of the datasets are most readily apparent in the time from ~1200 to the present, where the sampling resolutions are more similar. The low-resolution CH-1 record has a sampling resolution over this period of about 25 yr/sample, and the Macal Chasm record has a resolution of about 23 yr/sample. Comparing the datasets shows some degree of expected aliasing in both records, demonstrating a key problem in time series analysis of climate records. The $\delta^{13}C$ values appear to be in more agreement than the $\delta^{18}O$ values; however there appears to be a slight lag of 10-50 years in the $\delta^{13}C$ values from CH-1. This lag is most likely due in part to aliasing, but also may be caused by uncertainties in the age models for both records, the specifics of which will be discussed below. The lag may be evidence of a spatial/temporal lag in shifts in flora, with the shifts occurring first in the central Belize region and subsequently affecting the drier Yucatán.

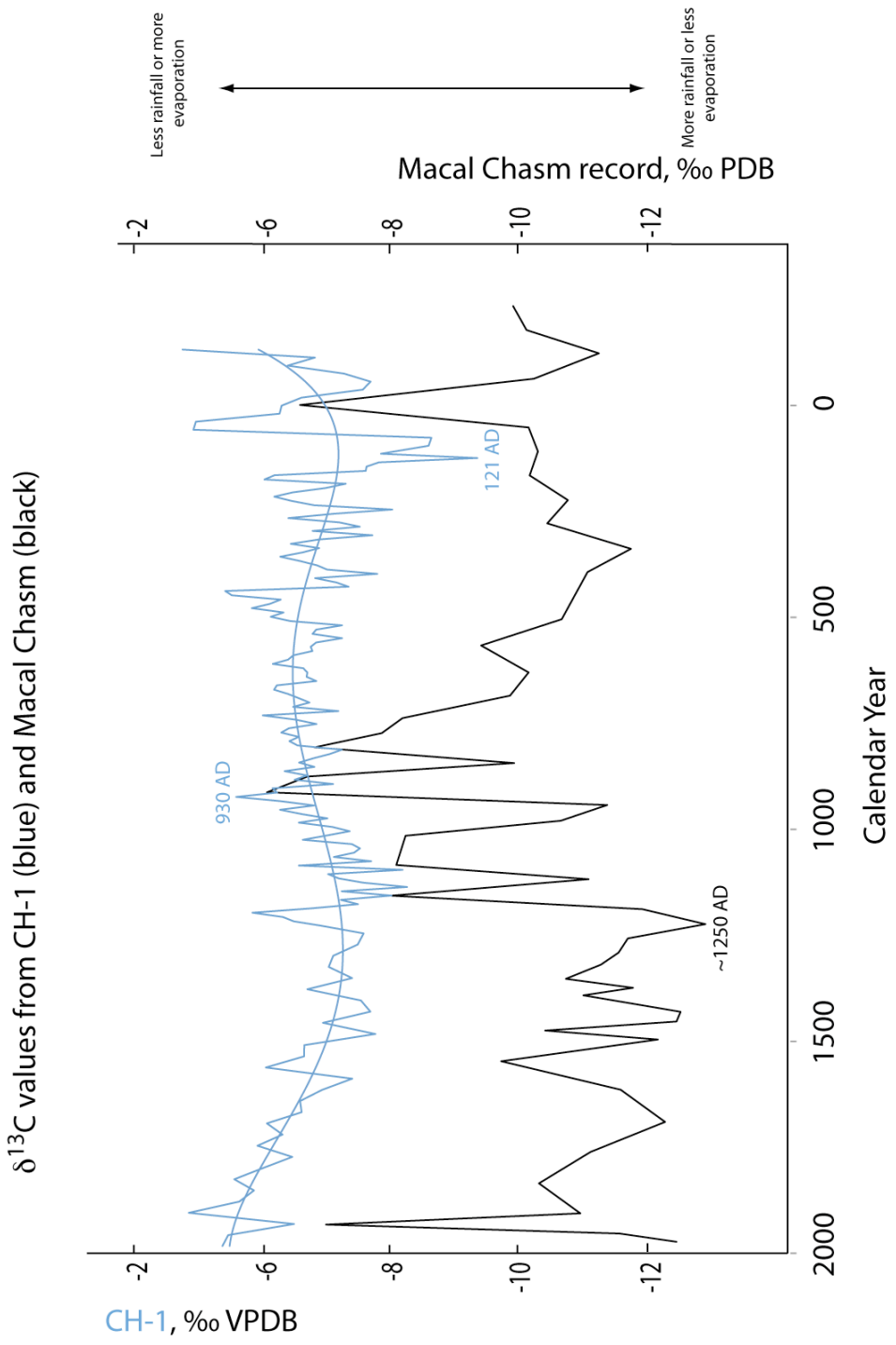

Figure 38. Low-resolution (1 mm, discrete) $\delta^{13}C$ values compared to the Macal Chasm record from Webster et al. (2007). The CH-1 record is in blue, while Macal Chasm is in black.

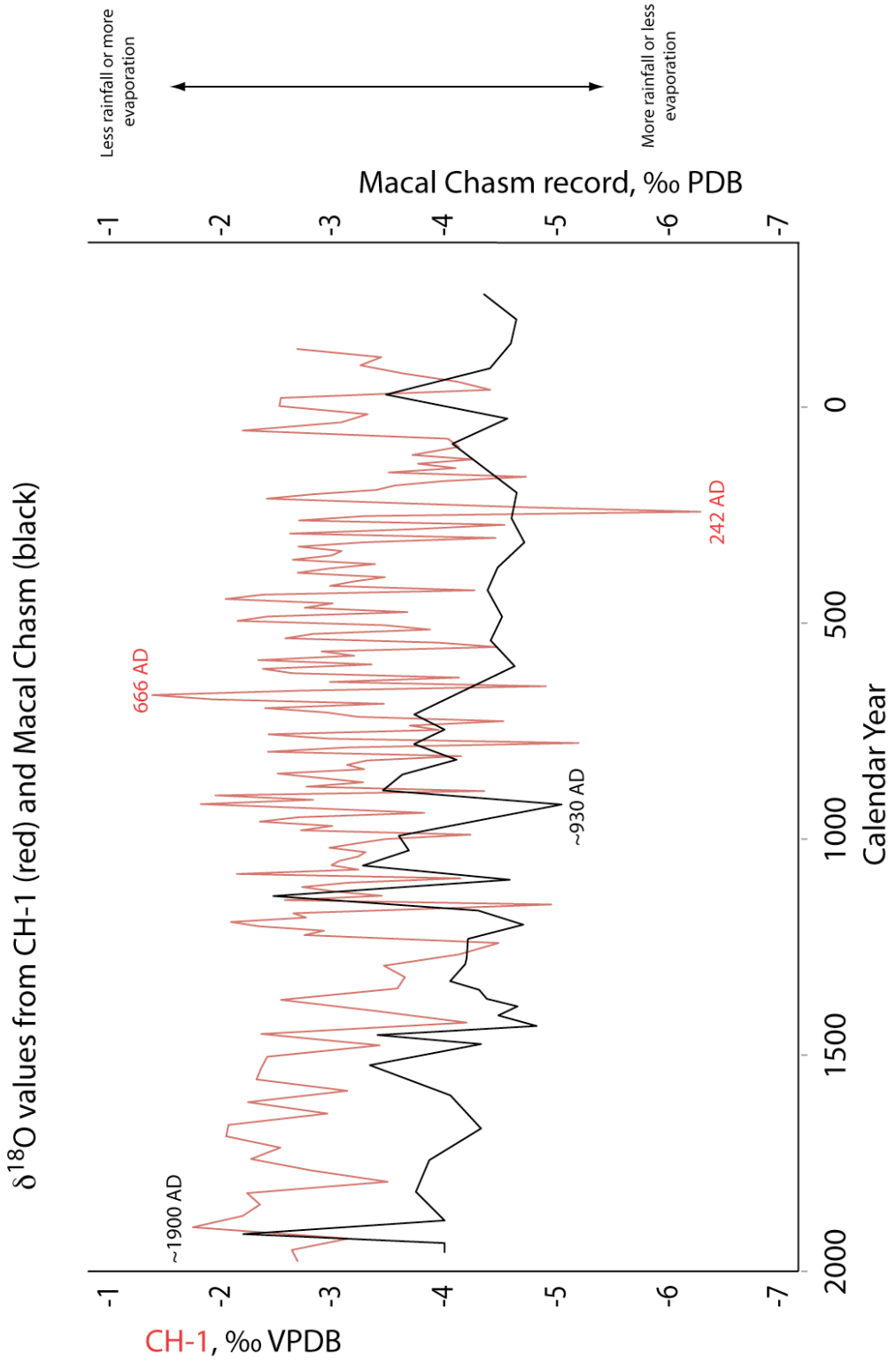

Figure 39. $\delta^{18}O$ from CH-1 in red compared to Macal Chasm in black.

The highest $\delta^{13}C$ value from Macal Chasm is ~ -6 ‰, and occurs around the year 900 AD. This corresponds to a high from CH-1, however it is not the highest $\delta^{13}C$ value from CH-1, which was from 1898 and had a value of -2.8 ‰. The lowest point in the Macal Chasm record has a value of ~ -14 ‰ occurring around the year 1250 AD. The lowest point in the $\delta^{13}C$ values occurs in the year 121, and has a value of -9.11 ‰. The difference in extremes between the two records is very similar, even though the time periods that extremes are recorded in both are very different.

The $\delta^{18}O$ values illustrate the climatic observation that rainfall in Belize is higher than in northern Yucatán by the lower values from Macal Chasm. While some droughts appear to have affected the region more broadly, evidence for droughts in CH-1 (centered around 930 AD and 1200 AD) that is not present in the Macal Chasm record suggest that northern Yucatán is more prone to localized droughts than the more tropical Belize region.

Both records show large shifts in $\delta^{18}O$ and $\delta^{13}C$ values on approximately the centennial scale. Longer-term trends from Macal Chasm are hard to see in both $\delta^{18}O$ and $\delta^{13}C$ values. CH-1 provides more evidence of long-term variation. The $\delta^{13}C$ values display longer-term variability. There appears to be a millennial scale cycle in the CH-1 $\delta^{13}C$ record from ~100 AD to ~1100 AD, however with only one full period it is impossible to say if this is a regular millennial scale climate cycle. In fact, it appears that for the last 1000 years the $\delta^{13}C$ values have been increasing without any evidence of a decrease necessary to complete a 1000-year cycle. A possible explanation for this longer-term variation in $\delta^{13}C$ values is millennial scale climate change, i.e., a 1000-year

rainfall cycle. Under this interpretation, a period of decreased rainfall started in ~100 AD and continued drying until ~600 when the climate began to return to wetter conditions. The $\delta^{13}C$ values in CH-1 after ~1100 indicate a drying period that continues to the present, or very close to it. The high-resolution dataset suggests an increase in wetness during the last century. The $\delta^{18}O$ values from CH-1 show the same trends, however the long-term trends are more muted than in the $\delta^{13}C$ values.

Another possible explanation is millennial-scale land use or land cover changes related to the Mayan civilization present in the region over the time recorded by CH-1. Many Mayan sites have been excavated in the region sustaining tens of thousands of people, with settlements in the region starting as early as 500 BC and continuing through until at least 700 AD (Sweetwood et al., 2009). To sustain this size of population in a semi-arid area like the Yucatán required large-scale agriculture in the region, which has been recorded in the soil (Sweetwood et al., 2009). Positive shifts in $\delta^{13}C$ values have been correlated to maize production from a lake core spanning the time from 2470 ^{14}C ybp to the present (Lane et al., 2008), supporting a land use interpretation for the increase in $\delta^{13}C$ values from CH-1.

The highest $\delta^{13}C$ value is from a ~25 year period centered on the year 666 AD (due to large sampling interval of discrete drilling method) and is -1.41 ‰. Aliasing in the Macal Chasm record has made it impossible to tell if the same signal is present in it as well, however, lake core climate records from the Yucatán offer another chance to correlate potential extremes in climate.

Hodell et al. (2005) present a drought proxy based on core density from Lake Chichancanab in the state of Quintana Roo, ~ 100 km SSE of Cenote Chaltun-Ha. The authors identify a short drought dated to ~670, followed by a relatively wet period lasting for 100 years. This is in very good agreement with the $\delta^{18}O$ values in CH-1. Hodell et al. also present evidence supporting the timing of this drought and others from the Cariaco basin in Venezuela from Haug et al. (2003).

Anti-correlations between $\delta^{18}O$ and Ti % from the Cariaco basin are also generally in good agreement, with very similar frequencies of wet and dry, as well as the general, longer-scale trend noted earlier. The 666 AD high in $\delta^{18}O$ values are correlated to a low in Ti %, meaning drought, although the signal is not as extreme from the Cariaco basin (Figure 40). Other possible droughts that correlate are at 919 and 1081 AD. This may be due to the location of the Yucatán. The Cariaco basin is located at 10° N, while the Cenote Chaltun-Ha is located at 20.7° N. The Cariaco basin is part of the same Caribbean climate that dominates the Yucatán (Hodell et al., 2005a), with seasonal rainfall dominated by the ITCZ. If the ITCZ were to migrate slightly south, the Yucatán would likely be affected more severely, as well as earlier and for a longer time as the ITCZ rebounded back to a more average location. Haug et al. (2001) present evidence from the Cariaco basin that the ITCZ has been generally shifting to the south during the Holocene.

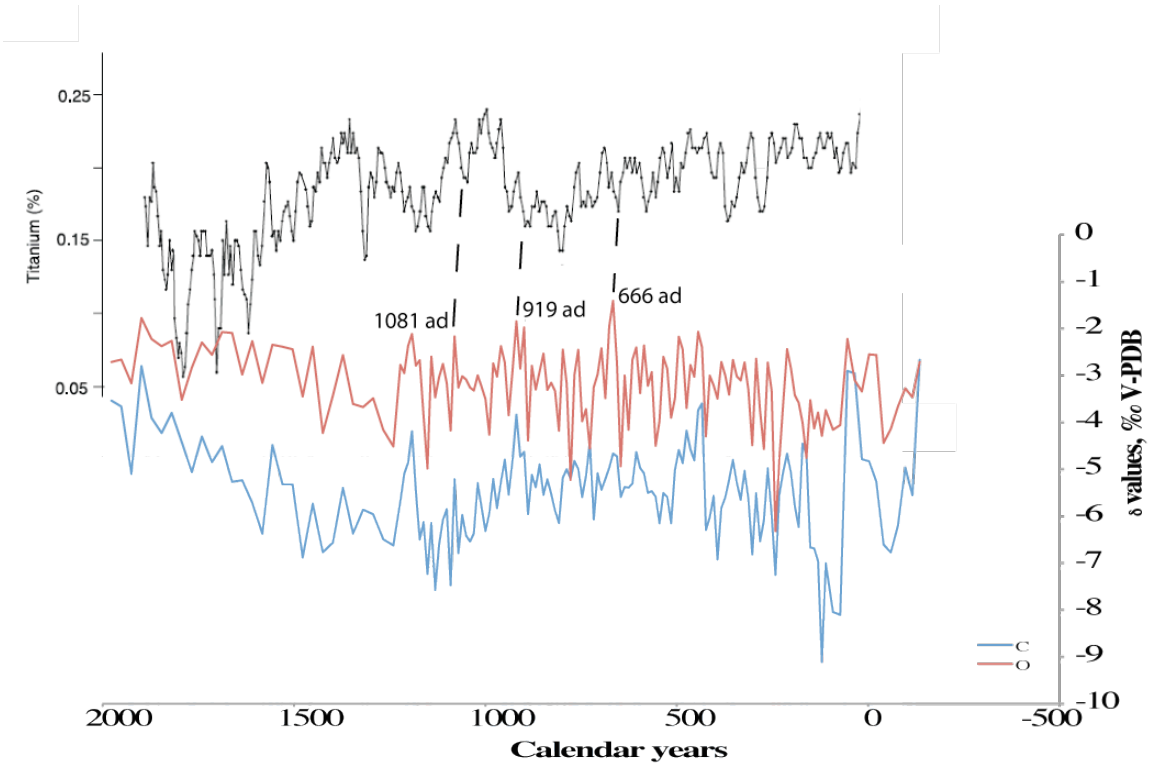

Figure 40. Cariaco basin Ti record compared to the low-resolution CH-1 record.

Some areas of the two records are in disagreement, e.g., ~1800. This is the lowest $\delta^{18}O$ value recorded in CH-1 for the last 500 years, yet it is occurs at the same time as one of the driest times in the Cariaco Basin record. This could be due to uncertainties in the age models, or aliasing, although the high-resolution CH-1 dataset also shows this low point. In the high-resolution dataset, the extreme low occurs in 1816, and is the lowest point from the high-resolution dataset that spans 365 years. This low $\delta^{18}O$ value at 1816 correlates exactly to "the year without a summer," so called because of the cold period that followed the Tambora volcanic eruption of 1815. This is probably the coldest period during the last 500 years (Cole-Dai et al., 2009). Other explanations for this anomaly may be a season with frequent and/or intense TC activity, decreasing the

average $\delta^{18}O$ value of the water dripping onto CH-1. However, no mud layer is present in this section of CH-1 to support this hypothesis. Rainwater $\delta^{18}O$ values can also be low due to a decrease in the isotopic composition of the water in the moisture source region driven by lower evaporation or changing ocean circulation, or a shift in storm tracks to deliver water from a more distant moisture source. Dripwaters can also shift to lower $\delta^{18}O$ values if evaporation is inhibited. I favor the interpretation that the low $\delta^{18}O$ values ~ 1800 recorded by CH-1 resulted from the Tambora eruption, and the cold period that followed because it is the simplest explanation.

Curtis et al. (1996) present $\delta^{18}O$ values from various ostracod and gastropod shells from cores taken from lake Punta Laguna, Quintana Roo, ~160 km to the east of Cenote Chaltun-ha. The general trend of lower $\delta^{18}O$ values from ~100 BC until about 100 AD followed by a period of higher values is the same in both CH-1 and the Punta Laguna, however the trend in Punta Laguna is interpreted to be more of a stable record with abrupt and rapid changes (Figure 41). This is especially evident ~1100 AD, where $\delta^{18}O$ values in Punta Laguna drop by ~3.5 ‰ in less than 100 years. CH-1 also displays a rapid shift from high to lower values of ~2.5 ‰ in 60 years, starting in 1192. The shift from wetter to drier conditions was diachronous in the three locations. The drying at Lake Chichancanab began ~900 AD, at Punta Laguan ~1100 AD, and at Cenote Chaltun-Ha at 1191 AD. This illustrates the spatial and temporal resolution needed to understand the paleoclimate of the Yucatán and its implications for the archeology of the Mayan civilization.

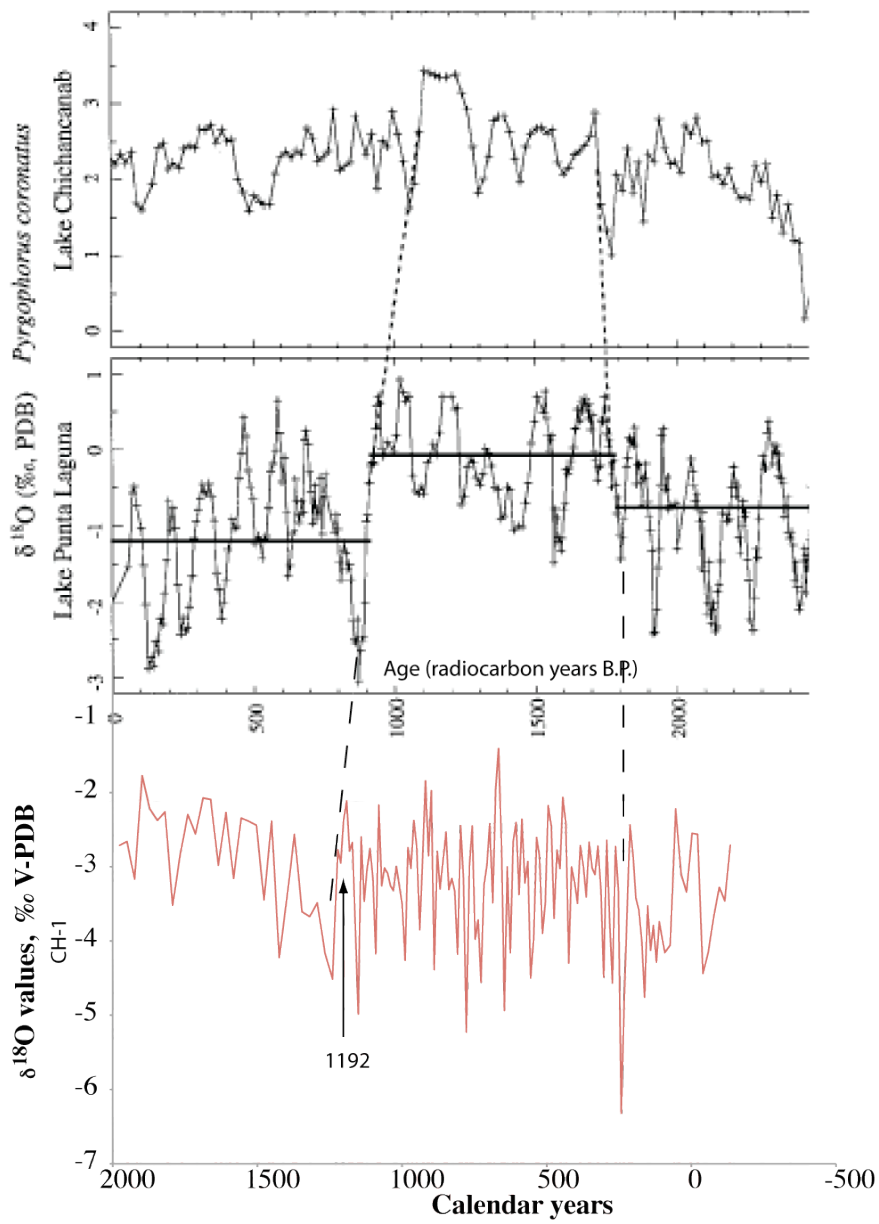

Figure 41. Comparison of three $\delta^{18}O$ value records from the Yucatán Peninsula.

The Punta Laguna record shows a general decrease in $\delta^{18}O$ values over the last 1000 years, whereas CH-1 displays a positive trend. Reasons for the disagreement in trends of the $\delta^{18}O$ values may be Punta Laguna's relative proximity to the Caribbean Sea.

This may be evidence of local climate change during this period, with the east coastal region of the northern Yucatán remaining relatively wet, while the interior got progressively drier over this interval. Punta Laguna currently receives ~500 mm/yr more precipitation than Cenote Chaltun-Ha. This interpretation would suggest that the present longitudinal rainfall gradient across the northern peninsula was much more equitable 1000 years ago.

The general agreement between the $\delta^{18}O$ and $\delta^{13}C$ values between CH-1 and the other regional stalagmite and lake core paleoclimate records, as well as the timing of some specific high points (droughts) and low points (wet periods), adds confidence to the climate signal present in CH-1. The fact that the extremes in CH-1 are not always the same extremes as the other records may be due to the dating or sensitivity or sampling rate of the different climate records, or may be evidence of shifts in climate occurring on a small regional scale. A more comprehensive paleoclimate study from CH-1 may be a useful undertaking in the future.

b. *Hypothesis testing*

The first step in establishing a paleoclimate proxy is to test the desired climate signal against the instrumental record. For this study, that means assessing when the mud layers were deposited, and assessing how frequently these mud layers were deposited in years with a recorded TC. These assessments are based on assumptions made about the nature of the regional water table in the Yucatán, as well as field observations relating cave flooding to TCs. For this study, an attempt was made to correlate a known TC

proxy ($\delta^{18}O$ anomaly) within the same stalagmite to add to the confidence level in the accuracy of the proxy.

The TC record for the Yucatán based on meteorological observations spans the years from 1852 to the present. From 1852 until 2006 (the last TC season recorded by CH-1), at least 195 TCs ranging in intensity from tropical depression (TD) to category 5 hurricanes on the Saffir-Simpson scale passed within 370 km of Cenote Chaltun-Ha. Figure 42 shows a histogram plotting the frequency of years with 0-5 TCs/year. During this time, 72% of years had at least one TC. Table 10 summarizes the frequency of number of TCs/year and TCs/mud layer.

Number of TCs (bin)	0	1	2	3	4	5
Years w/	43	56	30	13	6	4
Mud layers w/	0	8	6	2	2	1
% of years/mud	0.0	14.3	20.0	15.4	33.3	25.0

Table 10. Summarizing TC frequency by year and mud layer deposit from 1852-2006.

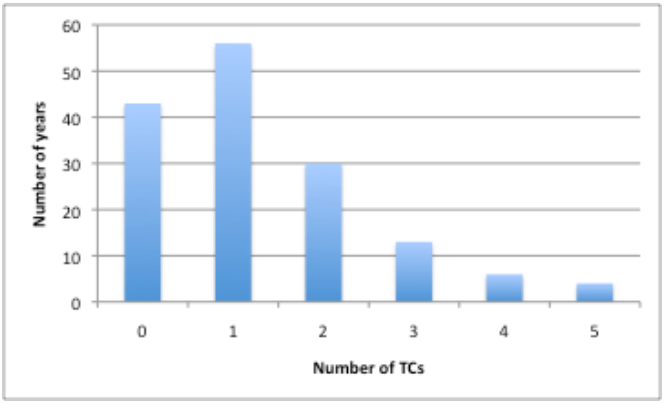

Figure 42. Histogram of TCs/year, illustrating that years with at least 1 TC are far more common than years without any TCs.

There are 19 mud layers present in CH-1 during this time, all of which occurred during the same year as a TC. Figure 43 shows a histogram of the number of mud layers corresponding to the number of TCs per year of the mud layer. Figure 44 illustrates the

total number of TCs compared to the total number of mud layers, broken up into bins defined by number of TCs/year.

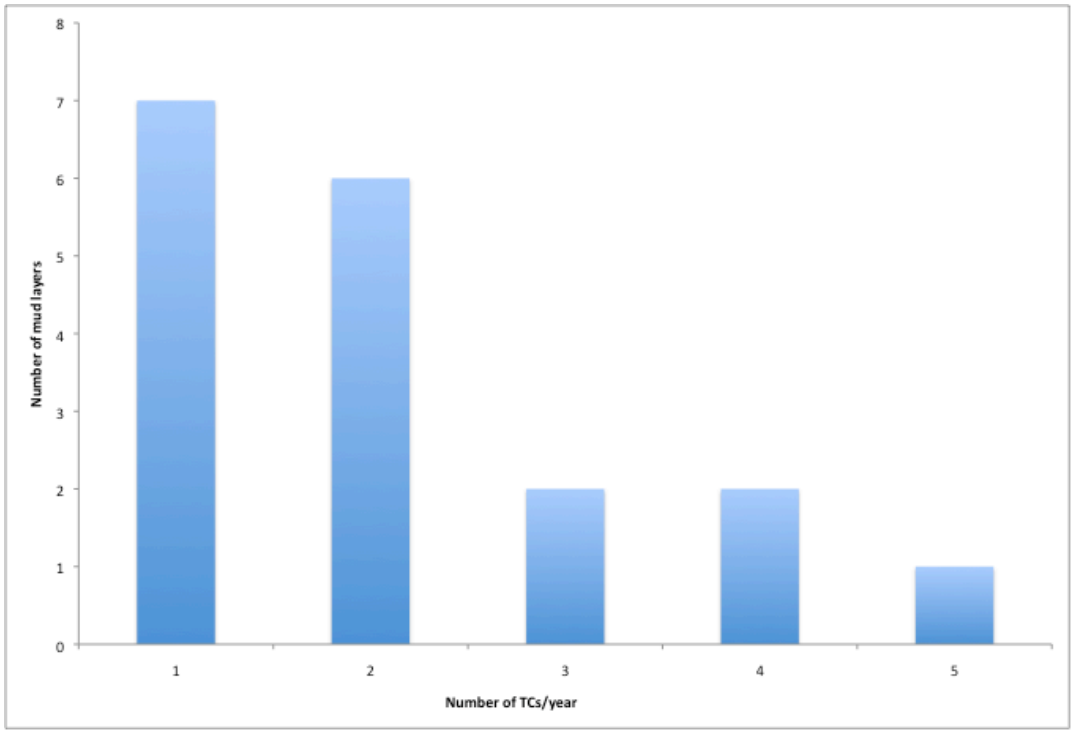

Figure 43. Histogram of TCs/year with a mud layer.

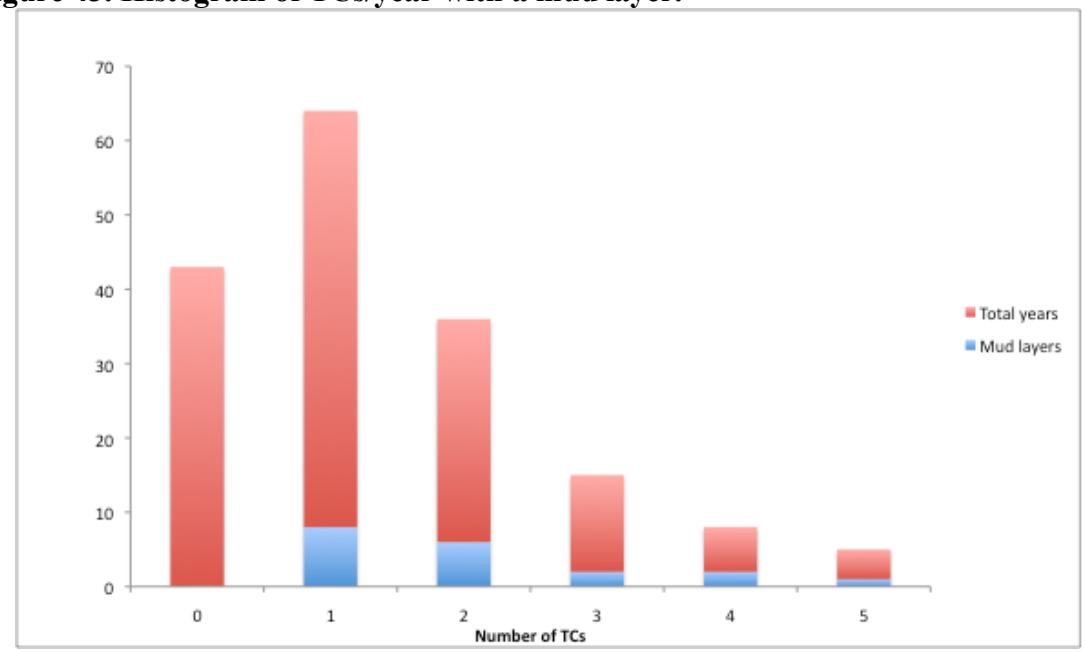

Figure 44. Histogram showing the total number of TCs/year in red, and the number of years with mud layers, and how many TC strikes occurred in blue.

The proportion of years with greater than one storm being recorded by a mud layer is nearly twice as high as years with mud layers recording only one storm. The average number of TCs/year with a mud layer is 2. Mud layers in CH-1 did not record each of the 92 years with TCs. No single year has more than one mud layer, so the mud layer proxy is only recording years with at least one TC, and not individual TCs.

In an attempt to quantify if the mud layers were recording more intense TCs, a numerical intensity scale was assigned based on the Saffir-Simpson scale as seen in table 11. The average intensity based on the scale in table was 2.7, or close to category 1 hurricane. The mode was 2, or tropical storm, leading to the conclusion that the number of TCs per year was a more important factor in the emplacement of a mud layer than intensity.

TD	1
TS	2
H1	3
H2	4
H3	5
H4	6
H5	7

Table 11. The code numbers assigned to Saffir-Simpson scale intensities of TCs.

The TCs recorded by CH-1 as mud layers passed by Cenote Chaltun-Ha at distances ranging from 0 to 337 km, with a minimum average distance of 166 km, supporting the assumption that the water table in the Yucatán is sensitive to rapid recharge on a regional scale.

The mud layer proxy shows excellent potential for a quantitative paleotempestology tool. Some of the strengths are the relative simplicity and low price of collecting proxy data spanning long time intervals (100s to 1000s of years) compared to high-resolution stable isotope sampling in stalagmites. It may also be possible to collect multiple stalagmites from the same cave at varying elevations providing records with different sensitivities from the same location. Finally, the analysis method is non-destructive, preserving the stalagmite sample for other studies. Some weaknesses of the method include the fact that it will only be applicable in regions with low-lying, highly interconnected karst to allow for a regional rise in the water table. The proxy has the inability to resolve more than one TC per year and there is a possibility that the flooding due to heavy rain from a frontal storm could deposit a mud layer, adding false positives to the TC record.

To avoid some of these pitfalls, and to make the conclusions and more robust, I suggest making every attempt to collect at least two stalagmites from the same cave at different elevations above the water table.

The $\delta^{18}O$ value anomaly proxy was not successful in CH-1. I believe this is due to the difficulties specific to CH-1 mentioned above. However, in future studies with other stalagmites, if the $\delta^{18}O$ value anomalies were to be faithfully being recorded and measurable, I would expect a higher percentage of success in years without mud layers than with, opposing the hypothesis that $\delta^{18}O$ value anomalies would help verify that a mud layer was recording a TC.

The $\delta^{18}O$ value anomaly was only ~50% effective at supporting the cyclogenic nature of the mud layers, and the mud layers do not always get pushed to the side creating lobes, which will be discussed below, but the data supports the hypothesis that the mud layers are indeed recording TC events.

d. Other Interpretations:

i. Shape of CH-1:

Kaufmann and Dreybrodt (2004) have modeled the growth of stalagmite shape and layer characteristics with the climatic controls of temperature, soil activity, and precipitation. The results reported describe the growth styles of many stalagmites used for paleoclimatic studies. However, of the six different model runs, none of the shapes predicted satisfactorily describe the shape and laminae growth of CH-1 (Figure 45). CH-1 has, to my knowledge from the field as well as published stalagmite records, a fairly unique shape, it is almost perfectly 4 cm in diameter for most of its growth history, and has a flat as opposed to conical or convex lamina deposition style when there are no mud lobes present. I suggest that this shape is due to the mud layers themselves.

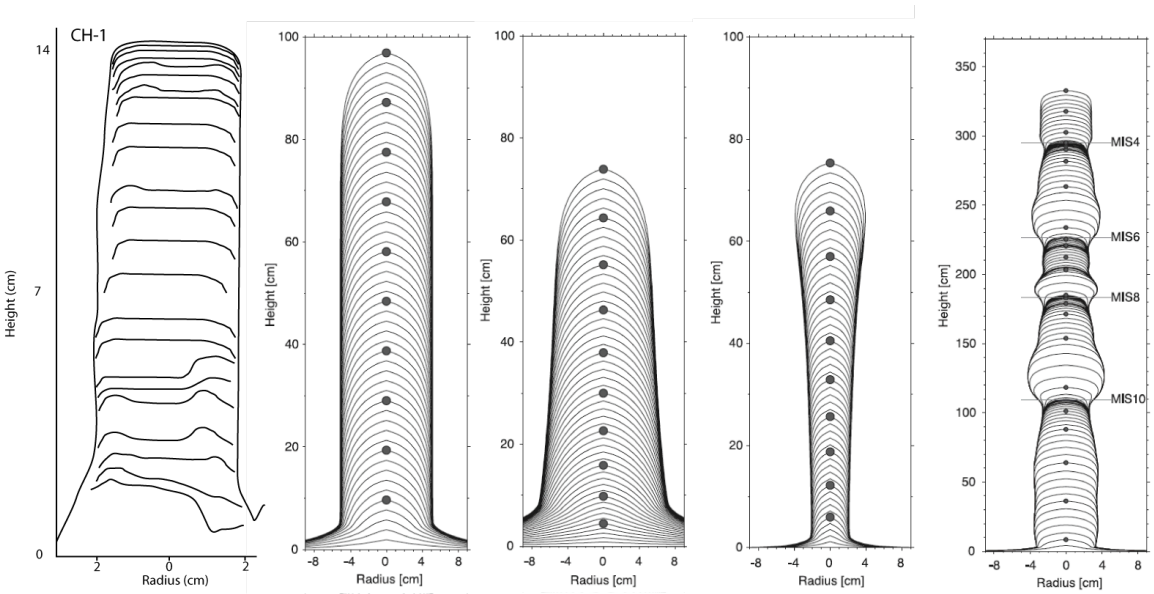

Figure 45. Tracing of the laminae morphology from CH-1 with the modeled stalagmite layer morphology from Kaufmann and Dreybrodt (2004), illustrating a new stalagmite morphology described from CH-1.

Unpublished work done by Dorale et al. (2005) report on flooding proxies from dendritic caves in the central US, but mud is something that is normally avoided in the selection of stalagmites for most paleoclimate studies. The only published study I am aware of that is based on a record from muddy stalagmites is that of Niggemann et al. (2003). The authors report a record of three stalagmites from B7 cave in western Germany which contain ~8 mud layers correlated to each other. The cross-sectional shapes and internal lamination of the three stalagmites have the very typical inverted cone shape expected from modeling for a stalagmite with an approximately constant growth rate. The growth rates are not constant, ranging from 9-280 μm/yr, which likely contributed to some expected variation in diameter of the stalagmites from B7 cave. The stalagmites from B7 cave span between 6,000 and 12,000 years, and contain 8 mud layers.

One hypothesis explaining why the B7 cave stalagmites did not exhibit the same growth shape and lamina pattern as CH-1 was differing growth rates, however, the growth rates are similar to those of CH-1.

The explanation I propose is that the density of mud layers played the largest role in controlling stalagmite shape. Stalagmite B7-7's average distribution of mud layers is one per 7.75 cm of growth. This contrasts to the average of one mud layer every 0.06 cm in CH-1, approximately two orders of magnitude greater. The frequency of flooding in Cenote Chaltun-Ha may have been responsible for the unusually nearly symmetrical growth shaft and flat depositional surface of CH-1.

The model of growth for CH-1 and similar stalagmites that I propose is as follows: After deposition of the flood derived mud layer, as the force of drip impact and flow of dripwater begins to push the mud away from the drip center as proposed in the hypothesis for this study, a mud lobe is created as the dripwater preferentially flows down one side of the stalagmite. This mud lobe, viewed as a sort of lag deposit, has been observed to form on only one of the visible sides of stalagmite CH-1 when viewed in cross-section in most cases (Figure 23). The presence of the mud lobe on only one side of the stalagmite creates a boundary that subsequent dripwater cannot readily flow over. This leaves a portion of the top of the stalagmite relatively lower, allowing drip water to deposit calcite in the drip center and along flow off the top of the stalagmite in this direction, creating the onlapping relationships observed in the post-mud layer calcite (Figure 23). When the next flood occurs and mud is again deposited, it is likely that the flow direction will still be the same, unless enough of a new lobe of mud is created on the

opposite side of the periphery of the stalagmite top. This model of alternating mud lobe emplacement may explain the uncommon flattop geometry of CH-1, and also may explain why the observed mud layers create lobes on only one side of CH-1. To test if the mud lobes really are only present on a part of the rim of the top of CH-1, a section of CH-1 would need to be quartered to gain another perspective on the outer rim of CH-1. These conclusions have implications for the future selection of stalagmites for this type of study, as well as where mud deposited from TCs that is not visible in the cross section of CH-1 may actually be preserved.

ii. *Why some TCs leave mud layers and some do not*

An unsolved question remaining is why some TC/flood events deposit mud layers, and some don't. In an attempt to understand this, years with mud layers from 1965 to 2005 were compared to monthly rainfall anomalies averaged from the 4 locations with rainfall data as well as the total precipitation in the 4 locations during the days the TCs were in the region of Chaltun-Ha (Figure 20). Daily rain data were not available before 1969, and after 2000 was only available from Acanceh. These years with mud layers were compared to 3 years during the time without mud layers that had TCs similar in nature to years with mud layers. These comparisons can be seen in Figure 46, A-H. The letters in the rain charts in the figures illustrate the areas below 0, and the numbers illustrate the areas above 0 that were integrated in an attempt to find a climate variable responsible for mud layer deposition. These areas are highlighted for 2005 (red – above zero, blue – below zero). Parameters considered were monthly rainfall anomalies, and the yearly

integration of these curves, subtracting the total area under the curve above zero to the total area under the curve below zero. The results of this comparison did not reveal any detectable trend, or reason some TCs should flood Cenote Chaltun-Ha and others should not, as is summarized in Table 12. Red highlighted years contain a mud layer. The reader will notice that there is no discernable trend in storm intensity, number of storms per year, single storm rainfall, distance from the cave site, or difference from the average monthly rainfall (plus or minus). Of special interest is 1988. Hurricane Gilbert passed nearly directly over Chaltun-Ha, and dropped large amounts of rain on the region, creating the largest positive anomaly in the years investigated, yet did not deposit a mud layer. No mud layer could be confidently identified upon re-investigation of CH-1 in fluorescent light to look for a mud layer that may not have been originally identified from 1988.

Year	Mud layer present	# of TCs	Max intensity	Max single storm rainfall (avg of 4 locations, mm)	Avg distance to closest pass of best track (km)	Negative anomaly integration	Positive anomaly integration	Positive - negative anomaly
2005	x	4	H5	79	85	3555	6700	3145
2003		2	TS	28	95	2422	4214	1792
2001	x	1	TS	40	262	2488	1953	-535
1998	x	1	TS	46	19	2785	2987	202
1993	x	2	TS	112	275	4704	2549	-2155
1988		4	H5	135	160*	1704	15622	13918
1980		3	H5	14	211	6013	2830	-3183
1965	x	2	TD	N/A	168	8258	5180	-3078

* - Hurricane Gilbert (H5) passed within 16 km of Chaltun-Ha

Table 12. Summarizing the results of different potential factors for the deposition of mud layers. Highlighted years contain a mud layer.

The conclusion from this exercise is that the data available at this time provides no discernable connection between any climatalogical parameters of individual storms or storm seasons of interest to paleotempestology. Future research may be valuable in determining a useful correlation.

2005 - Thick mud layer present

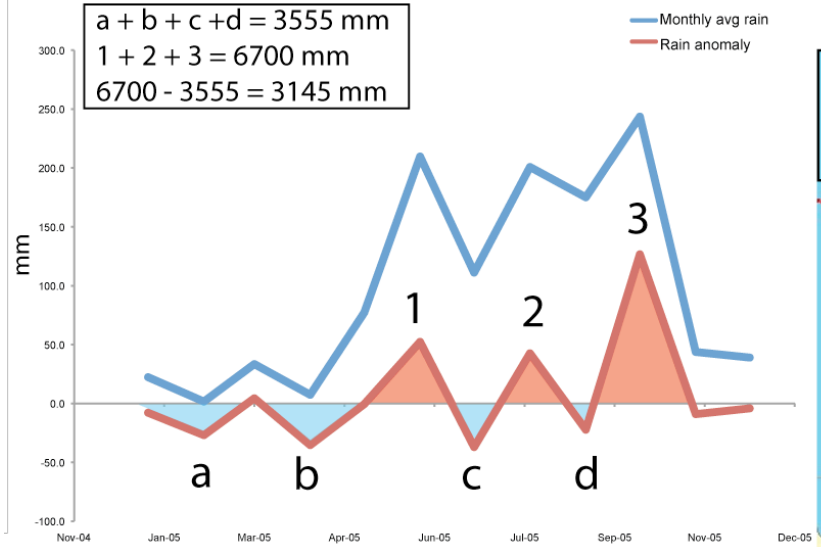

TCs	dates:	Total rainfall (mm) from days when TC was in region Santa Elena	Holca	Sotuta	Acanceh
Cindy	7/3-7/5	N/A	N/A	N/A	24
Emily	7/18-7/19	N/A	N/A	N/A	35
Stan	10/1-10/3	N/A	N/A	N/A	30
Wilma	10/21-10/23	N/A	N/A	N/A	79

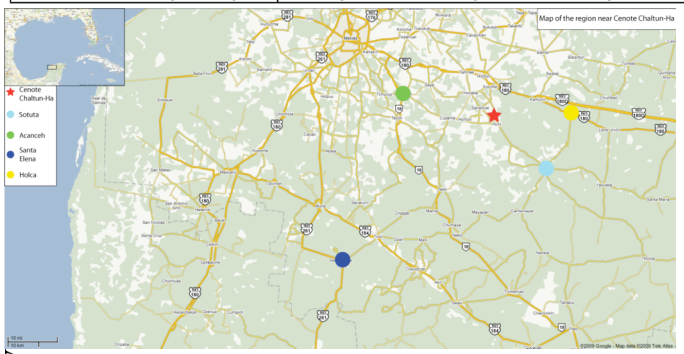

2003 - No mud layer present

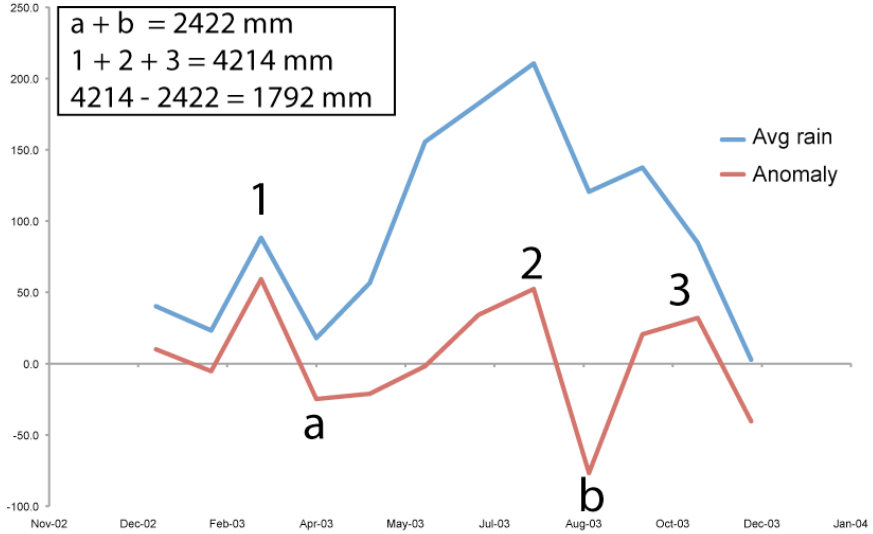

TCs	Dates	Total rainfall (mm) from days when TC was in region			
		Santa Elena	Holca	Sotuta	Acanceh
Bill	6/29-6/30	N/A	N/A	N/A	28
Claudette	7/11-7/12	N/A	N/A	N/A	26

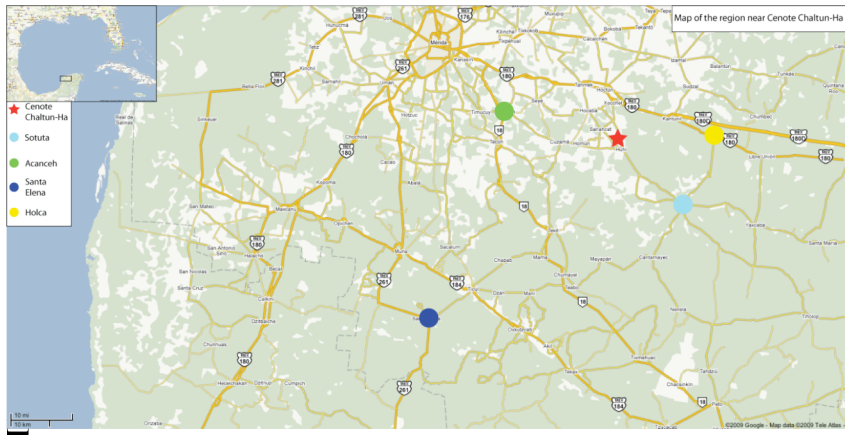

B

2001 - Mud layer present

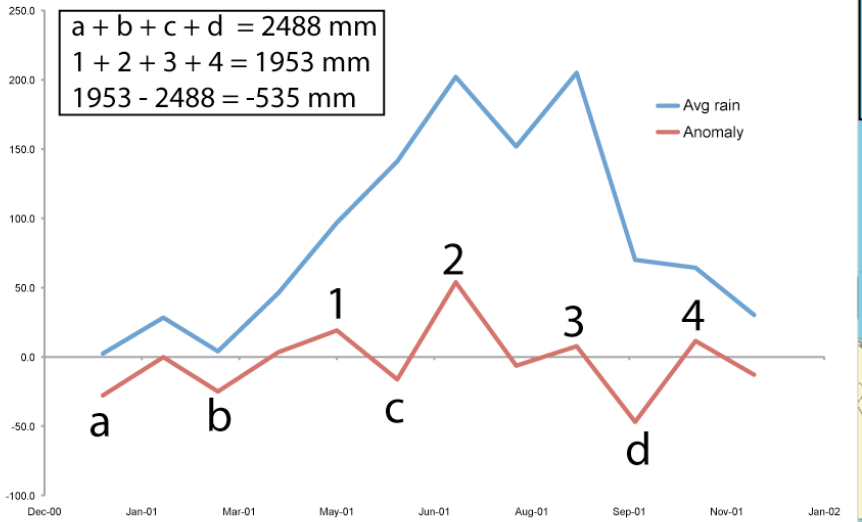

TCs	Date	Total rainfall (mm) from days when TC was in region Santa Elena	Holca	Sotuta	Acanceh
Chantal	8/20-8/22	N/A	N/A	N/A	40

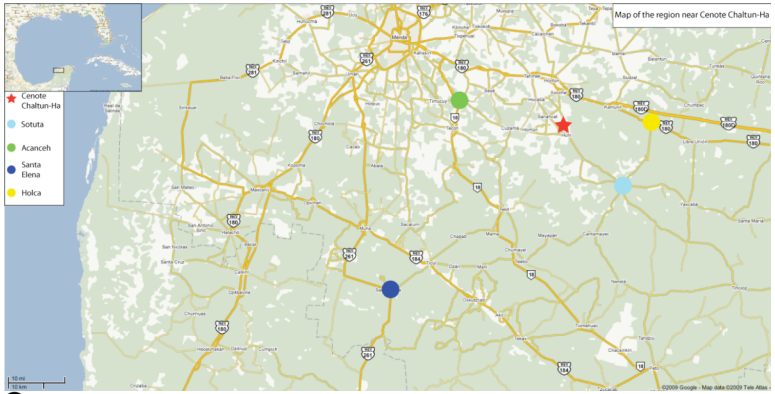

C

1998 - Mud layer present

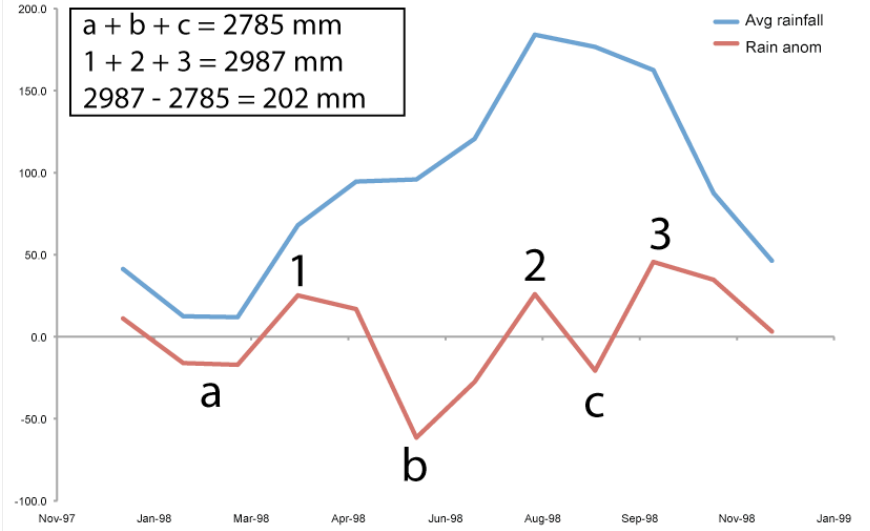

		Total rainfall (mm) from days when TC was in region			
TCs	Date	Santa Elena	Holca	Sotuta	Acanceh
Mitch	11/3-11/4	3.5	49	9.5	120

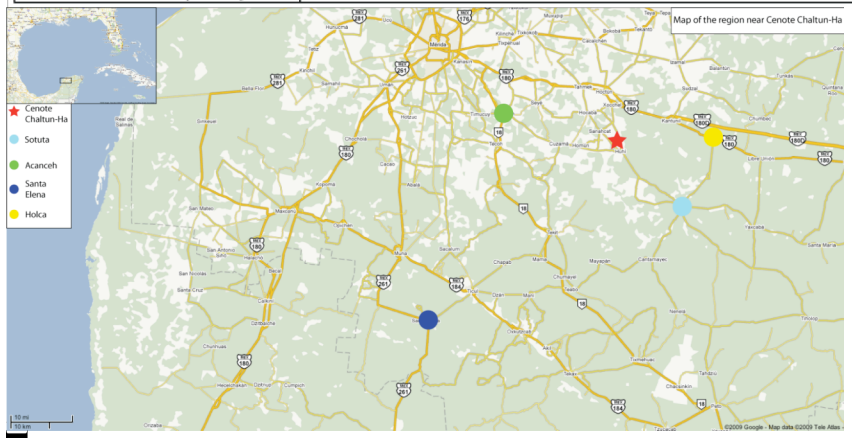

D

1993 - Mud layer present

a + b = 4704 mm
1 + 2 = 2549 mm
2549 - 4704 = -2155 mm

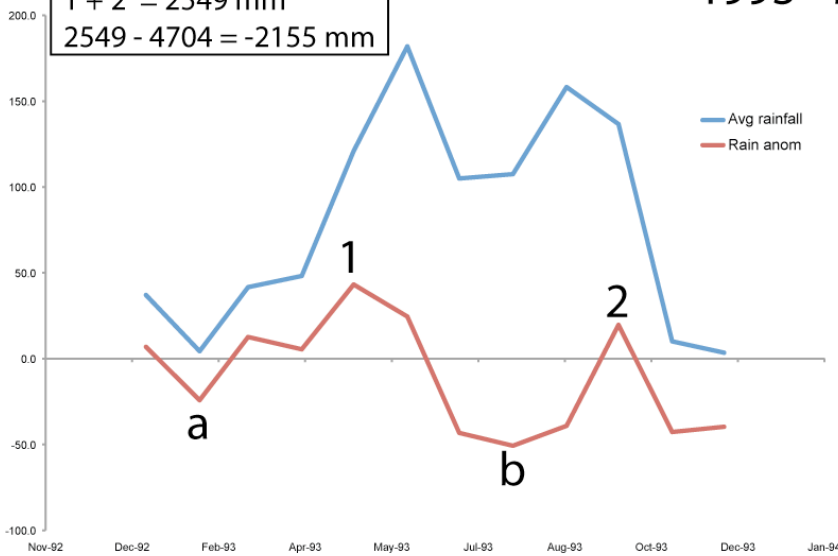

TCs	date	Total rainfall (mm) from days when TC was in region Santa Elena	Holca	Sotuta	Acanceh
Arlene	6/18-6/19	150	111	65	123
Gert	9/18-9/19	119	42	15	25

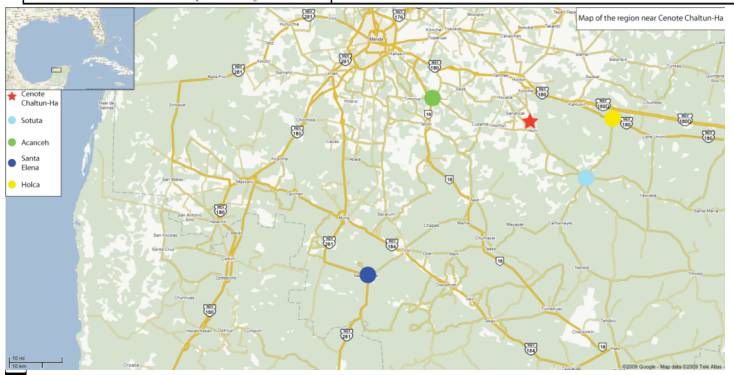

1988 - No mud layer present

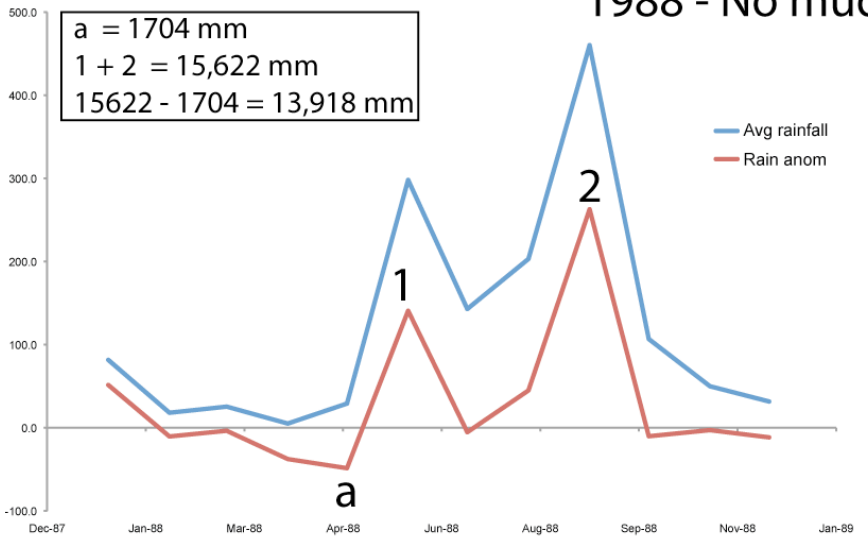

TCs	Dates	Total rainfall (mm) from days when TC was in region			
		Santa Elena	Holca	Sotuta	Acanceh
Debby	8/31-9/1	10.4	0	48.5	20
Florence	9/7-9/9	0	0	0	20.2
Gilbert	9/14-9/15	0	245	178.8	115.6
Keith	11/20-11/22	0	71	24	0

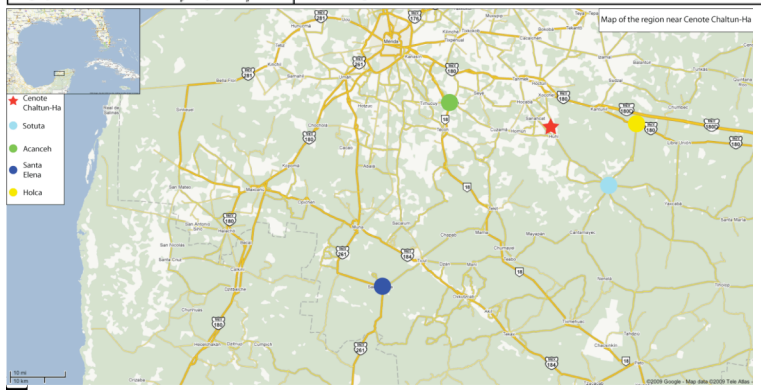

F

1980 - No mud layer present

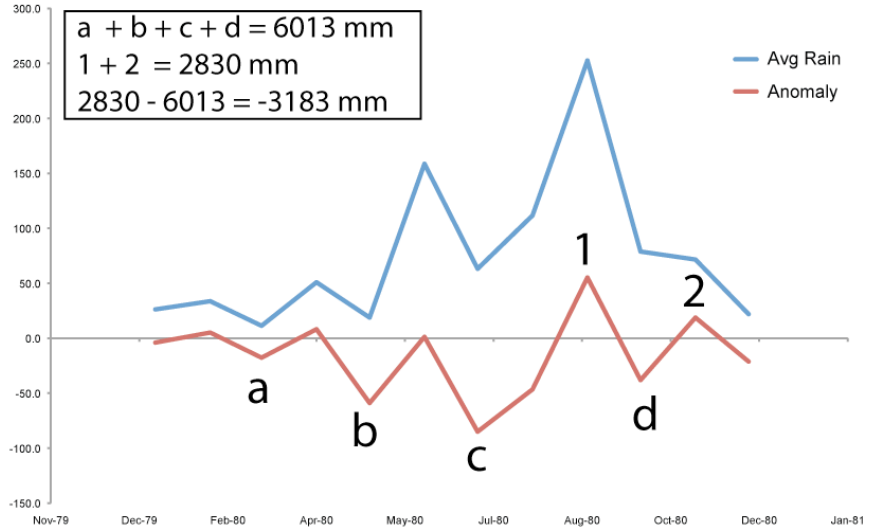

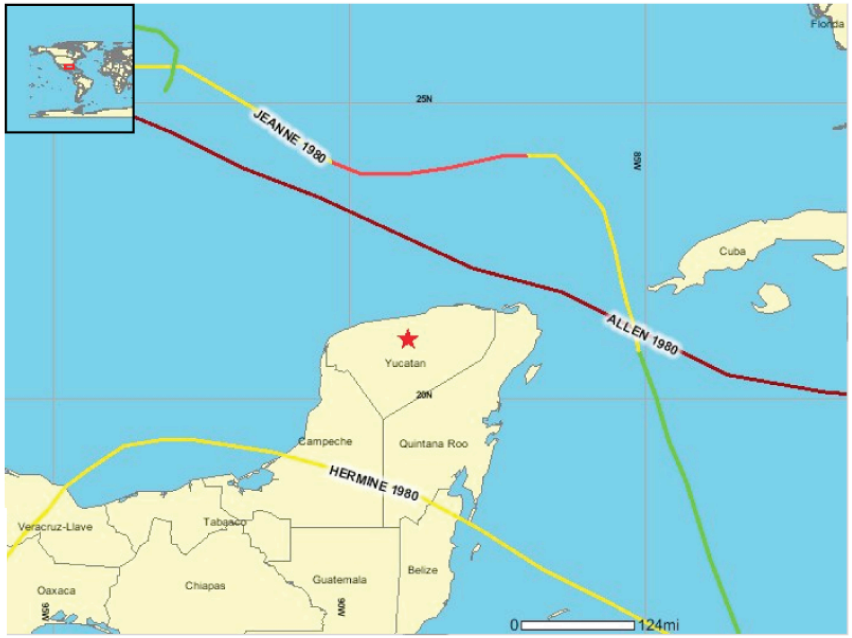

TCs	dates	Total rainfall (mm) from days when TC was in region Santa Elena	Holca	Sotuta	Acanceh
Allen	8/7-8/8	22.6	4.8	N/A	4.7
Hermine	9/22-9/23	20.6	22.1	N/A	0
Jeanne	11/12-11/13	0	2.7	N/A	0

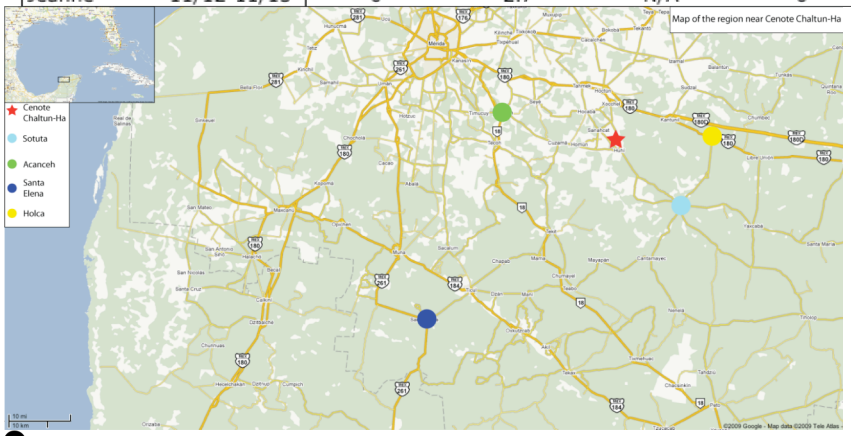

G

1965 - Mud layer present

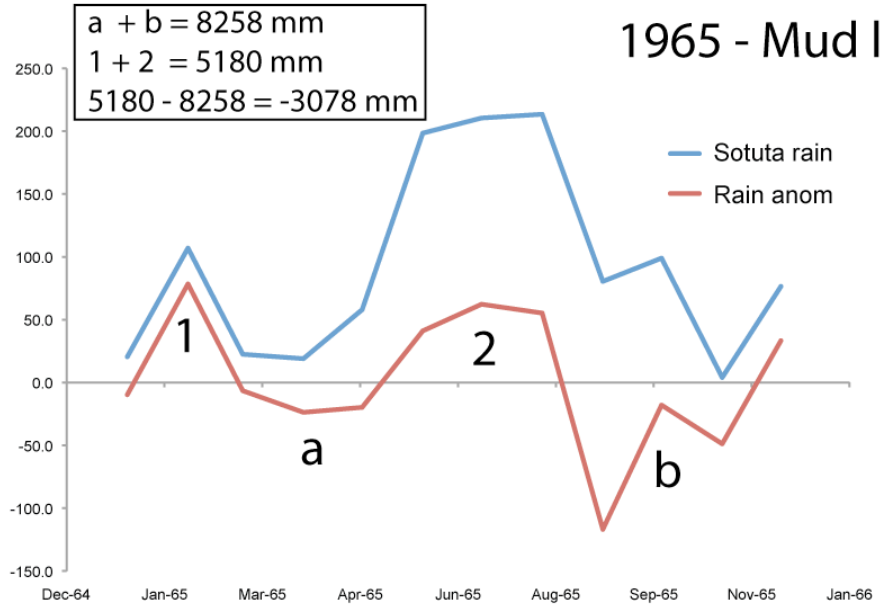

tcs	dates	
Notnamed	6/12-6/13	No daily rainfall data
Debbie	9/25-9/27	

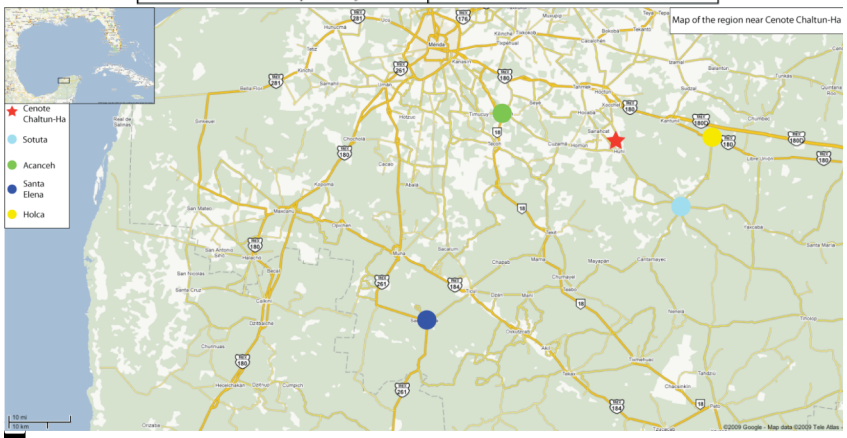

H

Figure 46, A-H. Composite figures showing the monthly rainfall totals and anomalies associated, best track data courtesy of NOAA, and a map of the locations of the weather data of 5 years with mud layers and 3 without.

One year of interest is 1993 (Figure 46, E). The maximum intensity of any storm that passed the region of Chaltun-Ha was tropical storm Arlene. Arlene became a TC in the Gulf of Mexico, west of the Yucatán. Since TCs generally move to the west or northwest, one would not expect the storm track to move over the Yucatán, which is what is observed. However, Arlene dropped over a meter of rain in the area of Chaltun-Ha during the two days it was near the Yucatán. The reason for this is likely due to the cyclical nature of TCs, and the ability of these storms to pull large amounts of moisture from warm oceans left behind in its trail. Satellite images of this storm explain why this type of storm may be likely to flood the region (Figure 47). This provides evidence that a TC may not even have to pass over or originate to the east of the Yucatán to deposit a mud layer. This also shows that the mud layer proxy may be sensitive to storms that the $\delta^{18}O$ value anomaly proxy is not, including unusually large frontal rainstorms.

e. *Climatic interpretations*

i. *Growth rate*

The growth rate of stalagmites is controlled by surface temperature, the rate of CO^2 degassing, which is related to the concentration of CO^2 in drip water compared to the cave atmosphere, and the water drip interval, which is related to precipitation (Kaufmann and Dreybrodt, 2004). With this in mind, an investigation into the variation

of growth rates observed in CH-1 was performed. Since most of the variables are unknown to us for the ~2000 years of growth recorded by CH-1, $\delta^{18}O$ values and the number of mud layers recorded in CH-1 were used as proxies for precipitation amount. Since TCs account for such a large portion of the precipitation that the Yucatán receives on an annual basis, it stands to reason that periods with a higher frequency of mud layers would be relatively wetter than times with fewer mud layers, causing higher growth rates.

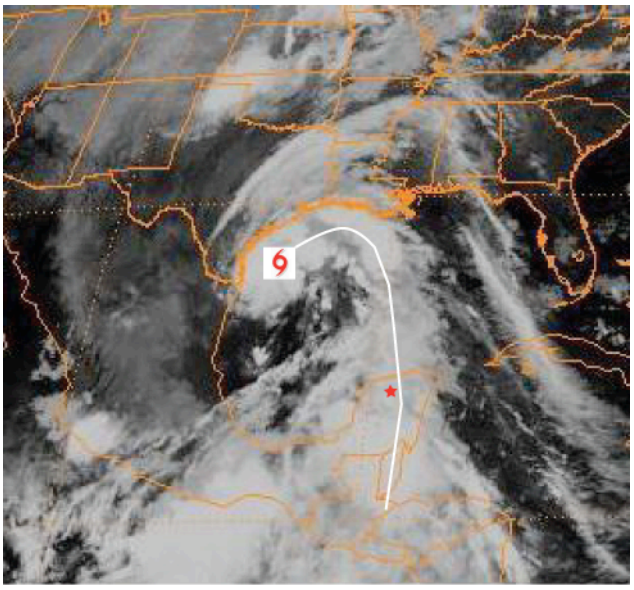

Figure 47. Satellite image of tropical storm Arlene, which originated in the Gulf of Mexico to the west of the Yucatán. The hurricane symbol denotes the eye of the storm in the picture, the red star is the location of Chaltun-Ha, and the drawn-in white line should draw the reader's attention to the trail of clouds that this system brought with it.

Gray scale analysis of the fluorescence between sections 1 and 2 in the main growth axis reveals a higher mean (Table 13) for section 2 than for section 1 with greater than 99.998% confidence, signifying higher influx of humic and fulvic acids from increased plant productivity on the surface between 118 AD and 1222 AD, which is often

attributed to wetter conditions (Baker et al., 2008). The $\delta^{18}O$ values from section 2 have a mean that is 0.37‰ lower than section 1, also indicating wetter conditions. The means of the $\delta^{18}O$ values from the two sections are different with greater than 99.95% confidence. The higher growth rate, higher fluorescence intensity, and lower $\delta^{18}O$ values of section 2, deposited between 118 AD and 1222 AD, are consistent with significantly wetter conditions than section 1, deposited between 1222 AD and 2007 AD. The images used to assess fluorescent gray scale variation were incomplete for section 3, leaving the analysis of the fluorescence levels between sections 2 and 3 unfinished.

	Fluorescent light gray scale	
Section	1 (0-30.1 mm)	2 (30.1-140.9 mm)
Mean	47.5	52.2
St Dev	11.6	10.7
n	1279	4505
Se	0.346	
Sp	10.905	
t	-13.603	
H_0: Mean of Section 1 = Mean of Section 2		
H_1: Mean of Section 1 ≠ Mean of Section 2		
α = 0.002		
Critical value for a two-tailed t-test with v = ∞ at 0.002 significance level	3.0902	

Table 13. T-test results evaluating the means of the fluorescent gray scale values from the top 30.1 mm and 30.1-140.9 mm. The t-test allows us to reject the null hypothesis with greater than 99.998% confidence.

Another possible reason for an increase in growth rate during time periods in CH-1 with high mud layer frequency is the material deposited by the flood, the mud layer itself. Even though most of the mud layers added very little material to the center of CH-

1 where the distances used to calculate the growth rates were measured, it is conceivable that they contributed material to the overall growth rate. Mud layers with measurable thicknesses in the center of CH-1 were found only in the top 6 mm of CH-1. An exercise to determine how much the mud layers affected the growth rate was performed on the top ~ 6 mm. The thicknesses of the mud layers with measurable thickness were subtracted from the total thickness of the section, and the growth rate based on the ^{210}Pb radiometric dating was calculated from this shorter distance. The resulting growth rate of 0.038 mm/year was well within the 0.04 ± 0.004 mm/yr provided by using the length including the mud layers, meaning mud layer thickness is unlikely to play a role in the growth rates of CH-1.

Mud layers with measurable widths were found only in the top 6 mm of CH-1, yet their physical presence or the presence of mud lobes outside the central growth axis may still have had an effect on growth rates by creating a pool for the water, thereby reducing the total surface area available for the deposition of calcite on the top surface of CH-1. If deposition took place in the bottom of a shallow pool created by mud lobes instead of down the entire length of CH-1 as is the case in most stalagmites, then the stalagmite's growth would have been preferentially upward, which has been observed in its shape as noted earlier.

Figure 48 is a composite of four datasets; growth rate, δ^{18}O values, mud lobe frequency, and the location of the rapid drop in mud layer frequency. Some correlation between the growth rate and climate may be present in the top 3 + mm where a trend of increasing δ^{18}O values (drier conditions) corresponds to the slowest growth rate in CH-1.

A correlation between the growth rate in the top 3 cm based mainly on layer counting, and the drop in mud layer frequency at ~1200 AD may suggest a correlation between the dating technique and the drop in frequency at first glance. However this correlation has to be discounted due to the increase in mud layer frequency over the last ~150 years, during which time the same dating technique was employed as during the rest of the period after 1200 AD. Furthermore, I suspect that the change in growth rate decreased earlier in the record than could be measured. The layer counting technique used on the top 30 mm is dependent upon having high-resolution fluorescent images to count small-scale variations in brightness of fluorescence. High-resolution images were not taken of the section of CH-1 spanning the 109 mm below the top section, so the last age data point was at 30 mm before the U/Th 3 data point. This leaves a majority of CH-1, 109 mm, of the dating to interpolation between two data points. An important piece of future work for this project will be to acquire high-resolution images of the entire length of CH-1 to perform fluorescence layer counting and remove much of the uncertainty in the integrated age model, to refine the timing of the drop in mud layer frequency observed in CH-1.

Figure 48 also illustrates a trend in $\delta^{18}O$ values related to mud layer frequency. After ~1200 AD when mud layer frequency decreases, $\delta^{18}O$ values generally increase. This relationship may be evidence of the waning influence of cyclogenic water, and its associated negative $\delta^{18}O$ value anomalies during that period of low TC activity. This assumes that the proportion of TCs recorded by mud layers has been consistent throughout this entire record. Nevertheless, if these trends are related, it would suggest

that TCs have been a non-trivial source of the Yucatán's precipitation for at least 2,000 years.

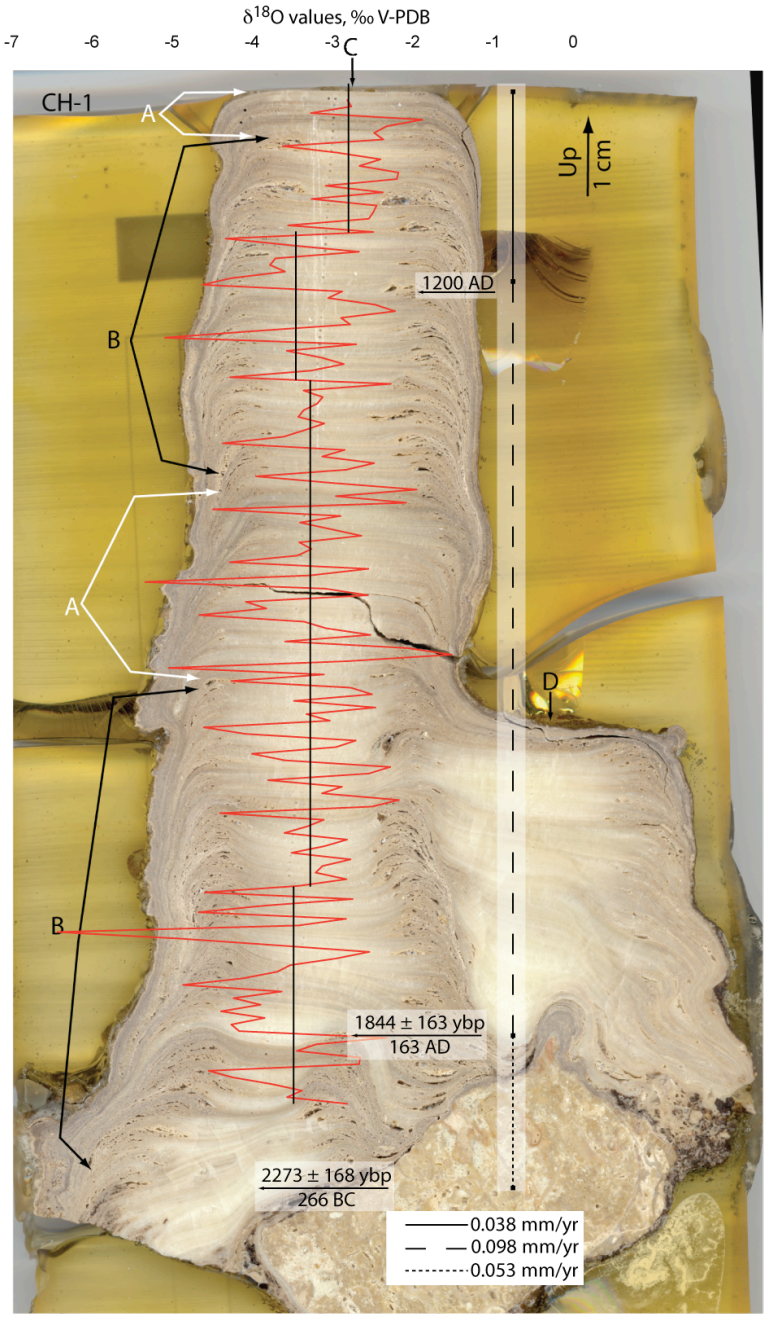

Figure 48. Integration of CH-1 data, displaying $\delta^{18}O$ values with approximate averages drawn in black, age model, mud lobe location, and TC frequency drop location, denoted by white arrow at 1200 AD.

ii. *Land use*

The high-resolution $\delta^{18}O$ and $\delta^{13}C$ datasets have revealed another interesting feature. After the year 1915, the $\delta^{13}C$ values begin to drop dramatically to the lowest point since 1662 AD. By 1929, the $\delta^{13}C$ values were -6.05‰, 3.19‰ lower than in 1915 (Figure 49). After this low-point, the $\delta^{13}C$ values return to about the average levels for the remainder of the record, with much higher variability in this time than any time previous. The $\delta^{18}O$ values follow the same trends, but not to any extreme that would make them appear out of the ordinary compared to the remainder of the high-resolution record. Potential hypotheses to describe this $\delta^{13}C$ value anomaly include: 1915 corresponded to the time when the stalactite that previously fed drip water to CH-1 was broken off, and the drip source became the soda straw that currently exists, leading to different fractionation of the $\delta^{13}C$ values en route to CH-1. Calculations done based on work from Baskaran and Illife (1995) on the growth rate of a soda straw from Texas led to the conclusion that the soda straw was too long for this to be a satisfactory explanation.

A possible connection between land use and $\delta^{13}C$ values became the explanation of choice when it was realized that the anomaly corresponded to a region-wide boom in *Agave Fourcroydes*, (Henequen) production. *Agave Fourcroydes* is a succulent plant cultivated for its coarse, strong fibers, which are used to make twine and many other types of textiles (Nobel, 1985). It is grown almost exclusively in the Yucatán peninsula, and has dominated the local economy since ~1900. The peak in *Agave Fourcroydes* cultivation on the peninsula occurred in 1916, but has remained an important crop. In

1965, *Agave Fourcroydes* from the Yucatán supplied 18% of the world total of hard fibers (Nobel, 1985). Production of *Agave Fourcroydes* decreased with the invention of synthetic fibers in the 1950s. *Agave Fourcroydes* is cultivated in rows with space between the rows enough for harvesters to weed and harvest the plants (Figure 50)

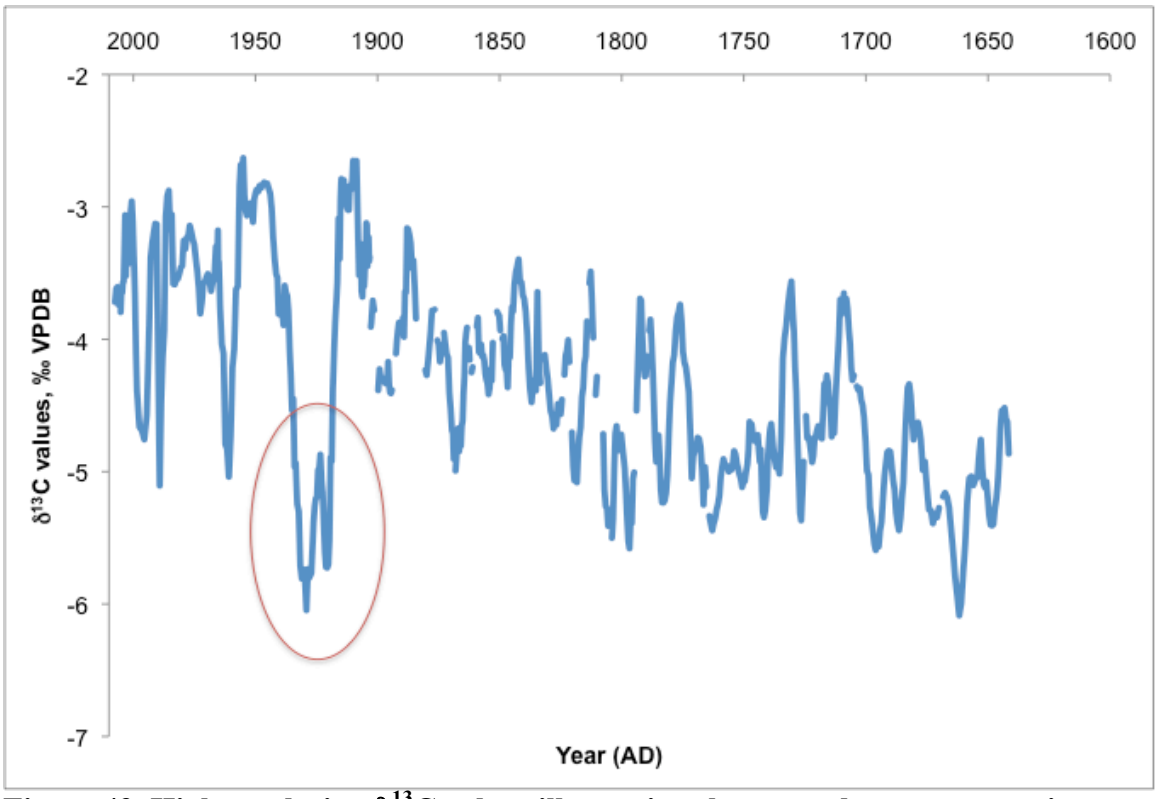

Figure 49. High-resolution $\delta^{13}C$ values illustrating the anomaly present starting at ~1915 (circled).

. *Agave Fourcroydes'* photosynthetic pathway is Crassulacean acid metabolism (CAM), like most succulents. CAM plants, like C_4 plants, thrive in arid, high-temperature regions, and are characterized by $\delta^{13}C$ values ~13‰ higher than C_3 plants, or on average ~ -13‰ (Bender, 1968; Sharp, 2007; Smith and Epstein, 1971). C4 and CAM plants like maize and other shrubs and cactus dominate the Yucatán, so this drop may

seem somewhat unexpected. Two potential explanations are 1) Intense cultivation of *Agave Fourcroydes* may have increased the total plant material produced on the land at Rancho Chaltun-Ha making the $\delta^{13}C$ values of the soil CO_2 under Rancho Chaltun-Ha migrate towards the -13‰ value expected of CAM and C_4 plants. 2) A total reduction in plant productivity due to the removal of native forests and brush land and replacement with an *Agave Fourcroydes* plantation, having a net negative effect on the $\delta^{13}C$ values of soil CO_2. The recovery of the $\delta^{13}C$ values and subsequent extremes may be due to the waxing and waning of *Agave* production on the hacienda above Chaltun-Ha in response to fluctuations in the world henequen market

Figure 50. A modern *Agave Fourcroydes* plantation. Photo courtesy of Amy Frappier.

.

Although these findings are preliminary, and work correlating the $\delta^{13}C$ values to better constrained land-use histories would need to be done before this record could be assumed to be a proxy for land-use, it at least provides hope that a $\delta^{13}C$ value land-use proxy may exist in stalagmites, and may help archeologists determine how ancient cultures used their land. A continuation of the high-resolution data set farther back in time in CH-1 may help resolve other land use changes during the time of the Maya.

f. *Sources of error*

Specific sources of error include placing high-resolution stable isotope data points in the precise stratigraphic location from which they were collected from due to the small scale required to measure high-resolution climate variability (Figure 51). At ~ 5 samples per mm, it is difficult to assign an exact location to individual samples within CH-1.

The error involved in the age model stems from the errors reported from the radiogenic dating methods, as well as human error in counting fluorescence gray scale intensity cycles. Further errors are introduced to the fluorescence gray scale intensity peak counting when the lines used to analyze the gray scale intensity go over a small blemish, crystal edge, or abnormality in CH-1 polished cross-section, which may add a year to the counting. Mud layers may also add to the total number of years counted by being darker than the surrounding calcite, creating a low gray scale intensity region that can be naively counted as a false year. Attempts to minimize this potential error were undertaken as described in Chapter 2; by subtracting visible mud layers that were thick

enough to be evident in the fluorescence intensity curves from the final age assigned to each individual layer

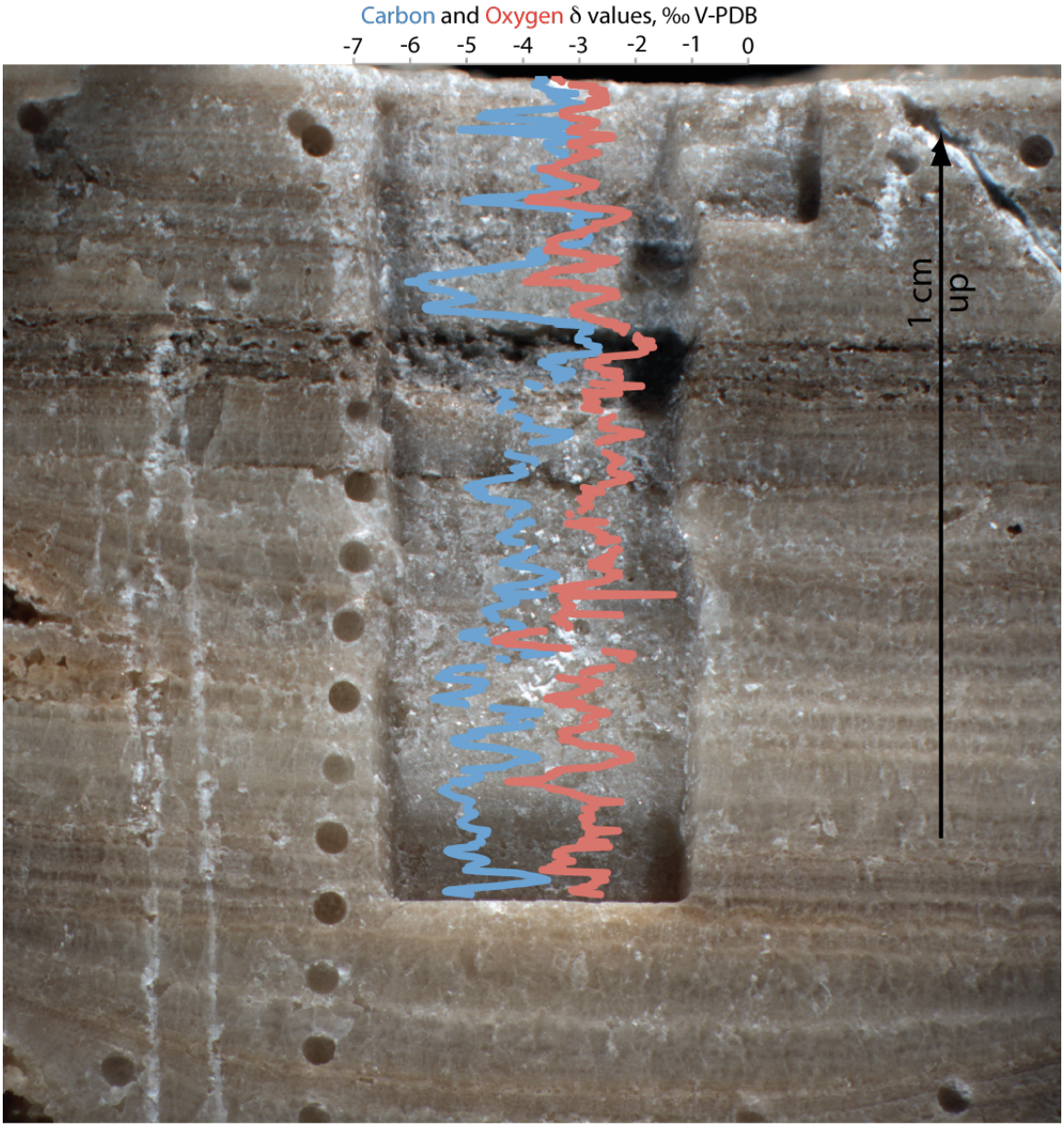

Figure 51. Showing the approximate locations of the first 560 samples.

.

The slow growth rate of CH-1 made using short-lived radioisotopes like ^{210}Pb difficult, because there was only a very thin amount of calcite at the top of CH-1 young enough to contain the necessary excess ^{210}Pb isotopes before they all decayed. This also made it impossible to use anthropogenic isotopes for dating, such as ^{137}Cs, because this dating method would have required many samples from a 1.6 mm section of CH-1. Mud in the calcite made U/Th dating difficult due to the excess initial Th problem, leaving the majority of CH-1, ~109 mm, with age constraints only available on either end.

6. Conclusions

Overall, the mud layer paleotempestology proxy in CH-1 was successfully demonstrated by the results of this study. Multiple lines of evidence including direct evidence from the correlations with the mud to the historical TC record made in CH-1 with 100% accuracy, the presence of the same trends in TC frequency recorded in other proxies from the Caribbean, and the general reproducibility of the climate signal from other paleoclimate records from the region lead to the conclusion that CH-1's mud layers correlate to TCs. Exactly why some TCs are responsible for depositing mud onto CH-1 and others are not still needs to be determined. Other climate signals present in CH-1 may be of interest to some researchers, and need to be investigated further in the future, i.e., how TC frequency in the Yucatan has changed in relation to other sites in the Atlantic Basin, or how TC activity or drought may have affected the Mayan civilization.

This study described a new stalagmite morphology related to flood frequency and postulated that identifying this shape in the field may be useful for the selection of stalagmites for future paleotempestology studies using this mud layer proxy.

CH-1 recorded TC strikes, mega-droughts, land-use changes related to the henequen boom in the early 20th century recorded in $\delta^{13}C$ values, and possibly global climatic events, including "The Year Without a Summer" and the Little Ice Age.

The comparison of CH-1 to other paleoclimate records from the Yucatán revealed trends in the timing and onset of some droughts. The drought that begun ~1000 AD appears to have begun in the south, near Lake Chichancanab, and east, near Punta Laguna, before it affected the northwestern portion of the Yucatán peninsula near Rancho Chaltun-Ha.

The TC frequency trend recorded in CH-1 suggests that TC frequency in the Yucatán is on the rise, and could mean that the Yucatán, as well as much of the rest of the Caribbean, is going to be experiencing TC seasons unlike any in memory or recorded history.

The importance of developing multiple TC proxies in climatic records is evident in the amount of damage that TCs can do. Many people lose their lives from flooding associated with TCs and many more lose their homes and other possessions. If the trend in Caribbean TCs observed in CH-1 continues with an increase in storms back to some "normal" level, people living in the region may have tough times ahead. To know if this trend is truly related to the total number of TCs in the basin as is suggested by the geographical differences between the published TC records of Liu and Fearn (2000), and

Donnelly and Woodruff (2007), and the record reported here from CH-1, more studies from geographically varied locations is necessary. Not all TC proxies are applicable everywhere, and so a variety of tools are needed for the science of paleotempestology to learn more about the past and make predictions for the future.

7. Works Cited:

Appleby, P.G., and Oldfield, F., 1978, The calculation of lead-210 dates assuming a constant rate of supply of unsupported 210Pb to the sediment: Catena, v. 5, p. 1-8.

—, 1983, The Assessment of Pb-210 Data from Sites with Varying Sediment Accumulation Rates: Hydrobiologia, v. 103, p. 29-35.

—, 1992, Application of Pb-210 to sedimentation studies, *in* Ivanovich, M., and Harmon, R.S., eds., Uranium-series Disequilibrium: Applications to Earth, Marine, and Environmental Problems: Oxford, Claredon Press, p. 731-778.

Ayalon, A., Bar-Matthews, M., and Sass, E., 1998, Rainfall-recharge relationships within a karstic terrain in the eastern Mediterranean semi-arid region, Israel: delta O-18 and delta D characteristics: Journal of Hydrology, v. 207, p. 18-31.

Baker, A., Smith, C.L., Jex, C., Fairchild, I.J., Genty, D., and Fuller, L., 2008, Annually laminated speleothems: a Review: International Journal of Speleology, v. 37, p. 193-206.

Baldini, J.U.L., McDermott, F., Hoffmann, D.L., Richards, D.A., and Clipson, N., 2008, Very high-frequency and seasonal cave atmosphere P-CO2 variability: Implications for stalagmite growth and oxygen isotope-based paleoclimate records: Earth and Planetary Science Letters, v. 272, p. 118-129.

Baskaran, M., and Iliffe, T.M., 1993, Age determination of recent cave deposits using excess 210Pb - a new technique: Geophysical Research Letters, v. 20, p. 603-606.

Bender, M.M., 1968, Mass Spectrometric Studies of Carbon 13 Variations in Corn and Other Grasses: Radiocarbon, v. 10, p. 468-&.

Bischoff, J.L., and Fitzpatrick, J.A., 1991, U-Series Dating of Impure Carbonates - an Isochron Technique Using Total-Sample Dissolution: Geochimica Et Cosmochimica Acta, v. 55, p. 543-554.

Bosch, R.F., and White, W.B., 2007, Lithofacies and transport of clastic sediments in karstic aquifers, *in* Ira D. Sasowsky, and Mylroie, J., eds., Studies of Cave Sediments: Dordrecht, Springer.

Cole-Dai, J., Ferris, D., Lanciki, A., Savarino, J., Baroni, M., and Thiemens, M.H., 2009, Cold decade (AD 1810-1819) caused by Tambora (1815) and another (1809) stratospheric volcanic eruption: Geophysical Research Letters, v. 36, p. 6.

Curtis, J.H., Hodell, D.A., and Brenner, M., 1996, Climate variability on the Yucatan Peninsula (Mexico) during the past 3500 years, and implications for Maya Cultural Evolution: Quaternary Research, v. 46, p. 37-47.

Dansgaard, W., 1964, Stable isotopes in precipitation: Tellus, v. 16, p. 436-468.

Doehring, D., 1971, Cave development during a catastrophic storm in Great Valley of Virginia: Science, v. 174, p. 1327.

Donnelly, J.P., Bryant, S.S., Butler, J., Dowling, J., Fan, L., Hausmann, N., Newby, P., Shuman, B., Stern, J., Westover, K., and Webb, T., 2001a, 700 yr sedimentary record of intense hurricane landfalls in southern New England: Geological Society of America Bulletin, v. 113, p. 714-727.

Donnelly, J.P., Butler, J., Roll, S., Wengren, M., and Webb, T., 2004, A backbarrier overwash record of intense storms from Brigantine, New Jersey, p. 107-121.
Donnelly, J.P., Roll, S., Wengren, M., Butler, J., Lederer, R., and Webb, T., 2001b, Sedimentary evidence of intense hurricane strikes from New Jersey: Geology, v. 29, p. 615-618.
Donnelly, J.P., and Woodruff, J.D., 2007, Intense hurricane activity over the past 5,000 years controlled by El Nino and the West African monsoon: Nature, v. 447, p. 465-468.
Dorale, J.A., Gonzalez, L.A., Reagan, M.K., Pickett, D.A., Murrell, M.T., and Baker, R.G., 1992, A High-Resolution Record of Holocene Climate Change in Speleothem Calcite from Cold Water Cave, Northeast Iowa: Science, v. 258, p. 1626-1630.
Dorale, J.A., Lepley, S., and Edwards, R.L., 2005, The ultimate flood recorder: flood-deposited sediments preserved in stalagmites, European Geoscience Union.
Dorale, J.A., and Liu, Z.H., 2009, Limitations of Hendy Test Criteria in Judging the Paleoclimatic Suitability of Speleothems and the Need for Replication: Journal of Cave and Karst Studies, v. 71, p. 73-80.
Dreybrodt, W., 1980, Deposition of calcite from thin films of natural calcareous solutions and the growth of speleothems: Chemical geology, v. 29, p. 89-105.
Drysdale, R.N., Zanchetta, G., Hellstrom, J.C., Fallick, A.E., Zhao, J.X., Isola, I., and Bruschi, G., 2004, Palaeoclimatic implications of the growth history and stable isotope (delta O-18 and delta C-13) geochemistry of a Middle to Late Pleistocene stalagmite from central-western Italy: Earth and Planetary Science Letters, v. 227, p. 215-229.
Edwards, R.L., Chen, J.H., and Wasserburg, G.J., 1987, U-238 U-234-Th-230-Th-232 Systematics and the Precise Measurement of Time over the Past 500000 Years: Earth and Planetary Science Letters, v. 81, p. 175-192.
Elsner, J.B., and Kara, A.B., 1999, Hurricanes of the North Atlantic: New York, Oxford.
Emanuel, K., 2003, Tropical cyclones: Annual Review of Earth and Planetary Sciences, v. 31, p. 75-104.
Escolero, O., Marin, L.E., Dominguez-Mariani, E., and Torres-Onofre, S., 2007, Dynamic of the freshwater-saltwater interface in a karstic aquifer under extraordinary recharge action: the Merida Yucatan case study, Springer, p. 719-723.
Fairchild, I.J., Smith, C.L., Baker, A., Fuller, L., Spotl, C., Mattey, D., and McDermott, F., 2006, Modification and preservation of environmental signals in speleothems: Earth-Science Reviews, v. 75, p. 105-153.
Fiorillo, F., 2009, Spring hydrographs as indicators of droughts in a karst environment: Journal of Hydrology, v. 373, p. 290-301.
Flynn, W.W., 1968, Determination of Low Levels of Polonium-210 in Environmental Materials: Analytica Chimica Acta, v. 43, p. 221-&.
Frappier, A., 2007, Interpreting stable isotopes in tropical stalagmites; masking of inter-annual climate proxy signals by residual tropical cyclone water from Hurricane Mitch: Abstracts with programs - Geological Society of America, v. 39, p. 98.

Frappier, A., Sahagian, D., Gonzalez, L.A., and Carpenter, S.J., 2002a, El Nino events recorded by stalagmite carbon isotopes: Science, v. 298, p. 565-565.
—, 2002b, El Nino events recorded by stalagmite carbon isotopes.: Science, v. 298, p. 565.
Frappier, A.B., 2008a, A stepwise screening system to select storm-sensitive stalagmites: Taking a targeted approach to speleothem sampling methodology: Quaternary International, v. 187, p. 25-39.
—, 2008b, Masking of inter-annual climate proxy signals by residual tropical cyclone water from Hurricane Mitch: Observations and challenges for low-latitude speleothem paleoclimatology, Goldschmidt Conference: Vancouver, Canada.
Frappier, A.B., Knutson, T., Liu, K.B., and Emanuel, K., 2008, Perspective: coordinating paleoclimate research on tropical cyclones with hurricane-climate theory and modelling: Tellus, p. 529-537.
Frappier, A.B., Sahagian, D., Carpenter, S.J., Gonzalez, L.A., and Frappier, B.R., 2007, Stalagmite stable isotopes record of recent tropical cyclone events: Geology, v. 35, p. 111-114.
Garcia-Herrera, R., Gimeno, L., Ribera, P., and Hernandez, E., 2005, New records of Atlantic hurricanes from Spanish documentary sources: Journal of Geophysical Research-Atmospheres, v. 110, p. 7.
Gedzelman, S., Lawrence, J., Gamache, J., Black, M., Hindman, E., Black, R., Dunion, J., Willoughby, H., and Zhang, X.P., 2003, Probing hurricanes with stable isotopes of rain and water vapor: Monthly Weather Review, v. 131, p. 1112-1127.
Giannini, A., Kushnir, Y., and Cane, M.A., 2000, Interannual variability of Caribbean rainfall, ENSO, and the Atlantic Ocean: Journal of Climate, v. 13, p. 297-311.
Goede, A., 1994, Continuous Early Last Glacial Paleoenvironmental Record from a Tasmanian Speleothem Based on Stable-Isotope and Minor Element Variations: Quaternary Science Reviews, v. 13, p. 283-291.
Gonzalez, L.A., and Lohmann, K.C., 1988, Controls on mineralogy and composition of spelean carbonates: Carlsbad Caverns, New Mexico, *in* James, N.P., and Choquette, P.W., eds., Paleokarst: New York, Springer-Verlag, p. 81-101.
Gray, W.M., 1968, Global View of Origin of Tropical Disturbances and Storms: Monthly Weather Review, v. 96, p. 669-700.
Haug, G.H., Gunther, D., Peterson, L.C., Sigman, D.M., Hughen, K.A., and Aeschlimann, B., 2003, Climate and the collapse of Maya civilization: Science, v. 299, p. 1731-1735.
Haug, G.H., Hughen, K.A., Sigman, D.M., Peterson, L.C., and Rohl, U., 2001, Southward migration of the intertropical convergence zone through the Holocene: Science, v. 293, p. 1304-1308.
Hendy, C.H., 1971, The isotopic geochemistry of speleothems--I. The calculation of the effects of different modes of formation on the isotopic composition of speleothems and their applicability as palaeoclimatic indicators: Geochimica et Cosmochimica Acta, v. 35, p. 801-824.

Hodell, D.A., Brenner, M., and Curtis, J.H., 2005a, Terminal Classic drought in the northern Maya lowlands inferred from multiple sediment cores in Lake Chichancanab (Mexico): Quaternary Science Reviews, v. 24, p. 1413-1427.

Hodell, D.A., Brenner, M., Curtis, J.H., Medina-Gonzalez, R., Can, E.I.C., Albornaz-Pat, A., and Guilderson, T.P., 2005b, Climate change on the Yucatan Peninsula during the little ice age: Quaternary Research, v. 63, p. 109-121.

Hodell, D.A., Curtis, J.H., and Brenner, M., 1995, Possible Role of Climate in the Collapse of Classic Maya Civilization: Nature, v. 375, p. 391-394.

Hutton, J., 1788, Theory of the earth; or an investigation of the laws observable in the composition, dissolution, and restoration of land upon the globe, Volume I of the Transactions of the Royal Society of Edinburgh.

Jones, P.D., and Mann, M.E., 2004, Climate over past millennia: Reviews of Geophysics, v. 42, p. 42.

Kaufmann, G., and Dreybrodt, W., 2004, Stalagmite growth and palaeo-climate: an inverse approach: Earth and Planetary Science Letters, v. 224, p. 529-545.

Kendall, A.C., and Broughton, P.L., 1978, Origin of Fabrics in Speleothems Composed of Columnar Calcite Crystals: Journal of Sedimentary Petrology, v. 48, p. 519-538.

Labonne, M., Hillaire-Marcel, C., Ghaleb, B., and Goy, J.L., 2002, Multi-isotopic age assessment of dirty speleothem calcite: an example from Altamira Cave, Spain: Quaternary Science Reviews, v. 21, p. 1099-1110.

Lachniet, M.S., 2009, Climatic and environmental controls on speleothem oxygen-isotope values: Quaternary Science Reviews, v. 28, p. 412-432.

Lachniet, M.S., Asmerom, Y., Burns, S.J., Patterson, W.P., Polyak, V.J., and Seltzer, G.O., 2004, Tropical response to the 8200 yr BP cold event? Speleothem isotopes indicate a weakened early Holocene monsoon in Costa Rica: Geology, v. 32, p. 957-960.

Landsea, C., Anderson, C., Charles, N., Clark, G., Fernandez-Partagas, J., Hungerford, P., Neumann, C., and Zimmer, M., 2000, The Atlantic hurricane database re-analysis project: Results for 1851-85, 24th Conference on Hurricanes and Tropical Meteorology/10th Conference on Interaction of the Sea and Atmosphere: Ft Lauderdale, Fl, Amer Meteorological Society, p. 542-543.

Landsea, C.W., Glenn, D.A., Bredemeyer, W., Chenoweth, M., Ellis, R., Gamache, J., Hufstetler, L., Mock, C., Perez, R., Prieto, R., Sanchez-Sesma, J., Thomas, D., and Woolcock, L., 2008, A reanalysis of the 1911-20 Atlantic hurricane database: Journal of Climate, v. 21, p. 2138-2168.

Lane, C.S., Mora, C.I., Horn, S.P., and Orvis, K.H., 2008, Sensitivity of bulk sedimentary stable carbon isotopes to prehistoric forest clearance and maize agriculture: Journal of Archaeological Science, v. 35, p. 2119-2132.

Lauritzen, S.E., 1993, High-Resolution Paleotemperature Proxy Record for the Last Interglaciation Based on Norwegian Speleothems, LIGA Symposium on the Last Interglaciation in Arctic and Subarctic Regions: Time Frame, Structure, and Duration: Saint-Michel Des Saints, Canada, p. 133-146.

Lawrence, J., and Gedzelman, S., 1996, Low stable isotope ratios of tropical cyclone rains: Geophysical Research Letters, v. 23, p. 527-530.
Lawrence, J.R., 1998, Isotopic spikes from tropical cyclones in surface waters: Opportunities in hydrology and paleoclimatology: Chemical Geology, v. 144, p. 153-160.
Linge, H., Lauritzen, S.E., and Lundberg, J., 2001, Stable isotope stratigraphy of a late last interglacial speleothem from Rana, northern Norway: Quaternary Research, v. 56, p. 155-164.
Liu, K.B., 2007, Uncovering prehistoric hurricane activity - Examination of the geological record reveals some surprising long-term trends: American Scientist, v. 95, p. 126-133.
Liu, K.B., and Fearn, M.L., 1993, Lake-Sediment Record of Late Holocene Hurricane Activities from Coastal Alabama: Geology, v. 21, p. 793-796.
—, 2000, Reconstruction of prehistoric landfall frequencies of catastrophic hurricanes in northwestern Florida from lake sediment records: Quaternary Research, v. 54, p. 238-245.
Liu, K.B., Shen, C.M., and Louie, K.S., 2001, A 1,000-year history of typhoon landfalls in guangdong, southern China, reconstructed from Chinese historical documentary records: Annals of the Association of American Geographers, v. 91, p. 453-464.
Mann, M.E., 2007, Climate over the past two millennia: Annual Review of Earth and Planetary Sciences, v. 35, p. 111-136.
Mann, M.E., Zhang, Z.H., Rutherford, S., Bradley, R.S., Hughes, M.K., Shindell, D., Ammann, C., Faluvegi, G., and Ni, F.B., 2009, Global Signatures and Dynamical Origins of the Little Ice Age and Medieval Climate Anomaly: Science, v. 326, p. 1256-1260.
Marin, L., 1990, Field investigation and numerical simulation of the karstic aquifer of northwestern Yucatán, Mexico [PhD thesis]: DeKalb, Northern Illinois University.
McCloskey, T.A., and Keller, G., 2006, 5000 year sedimentary record of hurricane strikes on the central coast of Belize, Workshop on Hurricanes and Typhoons - From the Field Records to the Forecast: Lafayette, LA, p. 53-68.
McDermott, F., 2004, Palaeo-climate reconstruction from stable isotope variations in speleothems: a review, p. 901-918.
Me-Bar, Y., and Valdez, F., 2003, Droughts as random events in the Maya lowlands: Journal of Archaeological Science, v. 30, p. 1599-1606.
Mickler, P.J., Banner, J.L., Stern, L., Asmerom, Y., Edwards, R.L., and Ito, E., 2004, Stable isotope variations in modern tropical speleothems: Evaluating equilibrium vs. kinetic isotope effects: Geochimica Et Cosmochimica Acta, v. 68, p. 4381-4393.
Mickler, P.J., Stern, L.A., and Banner, J.L., 2006, Large kinetic isotope effects in modern speleothems: Geological Society of America Bulletin, v. 118, p. 65-81.
Miller, D.L., Mora, C.I., Grissino-Mayer, H.D., Mock, C.J., Uhle, M.E., and Sharp, Z., 2006, Tree-ring isotope records of tropical cyclone activity: Proceedings of the

National Academy of Sciences of the United States of America, v. 103, p. 14294-14297.
Niggemann, S., Mangini, A., Richter, D.K., and Wurth, G., 2003, A paleoclimate record of the last 17,600 years in stalagmites from the B7 cave, Sauerland, Germany: Quaternary Science Reviews, v. 22, p. 555-567.
Nittrouer, C.A., Sternberg, R.W., Carpenter, R., and Bennett, J.T., 1979, Use of Pb-210 Geochronology as a Sedimentological Tool - Application to the Washington Continental-Shelf: Marine Geology, v. 31, p. 297-316.
NOAA, 2009, Historical Hurricane Tracks.
Nobel, P.S., 1985, Par, Water, and Temperature Limitations on the Productivity of Cultivated Agave-Fourcroydes (Henequen): Journal of Applied Ecology, v. 22, p. 157-173.
Nott, J., 2003, Palaeotempestology: the study of prehistoric tropical cyclones--a review and implications for hazard assessment: Environmental International, v. 30, p. 443.
Nott, J., Haig, J., Neil, H., and Gillieson, D., 2007, Greater frequency variability of landfalling tropical cyclones at centennial compared to seasonal and decadal scales: Earth and planetary science letters, p. 367-372.
Orland, I.J., Bar-Matthews, M., Kita, N.T., Ayalon, A., Matthews, A., and Valley, J.W., 2009, Climate deterioration in the Eastern Mediterranean as revealed by ion microprobe analysis of a speleothem that grew from 2.2 to 0.9 ka in Soreq Cave, Israel: Quaternary Research, v. 71, p. 27-35.
Palmén, E., 1948, On the formation and structure of tropical hurricanes: Geophysica, v. 3, p. 26-39.
Perry, E., Marin, L., McClain, J., and Velazquez, G., 1995, Ring of Cenotes (Sinkholes), Northwest Yucatan, Mexico - Its Hydrogeologic Characteristics and Possible Association with the Chicxulub Impact Crater: Geology, v. 23, p. 17-20.
Perry, E., Paytan, A., Pedersen, B., and Velazquez-Oliman, G., 2009, Groundwater geochemistry of the Yucatan Peninsula, Mexico: Constraints on stratigraphy and hydrogeology: Journal of Hydrology, v. 367, p. 27-40.
Pope, K.O., Ocampo, A.C., and Duller, C.E., 1991, Mexican Site for K/T Impact Crater: Nature, v. 351, p. 105-105.
Pope, K.O., Rejmankova, E., and Paris, J.F., 2001, Spaceborne imaging radar-C (SIR-C) observations of groundwater discharge and wetlands associated with the Chicxulub impact crater, northwestern Yucatan Peninsula, Mexico: Geological Society of America Bulletin, v. 113, p. 403-416.
Riehl, H., 1948, On the Formation of Typhoons: Journal of Meteorology, v. 5, p. 247-264.
Rosenfeld, J.H., 2001, Economic potential of the Yucatan Block of Mexico, Guatemala and Belize: Program and Abstracts - Society of Economic Paleontologists. Gulf Coast Section. Research Conference, v. 21, p. 713-723.
Rousseau, L., Beauchamp, J., Falgures, C., Emblanch, C., Genty, D., Bahain, J.J., and Blamart, D., 2005, Isotopic and biogeochemical markers help in reconstructing

the Lazaret Cave environment (Nice, France) during Upper Pleistocene (IOS 5): Comptes Rendus Geoscience, v. 337, p. 1348-1354.
Saurer, M., Borella, S., and Leuenberger, M., 1997, delta O-18 of tree rings of beech (Fagus silvatica) as a record of delta O-18 of the growing season precipitation: Tellus Series B-Chemical and Physical Meteorology, v. 49, p. 80-92.
Schwarcz, H.P., and Latham, A.G., 1989, Dirty Calcites .1. Uranium-Series Dating of Contaminated Calcite Using Leachates Alone: Chemical Geology, v. 80, p. 35-43.
Servicio Meteorologico Nacional, 2008, Conagua: Comision Nacional del Agua,, Volume 2008.
Sharp, Z., 2007, Prinicples of Stable Isotope Geochemistry: Upper Saddle River, NJ, Pearson Prentice Hall.
Shen, C.C., Edwards, R.L., Cheng, H., Dorale, J.A., Thomas, R.B., Moran, S.B., Weinstein, S.E., and Edmonds, H.N., 2002, Uranium and thorium isotopic and concentration measurements by magnetic sector inductively coupled plasma mass spectrometry: Chemical Geology, v. 185, p. 165-178.
Smith, B.N., and Epstein, S., 1971, 2 Categories of C-13/C-12 Ratios for Higher Plants: Plant Physiology, v. 47, p. 380-&.
Spotl, C., and Mattey, D., 2006, Stable isotope microsampling of speleothems for palaeoenvironmental studies: A comparison of microdrill, micromill and laser ablation techniques: Chemical Geology, p. 48-58.
Steinich, B., and Marin, L.E., 1996, Hydrogeological investigations in northwestern Yucatan, Mexico, using resistivity surveys: Ground Water, v. 34, p. 640-658.
Sweetwood, R.V., Terry, R.E., Beach, T., Dahlin, B.H., and Hixson, D., 2009, The Maya Footprint: Soil Resources of Chunchucmil, Yucatan, Mexico: Soil Science Society of America Journal, v. 73, p. 1209-1220.
Tooth, A.F., and Fairchild, I.J., 2003, Soil and karst aquifer hydrological controls on the geochemical evolution of speleothem-forming drip waters, Crag Cave, southwest Ireland: Journal of Hydrology, v. 273, p. 51-68.
Vargas, R., and Allen, M.F., 2008, Diel patterns of soil respiration in a tropical forest after Hurricane Wilma: Journal of Geophysical Research-Biogeosciences, v. 113, p. 10.
Vivó Escoto, J.A., 1964, Handbook of Middle American Indians, *in* Wauchope, R., and West, R.C., eds., Handbook of Middle American Indians, Volume I, Natural Environment and Early Cultures: Austin, University of Texas Press, p. 187-215.
Webster, J.W., Brook, G.A., Railsback, L.B., Cheng, H., Edwards, R.L., Alexander, C., and Reeder, P.P., 2007, Stalagmite evidence from Belize indicating significant droughts at the time of Preclassic Abandonment, the Maya Hiatus, and the Classic Maya collapse: Palaeogeography Palaeoclimatology Palaeoecology, v. 250, p. 1-17.
White, W.B., 2007, Cave sediments and paleoclimate: Journal of Cave and Karst Studies, v. 69, p. 76-93.
Woodruff, J.D., Donnelly, J.P., Mohrig, D., and Geyer, W.R., 2008, Reconstructing relative flooding intensities responsible for hurricane-induced deposits from Laguna Playa Grande, Vieques, Puerto Rico: Geology, v. 36, p. 391-394.

8. Appendix:

PB-210 raw data

10 samples drilled from the back of the slab of CH-1 were analyzed by Dr. Reide Corbett at East Carolina Universtiy in an Ortec Octete alpha detector. Samples ran from Mar 18th until Mar 22.

number	weight g	distance from top mm	XS Pb-210 (dpm/g)			Total Pb-210 (dpm/g)		
1	0.10148	0	**1.92**	+/-	**0.26**	2.10	+/-	0.26
2	0.10201	2.7	**0.18**	+/-	**0.14**	0.36	+/-	0.13
3	0.10698	6.3	**0.02**	+/-	**0.10**	0.20	+/-	0.08
4	0.10776	11	**0.06**	+/-	**0.13**	0.24	+/-	0.12
5	0.10883	22.1	**-0.01**	+/-	**0.12**	0.17	+/-	0.11
6	0.11164	41.1	**0.04**	+/-	**0.12**	0.22	+/-	0.11
7	0.1241	62.8	**0.02**	+/-	**0.14**	0.20	+/-	0.12
8	0.15913	95.6	**-0.06**	+/-	**0.09**	0.12	+/-	0.06
9	0.13698	141.3	**0.03**	+/-	**0.10**	0.21	+/-	0.07
10	0.13332	171.1	**-0.11**	+/-	**0.09**	0.07	+/-	0.07

SUMMARY OUTPUT

Regression Statistics	
Multiple R	0.9951926
R Square	0.9904084
Adjusted R	0.9808168
Standard E	0.3167557
Observatio	3

ANOVA

	df	*SS*	*MS*	*F*	*nificance F*
Regression	1	10.36028627	10.36	103	0.062
Residual	1	0.100334204	0.1		
Total	2	10.46062048			

	Coefficients	*Standard Error*	*t Stat*	*P-value*	*Lower 95%*	*Upper 95%*	*Lower 95.0%*	*Upper 95.0%*
Intercept	0.5071318	0.280428818	1.808	0.32	-3.06	4.070318	-3.056	4.07
X Variable	-0.7200922	0.070864179	-10.2	0.06	-1.62	0.180323	-1.621	0.18

U/Th data collected from 4 samples on the front of the slab of CH-1 and analyzed by Dr. Xianfeng Wang at the Minnesota Isotope Lab, Dept. of Geology & Geophysics, University of Minnesota, on May 15th.

^{230}Th dating results. The error is 2σ error.

Sample Number	^{238}U (ppb)	^{232}Th (ppt)	^{230}Th / ^{232}Th (atomic x10^{-6})	δ^{234}U* (measured)	^{230}Th / ^{238}U (activity)	^{230}Th Age (yr) (uncorrected)	^{230}Th Age (yr) (corrected)	$\delta^{234}U_{Initial}$** (corrected)	^{230}Th Age (yr BP)*** (corrected)
CH1-1	234.7 ±0.6	3214 ±65	28 ±2	-39.4 ±1.5	0.0229 ±0.0012	2636 ±138	**2221 ±325**	-40 ±2	**2163 ±325**
CH1-2	134.6 ±0.4	644 ±14	53 ±7	-36.1 ±1.8	0.0153 ±0.0021	1746 ±236	**1602 ±257**	-36 ±2	**1544 ±257**
CH1-3	215.4 ±0.5	718 ±15	86 ±7	-41.9 ±1.3	0.0174 ±0.0013	2003 ±146	**1902 ±163**	-42 ±1	**1844 ±163**
CH1-4	142.8 ±0.4	551 ±12	92 ±6	-29.2 ±1.8	0.0215 ±0.0013	2447 ±147	**2331 ±168**	-29 ±2	**2273 ±168**

* $\delta^{234}U = ([^{234}U/^{238}U]_{activity} - 1) \times 1000$. ** $\delta^{234}U_{initial}$ was calculated based on ^{230}Th age (T), i.e., $\delta^{234}U_{initial} = \delta^{234}U_{measured} \times e^{\lambda_{234}T}$. Corrected ^{230}Th ages assume the initial ^{230}Th/^{232}Th atomic ratio of 4.4 ±2.2 x10^{-6}. Those are the values for a material at secular equilibrium, with the bulk earth ^{232}Th/^{238}U value of 3.8. The errors are arbitrarily assumed to be 50%.
***B.P. stands for "Before Present" where the "Present" is defined as the year 1950 A.D.

The low-resolution (1 mm) and medium-resolution (0.2 mm) sampling and $\delta^{18}O$ and $\delta^{13}C$ analysis were both performed at the WHOI Micropaleontology Mass Spec Facility in Woods Hole, MA. A 100 sample sub-set of 0.02 mm was also obtained, although this dataset was not used in the study. 15-70 µg of powdered carbonate were analyzed for $\delta^{18}O$ and $\delta^{13}C$ values using a Finnigan-MAT 253 gas isotope ratio mass spectrometer (IRMS). 1.98 mm of microsampling and stable isotope analyses were both performed at the WHOI Micropaleontology Mass Spec Facility in Woods Hole, MA. CH-1 was milled along the growth axis at 20 µm intervals, at a trough depth of 140 µm. These analyses were performed during the months of Dec-Mar of 2008-2009. Results are reported in ‰, V-PDB. Samp id key: a – Axis 1, 1 mm. b – Axis 2, 1 mm. h1 – Hendy 1. h2 – Hendy 2. x – Hendy 3. y – Hendy 4. c – 0.2 mm. d – 0.002 mm.

Samp id	C13-MEAN	C13-STD	O18-MEAN	O18-STD	STD-VOLT	SAMP-VOLT	Depth cm	Wt. ug
I:a.01; c:First sample;	-3.53	0.04	-2.73	0.04	1.95	1.93	0.12	50
I:a.02;	-3.66	0.02	-2.67	0.02	2.15	2.14	0.22	53
I:a.03;	-5.10	0.01	-3.18	0.03	2.37	2.36	0.32	42
I:a.04; c:Within the top one of two distinct brown layers near the top;	-2.80	0.04	-1.78	0.09	0.76	0.77	0.42	23
I:a.05; c: Within the bottom of the two brown layers;	-3.90	0.03	-2.24	0.06	1.80	1.81	0.52	53
I:a.06;	-4.22	0.03	-2.38	0.11	1.07	1.07	0.62	34
I:a.07;	-3.79	0.03	-2.28	0.03	1.85	1.85	0.72	46
I:a.08;	-4.42	0.02	-3.53	0.03	1.52	1.51	0.82	37
I:a.09;	-5.06	0.01	-2.85	0.05	1.84	1.84	0.92	53
I:a.10;	-4.30	0.04	-2.30	0.07	1.17	1.16	1.02	33
I:a.11;	-4.84	0.02	-2.58	0.03	2.51	2.49	1.12	58

I:a.12;	-4.50	0.03	-2.08	0.06	1.10	1.12	1.22	31
I:a.13;	-5.26	0.04	-2.11	0.14	0.82	0.84	1.32	28
I:a.14;	-5.23	0.03	-2.99	0.04	1.65	1.67	1.42	43
I:a.15; c:Mud walled pool calcite;	-5.71	0.03	-2.29	0.06	1.66	1.66	1.52	45
I:a.16;	-6.37	0.06	-3.16	0.10	0.82	0.83	1.62	21
I:a.17;	-4.48	0.02	-2.36	0.03	1.68	1.68	1.72	42
I:a.18;	-5.32	0.08	-2.39	0.18	0.76	0.78	1.82	31
I:a.19;	-5.32	0.05	-2.46	0.09	1.10	1.13	1.92	36
I:a.20;	-6.87	0.07	-3.45	0.14	0.92	0.90	2.02	32
I:a.21;	-5.73	0.02	-2.40	0.04	1.49	1.50	2.12	38
I:a.22;	-6.76	0.03	-4.23	0.05	1.64	1.63	2.22	38
I:a.23;	-6.56	0.01	-3.45	0.04	0.55	0.56	2.32	29
I:a.24;	-5.39	0.02	-2.57	0.05	1.64	1.63	2.42	37
I:a.25;	-6.37	0.02	-3.62	0.08	1.16	1.15	2.52	30
I:a.26;	-5.85	0.05	-3.68	0.10	1.10	1.10	2.62	32
I:a.27;	-5.95	0.04	-3.50	0.09	1.08	1.06	2.72	31
I:a.28;	-6.49	0.02	-4.17	0.03	1.64	1.64	2.82	46
I:a.29;	-6.62	0.02	-4.53	0.07	0.74	0.72	2.92	27
I:a.30;	-5.67	0.03	-2.78	0.04	1.54	1.53	3.02	36
I:a.31;	-5.09	0.04	-2.97	0.07	1.23	1.25	3.12	36
I:a.32;	-4.85	0.05	-2.37	0.13	1.03	1.01	3.22	34
I:a.33;	-4.19	0.02	-2.13	0.02	2.35	2.33	3.32	56
I:a.34;	-5.46	0.03	-2.80	0.06	1.67	1.66	3.42	47
I:a.35; c:in a dark layer above the thickest light region;	-6.49	0.03	-2.69	0.07	0.62	0.64	3.52	23
I:a.36;	-6.12	0.02	-3.87	0.07	1.32	1.30	3.62	43
I:a.37;	-7.23	0.05	-5.00	0.10	1.50	1.52	3.72	45
I:a.38;	-6.14	0.03	-2.61	0.04	1.30	1.28	3.82	34
I:a.39;	-7.57	0.03	-3.48	0.07	1.73	1.73	3.92	46
I:a.40;	-6.61	0.03	-3.05	0.04	1.09	1.07	4.02	37
I:a.41;	-6.07	0.04	-2.77	0.07	1.25	1.24	4.12	33
I:a.42;	-5.84	0.03	-3.17	0.08	1.42	1.43	4.22	39
I:a.43;	-7.47	0.01	-4.19	0.03	2.52	2.61	4.32	58
I:a.44;	-5.20	0.04	-2.18	0.08	1.33	1.35	4.42	34
I:a.45;	-6.78	0.02	-3.27	0.04	2.33	2.32	4.52	56
I:a.46;	-5.97	0.04	-3.02	0.09	1.20	1.21	4.62	39

I:a.47;	-6.41	0.01	-3.10	0.02	2.45	2.43	4.72	54
I:a.48;	-6.54	0.02	-3.26	0.05	1.98	1.96	4.82	49
I:a.49;	-6.36	0.01	-3.34	0.02	2.23	2.66	4.92	60
I:a.50;	-5.29	0.04	-3.00	0.05	1.30	1.28	5.02	65
I:a.51;	-5.81	0.04	-3.26	0.10	1.07	1.07	5.12	29
I:a.52;	-6.31	0.03	-3.51	0.04	1.97	1.99	5.22	46
I:a.53;	-5.93	0.02	-4.28	0.02	1.08	1.07	5.32	27
I:a.54;	-5.20	0.05	-2.75	0.10	0.94	0.95	5.42	29
I:a.55;	-5.82	0.03	-3.04	0.05	1.07	1.04	5.52	23
I:a.56;	-5.26	0.04	-2.38	0.11	0.79	0.80	5.62	25
I:a.57;	-4.79	0.06	-2.74	0.07	0.97	0.99	5.72	29
I:a.58;	-5.54	0.05	-3.85	0.05	1.34	1.34	5.82	32
I:a.59;	-4.81	0.05	-2.92	0.13	0.72	0.74	5.92	23
I:a.60;	-3.83	0.04	-1.85	0.07	1.82	1.82	6.02	49
I:a.61;	-4.73	0.04	-2.87	0.05	0.56	0.55	6.12	19
I:a.62;	-4.63	0.06	-1.98	0.10	0.97	1.00	6.22	28
I:a.63;	-5.95	0.21	-4.40	0.40	0.46	0.34	6.32	18
I:a.64;	-5.11	0.03	-2.80	0.04	1.92	1.90	6.42	45
I:a.65;	-5.38	0.02	-3.32	0.06	0.72	0.74	6.52	21
I:a.66;	-4.89	0.12	-2.92	0.28	0.42	0.41	6.62	18
I:a.67;	-5.54	0.01	-2.55	0.02	2.64	2.63	6.72	63
I:a.68;	-5.21	0.02	-3.32	0.04	1.81	1.79	6.82	43
I:a.69;	-5.52	0.04	-3.17	0.08	1.22	1.22	6.92	33
I:a.70;	-5.88	0.03	-3.34	0.04	2.10	2.10	7.02	48
I:a.71;	-6.14	0.05	-4.19	0.11	0.71	0.69	7.12	23
I:a.72;	-5.17	0.02	-2.45	0.14	0.85	0.84	7.22	25
I:a.73;	-5.00	0.01	-3.19	0.02	2.65	2.62	7.32	60
I:a.74;	-5.20	0.02	-5.24	0.04	0.65	0.64	7.42	18
I:a.75; c:last layer above the crack;	-4.82	0.04	-3.01	0.04	0.76	0.76	7.52	24
I:a.76; c:First layer below the crack;	-4.98	0.01	-2.46	0.01	2.35	2.74	7.62	54
I:a.77;	-5.59	0.01	-3.99	0.02	2.91	2.90	7.72	63
I:a.78;	-5.14	0.04	-3.73	0.12	0.81	0.83	7.82	28
I:a.79;	-4.41	0.05	-4.57	0.10	0.74	0.74	7.92	25
I:a.80;	-6.07	0.01	-3.26	0.01	2.64	2.63	8.02	61
I:a.81; c: Drill hole off-	-5.08	0.04	-2.99	0.04	0.59	0.61	8.12	22

line.;
I:a.82; -5.43 0.00 -2.43 0.01 2.17 2.17 8.22 42
I:a.83; -5.20 0.02 -3.50 0.07 1.27 1.27 8.32 33
I:a.84; -4.97 0.03 -1.97 0.10 1.16 1.17 8.42 31
I:a.85; -4.66 0.01 -1.43 0.02 2.80 2.78 8.52 56
I:a.86; -4.72 0.04 -2.74 0.05 1.30 1.31 8.62 62
I:a.87; -5.58 0.04 -4.95 0.03 1.49 1.49 8.72 38
I:a.88; -5.37 0.01 -3.01 0.01 2.33 2.70 8.82 54
I:a.89; -5.39 0.01 -4.18 0.01 2.06 2.72 8.92 59
I:a.90; -5.30 0.01 -2.67 0.02 1.82 2.43 9.02 51
I:a.91; -4.63 0.01 -2.42 0.02 2.33 2.31 9.12 52
I:a.92; -4.97 0.01 -3.38 0.02 2.49 2.47 9.22 49
I:a.93; -5.08 0.04 -2.38 0.08 1.09 1.11 9.32 26
I:a.94; -5.50 0.02 -3.23 0.06 1.53 1.51 9.42 33
I:a.95; -5.46 0.05 -2.95 0.07 0.86 0.86 9.52 23
I:a.96; -5.58 0.03 -4.51 0.02 1.10 1.10 9.62 32
I:a.97; -6.15 0.03 -3.99 0.04 1.27 1.26 9.72 33
I:a.98; -5.50 0.04 -2.61 0.05 1.61 1.63 9.82 36
I:a.99; -5.58 0.03 -2.87 0.07 1.58 1.58 9.92 36
I:a.100 -6.14 0.03 -3.91 0.03 1.68 1.68 10.02 45
;
I:a.101 -5.01 0.02 -3.51 0.03 1.54 1.53 10.12 40
;
I:a.102 -4.59 0.02 -2.18 0.03 2.00 2.25 10.22 51
;
I:a.103 -4.87 0.04 -2.46 0.08 0.83 0.83 10.32 25
;
I:a.104 -4.17 0.01 -3.70 0.03 2.21 2.20 10.42 51
;
I:a.105 -4.57 0.05 -2.79 0.12 0.78 0.78 10.52 21
;c: First
offset
of the
line;
I:a.106 -4.80 0.04 -3.03 0.06 1.55 1.54 10.62 66
;
I:a.107 -3.74 0.04 -2.09 0.07 1.42 1.42 10.72 28
;
I:a.108 -3.59 0.03 -2.41 0.02 1.88 1.87 10.82 46
;
I:a.109 -6.29 0.01 -4.32 0.04 1.42 1.42 10.92 32
;c: in a
very
porous
layer;
I:a.110 -6.02 0.04 -3.01 0.04 1.48 1.47 11.02 65
;
I:a.111 -5.56 0.03 -3.23 0.06 1.33 1.35 11.12 64
;

I:a.112 -6.92 0.01 -3.50 0.03 2.23 2.21 11.22 47
;
I:a.113 -5.82 0.01 -2.73 0.03 1.83 1.81 11.32 42
;
I:a.114 -5.60 0.02 -3.00 0.04 1.58 1.56 11.42 38
;
I:a.115 -5.22 0.01 -3.42 0.02 1.79 1.78 11.52 37
;
I:a.116 -4.79 0.01 -2.68 0.02 1.91 2.77 11.62 65
;
I:a.117 -5.28 0.03 -3.04 0.11 1.38 1.36 11.72 37
;
I:a.118 -5.64 0.01 -3.11 0.02 2.78 2.76 11.82 61
;
I:a.119 -5.03 0.02 -2.74 0.04 1.85 1.83 11.92 39
;
I:a.120 -5.63 0.03 -3.32 0.02 1.36 1.37 12.02 37
;
I:a.121 -6.81 0.01 -4.50 0.02 1.75 1.89 12.12 41
;
I:a.122 -5.50 0.01 -2.65 0.03 1.55 1.59 12.22 35
;
I:a.123 -6.53 0.02 -3.76 0.05 1.37 2.57 12.32 52
;
I:a.124 -6.09 0.03 -4.57 0.03 1.69 1.69 12.42 44
;
I:a.125 -4.97 0.03 -2.74 0.08 1.52 1.50 12.52 35
;
I:a.126 -5.96 0.02 -3.33 0.03 2.02 2.00 12.62 54
;
I:a.127 -7.24 0.02 -6.34 0.01 2.48 2.49 12.72 49
;
I:a.128 -5.53 0.07 -4.79 0.08 0.92 0.92 12.82 26
;
I:a.129 -5.04 0.03 -3.61 0.06 0.83 0.81 12.92 24
;
I:a.130 -4.66 0.01 -2.44 0.03 1.28 1.28 13.02 28
;
I:a.131 -5.07 0.03 -2.87 0.04 1.33 1.33 13.12 32
;
I:a.132 -5.78 0.01 -3.43 0.03 2.21 2.20 13.22 45
;
I:a.133 -6.23 0.03 -3.60 0.03 1.73 1.71 13.32 36
;
I:a.134 -4.45 0.03 -4.01 0.05 1.76 1.76 13.42 39
;
I:a.135 -4.67 0.03 -4.78 0.05 1.02 1.05 13.52 36
;
I:a.136 -6.66 0.02 -3.53 0.03 1.61 1.60 13.62 45
;

I:a.137 ;	-6.68	0.01	-4.15	0.01	1.91	2.75	13.72	56
I:a.138 ;	-6.95	0.02	-3.80	0.05	2.05	2.05	13.82	55
I:a.139 ;	-9.10	0.02	-4.30	0.03	2.09	2.08	13.92	51
I:a.140 ;	-7.00	0.02	-3.75	0.03	1.66	1.66	14.02	36
I:a.141 ;	-8.04	0.01	-4.17	0.01	1.91	2.36	14.12	43
I:a.142 ;	-8.10	0.01	-4.06	0.03	1.69	2.85	14.22	63
I:a.143 ;	-2.90	0.04	-2.24	0.04	0.89	0.90	14.32	23
I:a.144 ;	-2.95	0.04	-3.11	0.06	1.28	1.27	14.42	28
I:a.145 ;	-4.78	0.04	-3.36	0.13	0.92	0.90	14.52	22
I:a.146 ;	-4.82	0.03	-2.56	0.05	1.32	1.34	14.62	32
I:a.147 ;	-5.26	0.06	-2.58	0.06	1.20	1.22	14.72	31
I:a.148 ;	-6.60	0.03	-4.45	0.05	0.86	0.87	14.82	22
I:a.149 ;	-6.77	0.02	-4.16	0.04	1.40	1.38	14.92	35
I:a.150 ;	-6.19	0.02	-3.67	0.05	1.58	1.59	15.02	36
I:a.151 ;	-4.96	0.03	-3.29	0.04	1.82	1.82	15.12	46
I:a.152 ;	-5.55	0.03	-3.47	0.04	1.77	1.75	15.22	51
I:a.153 ;c:Last sample in initial line;	-2.66	0.01	-2.73	0.02	1.90	1.88	15.32	51
I:h1.1; c:First Hendy test;	-5.44	0.01	-2.91	0.01	2.09	2.08	15.42	53
I:h1.2; c:First Hendy test;	-5.27	0.01	-2.54	0.02	2.00	2.25	15.52	52
I:h1.3; c:First Hendy test;	-5.53	0.03	-2.66	0.06	0.87	0.87	15.62	23
I:h1.4;	-18.64	0.92	-23.14	0.61	0.00	0.01	15.72	16

c:First Hendy test; I:h1.5;	-4.80	0.20	-3.66	0.18	0.42	0.31	15.82	19
c:First Hendy test; I:h1.6;	-12.13	0.58	-16.61	0.84	0.00	0.01	15.92	57
c:First Hendy test; I:h1.7;	-3.77	0.04	-2.10	0.08	1.10	1.12	16.01	30
c:First Hendy test; I:h2.1;	-5.19	0.03	-3.20	0.03	0.72	0.71	0.00	21
c: Second Hendy test; I:h2.2;	-5.12	0.03	-2.72	0.05	0.67	0.67	0.00	22
c: Second Hendy test; I:h2.3;	-3.56	0.02	-2.11	0.04	2.31	2.58	0.00	57
c: Second Hendy test; I:h2.4;	-4.34	0.04	-2.61	0.06	1.55	1.57	0.00	47
c: Second Hendy test; I:h2.5;	-5.35	0.02	-3.94	0.03	2.91	3.05	0.00	57
c: Second Hendy test; I:h2.6;	-4.64	0.04	-3.30	0.08	0.80	0.82	0.00	26
c: Second Hendy test; I:b.01;	-15.78	0.63	-27.74	0.45	0.00	0.01	0.07	54
c: Second line; I:b.02;	-4.21	0.01	-3.33	0.01	1.99	1.98	0.17	53

I:b.03;	-2.04	0.01	-3.33	0.01	2.15	2.70	0.27	57
I:b.04;	-3.45	0.22	-0.66	0.77	0.37	0.37	0.37	20
I:b.05;	-5.66	0.03	-3.06	0.09	0.90	0.89	0.47	21
I:b.06;	-7.10	0.01	-3.15	0.01	2.30	2.28	0.57	55
I:b.07;	-7.39	0.01	-4.14	0.02	2.69	2.99	0.67	59
I:b.08;	-7.25	0.02	-4.83	0.03	2.37	2.53	0.77	47
I:b.09;	-6.58	0.01	-2.66	0.02	2.03	2.01	0.87	43
I:b.10;	-6.89	0.01	-3.18	0.02	1.84	2.67	0.97	50
I:b.11;	-6.75	0.02	-4.22	0.02	1.33	1.33	1.07	40
I:b.12;	-7.46	0.03	-3.55	0.03	1.90	1.90	1.17	50
I:b.13;	-8.21	0.02	-3.57	0.03	2.12	2.11	1.27	41
I:b.14;	-5.93	0.01	-3.22	0.01	2.61	3.23	1.37	57
I:b.15;	-7.30	0.01	-5.25	0.03	1.44	1.42	1.47	32
I:b.16;	-6.67	0.02	-3.70	0.05	1.19	1.19	1.57	30
I:b.17;	-6.63	0.01	-3.73	0.02	1.94	1.92	1.67	43
I:b.18;	-7.47	0.01	-4.82	0.02	1.55	1.55	1.77	66
I:b.19;	-7.52	0.01	-3.45	0.01	1.53	2.36	1.87	60
I:b.20;	-7.59	0.00	-4.45	0.02	1.36	2.15	1.97	45
I:b.21;	-8.16	0.01	-5.18	0.04	1.20	2.41	2.07	49
I:b.22;	-7.65	0.02	-4.04	0.01	1.06	1.53	2.17	35
I:b.23; c:First hole drilled at 1.5 mm distance;	-7.01	0.06	-4.58	0.07	0.71	0.70	2.27	17
I:b.24;	-6.63	0.04	-2.91	0.09	0.86	0.86	2.37	28
I:b.25;	-6.32	0.02	-3.11	0.02	2.21	2.19	2.47	42
I:b.26; c: First hole drilled at 2 mm distance;	-7.27	0.06	-3.01	0.11	0.91	0.90	2.57	23
I:b.27;	-7.22	0.03	-3.46	0.08	1.52	1.52	2.67	32
I:b.28;	-8.39	0.02	-3.71	0.08	1.06	1.05	2.77	31
I:b.29;	-7.96	0.03	-3.22	0.04	1.25	1.25	2.87	33
I:b.30;	-7.81	0.01	-3.45	0.02	2.05	2.62	2.97	54
I:b.31;	-8.72	0.02	-4.04	0.04	1.92	1.91	3.07	48
I:b.32;	-9.35	0.03	-4.43	0.04	1.55	1.57	3.17	36
I:b.33;	-9.37	0.01	-4.92	0.02	2.64	3.14	3.27	61
I:b.34;	-7.45	0.02	-4.06	0.06	1.52	1.53	3.37	37
I:c.01;c: First	-4.15	0.05	-2.99	0.05	0.64	0.64	0.00	34

hi-res transect. 0.2 mm intervals;								
I:c.02;	-3.94	0.02	-2.90	0.02	2.03	2.03	0.01	47
I:c.03;	-3.51	0.01	-2.54	0.03	2.29	2.28	0.01	49
I:c.04;	-3.20	0.02	-2.46	0.03	2.51	2.50	0.01	47
I:c.05;	-4.12	0.02	-2.81	0.03	2.25	2.24	0.01	46
I:c.06;	-3.20	0.01	-2.74	0.02	2.13	2.11	0.01	39
I:c.07;	-3.49	0.03	-2.86	0.04	1.81	1.82	0.02	37
I:c.08;	-3.31	0.01	-3.00	0.07	1.54	1.52	0.02	66
I:c.09;	-3.40	0.02	-2.75	0.03	1.66	1.66	0.02	37
I:c.10;	-3.60	0.01	-2.89	0.01	1.86	2.37	0.02	52
I:c.11;	-3.67	0.02	-2.70	0.03	2.51	2.51	0.02	57
I:c.12;c: First sample taken with narrower line;	-2.91	0.03	-2.17	0.09	1.37	1.37	0.03	61
I:c.13;	-2.67	0.02	-2.88	0.06	1.37	1.37	0.03	61
I:c.14;	-3.44	0.01	-3.11	0.03	2.12	2.12	0.03	48
I:c.15;	-4.06	0.02	-2.64	0.01	2.35	2.33	0.03	49
I:c.16;	-5.65	0.03	-3.38	0.05	0.65	0.66	0.03	19
I:c.17;	-5.35	0.02	-2.46	0.03	2.05	2.57	0.04	52
I:c.18;	-5.55	0.02	-2.81	0.04	2.53	2.54	0.04	52
I:c.19;c:On the border between the top section and the 2 layers separated from the rest by the strange contact (distinct darker section);	-3.55	0.01	-2.54	0.02	2.98	2.96	0.04	60
I:c.20;c	-2.98	0.01	-1.95	0.03	2.25	2.23	0.04	51

: Inside the dark section;								
I:c.21;	-2.55	0.02	-1.74	0.03	1.72	1.70	0.04	44
I:c.22;	-3.31	0.02	-2.38	0.06	0.99	1.00	0.05	24
I:c.23;	-3.62	0.01	-2.34	0.06	1.96	1.97	0.05	42
I:c.24;	-4.36	0.01	-2.67	0.02	3.10	3.08	0.05	63
I:c.25;	-4.45	0.01	-2.44	0.02	2.79	2.78	0.05	55
I:c.26;	-4.07	0.01	-2.44	0.01	2.45	2.93	0.05	58
I:c.27;	-3.68	0.01	-2.19	0.00	2.17	2.22	0.06	45
I:c.28;	-4.20	0.01	-2.38	0.02	1.92	2.55	0.06	62
I:c.29;c : last sample inside dark section;	-4.10	0.02	-2.23	0.06	0.89	0.87	0.06	26
I:c.30;	-4.57	0.01	-2.37	0.05	2.26	2.26	0.06	45
I:c.31;	-4.53	0.04	-2.56	0.06	1.10	1.12	0.06	31
I:c.32;	-4.05	0.01	-2.85	0.02	2.50	2.48	0.07	47
I:c.33;	-4.23	0.02	-2.73	0.01	2.59	2.58	0.07	45
I:c.34;	-4.07	0.01	-2.35	0.01	2.22	2.21	0.07	37
I:c.35;	-4.16	0.01	-2.38	0.02	2.12	2.58	0.07	46
I:c.36;	-3.79	0.03	-2.32	0.03	1.22	1.22	0.07	22
I:c.37;	-3.76	0.02	-2.54	0.09	1.08	1.08	0.08	19
I:c.38;	-4.33	0.01	-3.13	0.05	2.26	2.25	0.08	46
I:c.39;	-4.37	0.01	-3.09	0.03	2.45	2.45	0.08	45
I:c.40;	-4.63	0.01	-3.29	0.05	1.60	1.59	0.08	32
I:d.01; c:First sample ;	-3.72	0.06	-3.43	0.18	0.52	0.53	0.00	26
I:d.02; c:;	-3.62	0.08	-3.36	0.09	0.87	0.85	0.00	20
I:d.03; c:;	-3.61	0.03	-3.34	0.03	0.67	0.65	0.00	21
I:d.04; c:;	-3.74	0.04	-3.31	0.12	1.11	1.10	0.01	29
I:d.05; c:;	-4.44	0.06	-4.40	0.05	0.52	0.42	0.01	21
I:d.06; c:;	-3.80	0.05	-3.14	0.09	0.61	0.61	0.01	21
I:d.07; c:;	-3.65	0.05	-2.71	0.07	0.62	0.62	0.01	24
I:d.08; c:;	-3.65	0.08	-2.70	0.09	0.80	0.79	0.01	23
I:d.09; c:;	-3.57	0.07	-2.73	0.07	0.83	0.80	0.02	24

I:d.10; c:;	-3.57	0.05	-2.56	0.06	1.13	1.12	0.02	29
I:d.11; c:;	-3.59	0.08	-2.77	0.07	0.79	0.78	0.02	27
I:d.12; c:;	-3.52	0.07	-2.69	0.07	1.08	1.09	0.02	28
I:d.13; c:;	-3.37	0.05	-2.47	0.06	0.67	0.67	0.02	25
I:d.14; c:;	-3.77	0.07	-3.33	0.18	0.47	0.46	0.03	21
I:d.15; c:;	-3.90	0.02	-3.40	0.14	0.47	0.45	0.03	20
I:d.16; c:;	-3.91	0.03	-3.05	0.05	1.71	1.70	0.03	36
I:d.17; c:;	-3.88	0.03	-3.05	0.10	0.74	0.75	0.03	30
I:d.18; c:;	-3.89	0.03	-3.08	0.06	0.58	0.60	0.03	23
I:d.19; c:;	-3.59	0.02	-2.74	0.04	2.00	1.98	0.04	42
I:d.20; c:;	-3.68	0.08	-2.86	0.12	0.50	0.48	0.04	20
I:d.21; c:;	-3.52	0.18	-3.06	0.23	0.41	0.40	0.04	19
I:d.22; c:;	-5.01	0.06	-5.83	0.07	0.37	0.27	0.04	20
I:d.23; c:;	-3.58	0.05	-2.86	0.07	0.64	0.63	0.04	22
I:d.24; c:;	-4.22	0.08	-4.26	0.16	0.35	0.32	0.05	19
I:d.25; c:;	-3.47	0.06	-2.72	0.12	0.68	0.68	0.05	22
I:d.26; c:;	-4.20	0.07	-4.69	0.15	0.45	0.38	0.05	23
I:d.27; c:;	-3.95	0.07	-4.32	0.19	0.44	0.40	0.05	21
I:d.28; c:;	-3.20	0.03	-2.47	0.04	0.93	0.93	0.05	25
I:d.29; c:;	-3.00	0.04	-2.25	0.06	0.83	0.82	0.06	24
I:d.30; c:;	-3.20	0.06	-2.34	0.07	0.70	0.69	0.06	22
I:d.31; c:;	-3.81	0.11	-3.13	0.21	0.44	0.42	0.06	23
I:d.32; c:;	-3.58	0.08	-2.53	0.11	0.79	0.78	0.06	21
I:d.33; c:;	-3.76	0.04	-3.16	0.09	0.48	0.46	0.06	20
I:d.34; c:;	-2.93	0.05	-2.34	0.09	0.75	0.75	0.07	21

I:d.35; c:;	-2.78	0.03	-2.55	0.04	0.86	0.86	0.07	24
I:d.36; c:;	-3.40	0.09	-3.85	0.21	0.42	0.39	0.07	19
I:d.37; c:;	-3.50	0.08	-2.79	0.03	1.14	1.12	0.07	17
I:d.38; c:;	-3.87	0.03	-2.81	0.04	1.07	1.06	0.07	20
I:d.39; c:;	-4.45	0.08	-2.97	0.06	0.96	0.96	0.08	17
I:d.40; c:;	-4.61	0.03	-3.01	0.08	0.90	0.90	0.08	18
I:d.41; c:;	-4.19	0.06	-3.12	0.05	0.65	0.65	0.08	20
I:d.42; c:;	-5.11	0.07	-3.14	0.11	0.59	0.58	0.08	20
I:d.43; c:;	-4.46	0.03	-3.17	0.10	0.89	0.90	0.08	26
I:d.44; c:;	-4.12	0.06	-2.94	0.09	1.09	1.08	0.09	21
I:d.45; c:;	-3.94	0.03	-2.87	0.07	0.70	0.71	0.09	19
I:d.46; c:;	-3.08	0.02	-2.44	0.08	1.63	1.61	0.09	28
I:d.47; c:;	-2.92	0.04	-2.41	0.09	1.02	1.02	0.09	20
I:d.48; c:;	-2.88	0.02	-2.45	0.04	2.51	3.01	0.09	40
I:d.49; c:;	-3.17	0.04	-2.92	0.09	1.04	1.04	0.10	22
I:d.50; c:;	-3.06	0.03	-2.78	0.04	1.83	1.80	0.10	30
I:d.51; c:;	-2.93	0.04	-2.81	0.04	1.36	1.34	0.10	24
I:d.52; c:;	-2.90	0.03	-2.82	0.07	1.18	1.17	0.10	23
I:d.53; c:;	-2.92	0.07	-2.83	0.10	1.10	1.09	0.10	21
I:d.54; c:;	-2.93	0.04	-2.87	0.04	1.28	1.27	0.11	22
I:d.55; c:;	-3.03	0.03	-2.95	0.06	1.21	1.20	0.11	23
I:d.56; c:;	-3.23	0.05	-3.10	0.08	1.21	1.18	0.11	19
I:d.57; c:;	-3.72	0.04	-3.35	0.04	1.33	1.31	0.11	21
I:d.58; c:;	-3.33	0.01	-3.06	0.03	1.72	1.71	0.11	30
I:d.59; c:;	-3.43	0.05	-2.98	0.07	0.80	0.80	0.12	19

I:d.60; c:;	-3.27	0.03	-2.72	0.05	1.43	1.42	0.12	27
I:d.61; c:;	-3.28	0.03	-2.80	0.03	1.88	1.85	0.12	33
I:d.62; c:;	-3.26	0.05	-2.68	0.04	0.89	0.88	0.12	20
I:d.63; c:;	-3.20	0.02	-2.72	0.03	1.88	2.21	0.12	36
I:d.64; c:;	-3.03	0.01	-2.73	0.04	1.77	2.12	0.13	33
I:d.65; c:;	-3.06	0.02	-2.82	0.05	1.80	1.78	0.13	27
I:d.66; c:;	-2.88	0.03	-2.72	0.05	1.70	1.68	0.13	27
I:d.67; c:;	-2.91	0.02	-2.84	0.05	1.37	1.35	0.13	27
I:d.68; c:;	-2.88	0.03	-2.85	0.04	1.49	1.47	0.13	27
I:d.69; c:;	-2.71	0.03	-2.89	0.04	0.68	0.69	0.14	18
I:d.10; c:;	-2.70	0.06	-3.00	0.15	0.51	0.49	0.14	15
I:d.71; c:;	-2.78	0.06	-3.11	0.06	0.87	0.85	0.14	22
I:d.72; c:;	-2.94	0.04	-3.16	0.10	0.76	0.75	0.14	16
I:d.73; c:;	-3.00	0.02	-3.11	0.06	1.38	1.36	0.14	24
I:d.74; c:;	-3.22	0.05	-3.19	0.05	0.68	0.66	0.15	19
I:d.75; c:;	-3.32	0.05	-3.36	0.07	1.24	1.22	0.15	22
I:d.76; c:;	-3.57	0.05	-3.49	0.10	1.06	1.05	0.15	23
I:d.77; c:;	-3.37	0.06	-3.32	0.06	1.18	1.17	0.15	26
I:d.78; c:;	-3.26	0.07	-3.12	0.07	1.11	1.09	0.15	22
I:d.79; c:;	-3.19	0.03	-2.92	0.04	2.37	2.48	0.16	44
I:d.80; c:;	-3.29	0.02	-3.14	0.04	0.95	0.94	0.16	26
I:d.81; c:;	-3.37	0.09	-3.15	0.11	0.93	0.92	0.16	21
I:d.82; c:;	-3.49	0.03	-2.64	0.09	1.15	1.14	0.16	25
I:d.83; c:;	-3.48	0.03	-2.75	0.02	2.03	2.01	0.16	36
I:d.84; c:;	-4.56	0.10	-5.81	0.15	0.57	0.38	0.17	16

I:d.85; c:;	-3.43	0.05	-2.83	0.04	1.30	1.29	0.17	30
I:d.86; c:;	-5.45	0.17	-7.94	0.05	0.54	0.25	0.17	20
I:d.87; c:;	-3.08	0.03	-2.56	0.04	1.37	1.35	0.17	25
I:d.88; c:;	-2.98	0.03	-2.40	0.04	1.54	1.52	0.17	24
I:d.89; c:;	-3.12	0.03	-2.64	0.06	1.03	1.02	0.18	17
I:d.90; c:;	-3.37	0.07	-2.70	0.03	1.22	1.21	0.18	15
I:d.91; c:;	-3.25	0.02	-2.68	0.03	1.91	1.89	0.18	24
I:d.92; c:;	-3.24	0.03	-2.65	0.02	2.07	2.04	0.18	27
I:d.93; c:;	-3.19	0.02	-2.79	0.05	1.74	1.72	0.18	18
I:d.94; c:;	-3.09	0.02	-2.79	0.03	2.00	1.97	0.19	23
I:d.95; c:;	-3.42	0.03	-3.04	0.03	2.18	2.15	0.19	24
I:d.96; c:;	-3.93	0.03	-3.36	0.02	1.74	1.71	0.19	16
I:d.97; c:;	-4.57	0.02	-3.59	0.02	1.73	1.70	0.19	15
I:d.98; c:;	-5.04	0.03	-3.55	0.04	1.25	1.23	0.19	17
I:d.99; c:;	-4.75	0.03	-3.50	0.08	1.31	1.31	0.20	20
I:d.100 ;c:;	-4.32	0.03	-3.05	0.03	1.97	1.94	0.20	30
I:x.01; c: Hendy;	-0.68	0.02	-2.21	0.03	2.18	4.10	0.00	49
I:x.02; c: Hendy;	-1.94	0.02	-2.36	0.01	2.07	3.50	0.10	43
I:x.03; c: Hendy;	-3.32	0.02	-2.82	0.03	1.98	3.95	0.20	46
I:x.04; c: Hendy;	-3.78	0.01	-2.87	0.02	1.88	2.44	0.30	62
I:x.05; c: Hendy;	-4.16	0.02	-3.01	0.02	2.67	4.65	0.40	52
I:x.06; c: Hendy;	-3.04	0.03	-3.01	0.05	2.34	2.32	0.50	50

I:x.07; c: Hendy;	-3.31	0.02	-2.79	0.04	2.40	2.65	0.60	67
I:x.08; c: Hendy;	-2.78	0.01	-2.70	0.05	2.29	2.31	0.70	45
I:x.09; c: Hendy;	-2.59	0.03	-2.85	0.02	2.17	4.27	0.80	52
I:x.10; c: Hendy;	-2.48	0.08	-3.52	0.19	0.47	0.45	0.90	20
I:y.01; c: Hendy;	-2.65	0.01	-1.83	0.02	1.47	1.46	0.00	32
I:y.02; c: Hendy;	-4.09	0.03	-2.62	0.04	1.64	1.62	0.10	35
I:y.03; c: Hendy;	-5.08	0.03	-2.44	0.02	2.55	2.74	0.20	46
I:y.04; c: Hendy;	-5.70	0.01	-2.38	0.04	2.42	3.02	0.30	34
I:y.05; c: Hendy;	-5.11	0.02	-2.28	0.04	2.30	5.07	0.40	52
I:y.06; c: Hendy;	-4.77	0.01	-2.56	0.01	2.19	3.24	0.50	35
I:y.07; c: Hendy;	-3.01	0.02	-1.94	0.04	2.08	3.15	0.60	40
I:y.08; c: Hendy;	-4.03	0.02	-2.11	0.02	1.98	5.13	0.70	56
I:y.09; c: Hendy;	-4.85	0.01	-2.71	0.03	2.63	3.67	0.80	45
I:y.10; c: Hendy;	-3.73	0.02	-2.73	0.03	2.50	4.75	0.90	61

High-resolution dataset was micromilled at ~20 um in the EAGLES lab at Boston College during the month of May, 2009. The top 15.1 mm of CH-1 were micro-milled at 20 um sampling the EAGLES isotope lab in Devlin 301 at Boston College in May of 2009. Powdered carbonate samples of 50-100 µg of carbonate were analyzed for $\delta^{18}O$ and $\delta^{13}C$ values using a ThermoFinnigan MAT 253 Dual Inlet System at the KPESIL - W. M. Keck Paleoenvironmental and Environmental Stable Isotope Laboratory at the University of Kansas. The results are in ‰, V-PDB.

Date	Sample ID-1	D mV	$\delta^{13}C$ (VPDB)	σ	$\delta^{18}O$ (VPDB)	σ
5/18/09	JP-7	-47.9%				
5/18/09	JP-8	-1.7%	-3.32	0.01	-2.78	0.03
5/18/09	JP-9	-2.2%	-3.06	0.01	-2.54	0.02
5/18/09	JP-10	-1.9%	-3.52	0.01	-2.64	0.02
5/18/09	JP-11	-3.1%	-3.22	0.01	-2.53	0.03
5/18/09	JP-12	-4.3%	-3.35	0.01	-2.67	0.02
5/18/09	JP-13	-3.7%	-3.43	0.01	-2.68	0.01
5/18/09	JP-14	-5.0%	-3.34	0.01	-2.83	0.01
5/18/09	JP-15	-1.9%	-3.18	0.01	-2.52	0.02
5/18/09	JP-16	-2.6%	-3.03	0.01	-2.81	0.02
5/18/09	JP-17	-4.3%	-2.96	0.01	-2.65	0.02
5/18/09	JP-18	-3.4%	-3.12	0.01	-2.85	0.01
5/18/09	JP-19	-2.5%	-3.38	0.01	-2.92	0.01
5/18/09	JP-20	-4.3%	-3.65	0.01	-3.13	0.01
5/18/09	JP-21	-3.7%	-4.09	0.01	-3.23	0.06
5/18/09	JP-22	-2.8%	-4.39	0.01	-3.30	0.01
5/19/09	JP-23	-2.7%	-4.66	0.01	-3.20	0.02
5/19/09	JP-24	-3.4%	-4.69	0.01	-3.30	0.02
5/19/09	JP-25	-4.1%	-4.76	0.01	-3.15	0.01
5/19/09	JP-26	-5.1%	-4.57	0.01	-3.16	0.01
5/19/09	JP-28	-3.4%	-3.91	0.02	-2.85	0.01
5/19/09	JP-29	-2.3%	-3.38	0.01	-2.76	0.04
5/19/09	JP-30	-3.3%	-3.27	0.02	-2.68	0.02
5/19/09	JP-31	-4.8%	-3.20	0.01	-2.73	0.01
5/19/09	JP-32	-3.5%	-3.13	0.02	-2.76	0.02
5/19/09	JP-33	-4.0%	-3.13	0.01	-2.84	0.01
05/15/09	JP-41	7.4%	-3.58	0.01	-3.16	0.03
05/15/09	JP-42	0.4%	-3.59	0.01	-3.16	0.02
05/15/09	JP-43	-1.8%	-3.54	0.02	-3.10	0.03
05/15/09	JP-44	-3.0%	-3.54	0.01	-2.94	0.00
05/15/09	JP-45	3.5%	-3.51	0.01	-2.92	0.04
05/15/09	JP-46	-2.9%	-3.46	0.01	-2.89	0.02
05/15/09	JP-47	-2.4%	-3.45	0.02	-2.97	0.02
05/15/09	JP-48	-3.3%	-3.25	0.00	-2.67	0.02
05/15/09	JP-49	2.9%	-3.32	0.01	-2.93	0.02
05/15/09	JP-50	-3.4%	-3.23	0.00	-2.83	0.02

05/15/09	JP-51	-2.3%	-3.22	0.02	-3.11	0.04
05/15/09	JP-52	-3.2%	-3.14	0.01	-3.03	0.01
05/15/09	JP-53	-2.0%	-3.19	0.01	-3.11	0.03
05/16/09	JP-54	-2.8%	-3.25	0.01	-3.22	0.02
05/16/09	JP-55	-1.9%	-3.28	0.01	-3.27	0.01
05/16/09	JP-56	-2.4%	-3.39	0.00	-3.39	0.02
05/16/09	JP-57	2.2%	-3.49	0.01	-3.40	0.02
05/16/09	JP-58	-0.4%	-3.61	0.01	-3.41	0.01
05/16/09	JP-59	-2.5%	-3.81	0.01	-3.70	0.02
05/16/09	JP-60	-3.1%	-3.72	0.01	-3.52	0.00
05/16/09	JP-61	-2.1%	-3.58	0.01	-3.48	0.02
05/16/09	JP-62	-2.4%	-3.57	0.01	-3.41	0.03
05/16/09	JP-63	0.9%	-3.54	0.01	-3.30	0.02
05/16/09	JP-64	-3.3%	-3.51	0.01	-3.24	0.01
05/16/09	JP-65	-3.2%	-3.55	0.01	-3.16	0.02
05/16/09	JP-66	-2.3%	-3.64	0.01	-2.98	0.02
05/16/09	JP-67	-3.3%	-3.57	0.01	-2.93	0.01
05/16/09	JP-68	1.5%	-3.53	0.01	-2.80	0.01
05/16/09	JP-69	-2.6%	-3.30	0.00	-2.70	0.02
05/16/09	JP-70	-3.8%	-3.29	0.01	-2.72	0.03
05/16/09	JP-71	-3.7%	-3.18	0.01	-2.73	0.01
05/16/09	JP-72	-1.0%	-3.45	0.02	-2.92	0.01
05/16/09	JP-73	-3.2%	-3.42	0.01	-2.94	0.00
05/16/09	JP-74	-2.0%	-3.52	0.01	-3.01	0.01
05/16/09	JP-75	-1.5%	-3.62	0.02	-3.12	0.05
05/16/09	JP-76	1.2%	-3.75	0.01	-3.19	0.03
05/16/09	JP-77	-4.0%	-4.04	0.01	-3.51	0.01
05/16/09	JP-78	-2.7%	-4.11	0.02	-3.42	0.01
05/16/09	JP-79	-2.4%	-4.79	0.01	-3.85	0.02
05/16/09	JP-80	-1.8%	-4.83	0.02	-3.80	0.02
05/17/09	JP-81	-3.4%	-5.04	0.01	-3.91	0.01
05/17/09	JP-82	3.9%	-4.73	0.01	-3.55	0.02
05/17/09	JP-83	-2.1%	-4.21	0.01	-3.24	0.01
05/17/09	JP-84	-3.8%	-4.08	0.01	-3.19	0.03
05/17/09	JP-85	-2.1%	-3.62	0.01	-2.89	0.02
05/17/09	JP-86	-1.1%	-3.60	0.01	-2.85	0.03
05/17/09	JP-87	-2.6%	-2.84	0.01	-2.42	0.01
05/17/09	JP-88	-3.5%	-2.68	0.00	-2.24	0.02
05/17/09	JP-89	-2.9%	-2.74	0.01	-2.29	0.03
05/17/09	JP-90	-3.5%	-2.63	0.01	-2.13	0.01
05/17/09	JP-91	-0.8%	-2.91	0.01	-2.27	0.02
05/17/09	JP-92	0.5%	-3.03	0.01	-2.19	0.01
05/17/09	JP-93	1.7%	-3.07	0.01	-2.34	0.02
05/17/09	JP-94	0.4%	-3.01	0.01	-2.32	0.01
05/17/09	JP-95	-3.8%	-2.98	0.01	-2.44	0.03
05/17/09	JP-96	6.5%	-2.97	0.01	-2.44	0.01
05/17/09	JP-97	-5.2%	-2.99	0.01	-2.73	0.07
05/18/09	JP-98	-3.7%	-3.12	0.01	-2.71	0.01
05/18/09	JP-99	-3.3%	-2.94	0.02	-2.74	0.01
05/18/09	JP-100	-4.1%	-2.90	0.01	-2.69	0.01

05/18/09	JP-101	-2.4%	-2.87	0.01	-2.89	0.03
05/18/09	JP-102	-4.1%	-2.89	0.01	-2.87	0.01
05/18/09	JP-103	-0.1%	-2.84	0.02	-3.02	0.01
05/18/09	JP-104	-0.9%	-2.86	0.02	-2.94	0.02
05/18/09	JP-105	-4.1%	-2.83	0.01	-3.23	0.03
05/18/09	JP-106	-3.0%	-2.82	0.01	-3.31	0.01
05/18/09	JP-107	-2.6%	-2.83	0.01	-3.41	0.01
05/18/09	JP-108	1.3%	-2.82	0.01	-3.45	0.03
05/18/09	JP-109	-2.5%	-2.86	0.02	-3.53	0.01
05/18/09	JP-110	-2.1%	-2.90	0.01	-3.43	0.02
05/18/09	JP-111	0.9%	-3.01	0.01	-3.51	0.02
05/18/09	JP-112	-1.8%	-3.23	0.01	-3.43	0.02
05/18/09	JP-113	-3.3%	-3.39	0.01	-3.49	0.02
05/18/09	JP-114	-3.2%	-3.51	0.01	-3.38	0.01
05/18/09	JP-115	-2.3%	-3.54	0.01	-3.58	0.02
05/18/09	JP-116	-4.5%	-3.81	0.01	-3.31	0.01
05/18/09	JP-117	-5.2%	-3.81	0.02	-3.12	0.01
05/18/09	JP-118	0.4%	-3.75	0.01	-2.85	0.01
05/18/09	JP-119	1.0%	-3.80	0.01	-2.84	0.02
05/18/09	JP-120	-0.2%	-3.89	0.00	-2.87	0.03
05/22/09	JP-121	-2.7%	-3.60	0.02	-2.50	0.01
05/22/09	JP-122	-5.9%	-3.65	0.01	-2.34	0.02
05/22/09	JP-123	-4.5%	-3.67	0.01	-2.45	0.02
05/22/09	JP-124	-3.6%	-3.79	0.01	-2.47	0.02
05/22/09	JP-125	0.9%	-4.07	0.01	-2.74	0.02
05/22/09	JP-126	-2.1%	-4.27	0.01	-2.86	0.02
05/22/09	JP-127	-4.7%	-4.54	0.02	-3.12	0.02
05/22/09	JP-128	-5.5%	-4.45	0.01	-2.75	0.04
05/22/09	JP-129	0.7%	-4.96	0.01	-3.48	0.02
05/22/09	JP-130	-5.2%	-4.94	0.01	-3.40	0.02
05/22/09	JP-131	1.9%	-5.25	0.02	-3.56	0.01
05/22/09	JP-132	-3.2%	-5.30	0.01	-3.61	0.01
05/22/09	JP-133	-4.3%	-5.71	0.01	-3.75	0.02
05/22/09	JP-134	-2.2%	-5.81	0.02	-3.82	0.02
05/22/09	JP-135	-1.9%	-5.74	0.01	-3.77	0.01
05/22/09	JP-136	-3.0%	-5.80	0.01	-3.55	0.01
05/22/09	JP-137	-1.0%	-6.05	0.01	-3.94	0.04
05/22/09	JP-138	0.8%	-5.74	0.01	-3.03	0.02
05/22/09	JP-139	-0.8%	-5.80	0.01	-3.11	0.01
05/23/09	JP-140	-1.4%	-5.79	0.02	-3.08	0.02
05/23/09	JP-141	-5.7%	-5.77	0.03	-3.05	0.02
05/23/09	JP-142	-2.4%	-5.58	0.01	-2.60	0.02
05/23/09	JP-143	-2.8%	-5.38	0.01	-2.49	0.02
05/23/09	JP-144	-3.3%	-5.26	0.01	-2.35	0.02
05/23/09	JP-145	-3.0%	-5.20	0.02	-2.35	0.01
05/23/09	JP-146	-2.5%	-5.19	0.01	-2.43	0.01
05/23/09	JP-147	-1.3%	-4.99	0.02	-2.33	0.03
05/23/09	JP-148	-0.8%	-4.98	0.02	-2.56	0.02
05/23/09	JP-149	-1.1%	-4.87	0.03	-2.58	0.02
05/23/09	JP-150	-0.9%	-5.07	0.01	-2.68	0.03

05/23/09	JP-151	-3.1%	-5.16	0.01	-2.77	0.03
05/23/09	JP-152	-3.3%	-5.40	0.02	-2.85	0.03
05/23/09	JP-153	-2.0%	-5.62	0.01	-2.97	0.03
05/23/09	JP-154	-0.7%	-5.72	0.01	-3.06	0.03
05/23/09	JP-155	-1.5%	-5.73	0.02	-3.10	0.02
05/23/09	JP-156	-2.2%	-5.70	0.01	-3.13	0.04
05/23/09	JP-157	1.9%	-5.52	0.01	-3.12	0.02
05/23/09	JP-158	-0.8%	-4.89	0.01	-2.96	0.02
05/23/09	JP-159	-2.9%	-4.92	0.01	-3.09	0.01
05/23/09	JP-160	-3.3%	-4.37	0.01	-2.90	0.01
05/23/09	JP-161	-3.6%	-4.11	0.01	-2.89	0.02
05/23/09	JP-162	-5.3%	-3.88	0.01	-2.76	0.03
05/23/09	JP-163	-1.0%	-3.73	0.01	-2.80	0.04
05/23/09	JP-164	-2.1%	-3.57	0.01	-2.58	0.02
05/23/09	JP-165	-3.3%	-3.09	0.00	-2.36	0.02
05/23/09	JP-166	-3.4%	-3.39	0.02	-2.54	0.02
05/23/09	JP-167	-3.6%	-2.94	0.01	-2.37	0.01
05/23/09	JP-168	-0.7%	-2.79	0.02	-2.16	0.02
05/23/09	JP-169	-2.2%	-2.83	0.02	-2.35	0.03
05/23/09	JP-170	-3.3%	-2.86	0.01	-2.20	0.01
05/23/09	JP-171	-4.0%	-2.80	0.01	-2.24	0.02
05/23/09	JP-172	-5.4%	-2.96	0.02	-2.22	0.03
05/23/09	JP-173	-41.5%	-3.25	0.02	-2.51	0.02
05/23/09	JP-174	-2.0%	-2.98	0.02	-1.97	0.04
05/23/09	JP-175	-2.6%	-3.01	0.01	-1.99	0.02
05/23/09	JP-176	-5.4%	-3.02	0.01	-1.92	0.02
05/23/09	JP-177	-4.6%	-3.02	0.01	-2.00	0.02
05/23/09	JP-178	-5.7%	-2.84	0.01	-1.71	0.01
05/23/09	JP-179	-2.1%	-2.84	0.01	-1.96	0.02
05/23/09	JP-180	-2.8%	-2.87	0.01	-1.89	0.02
05/24/09	JP-181	-2.0%	-2.80	0.02	-1.90	0.04
05/24/09	JP-182	-2.2%	-2.65	0.01	-1.68	0.02
05/24/09	JP-183	-1.9%	-2.66	0.01	-1.88	0.03
05/24/09	JP-184	-5.0%	-2.67	0.02	-1.84	0.04
05/24/09	JP-185	-3.4%	-2.69	0.01	-1.82	0.01
05/24/09	JP-186	-1.9%	-2.65	0.01	-1.89	0.04
05/24/09	JP-187	1.9%	-2.95	0.01	-1.96	0.02
05/24/09	JP-188	-6.0%	-3.25	0.01	-2.26	0.02
05/24/09	JP-189	-0.8%	-3.52	0.01	-2.60	0.01
05/24/09	JP-190	-1.9%	-3.29	0.02	-2.53	0.04
05/24/09	JP-191	-1.1%	-3.28	0.02	-2.50	0.03
05/24/09	JP-192	-0.7%	-3.64	0.01	-2.77	0.02
05/24/09	JP-193	-2.1%	-3.68	0.01	-2.85	0.03
05/24/09	JP-194	-5.2%	-3.49	0.01	-2.71	0.03
05/24/09	JP-195	-1.4%	-3.60	0.02	-2.86	0.03
05/24/09	JP-196	-1.1%	-3.53	0.01	-2.69	0.03
05/24/09	JP-197	-1.8%	-3.39	0.02	-2.63	0.02
05/24/09	JP-198	-1.1%	-3.32	0.01	-2.55	0.01
05/24/09	JP-199	-2.1%	-3.12	0.01	-2.29	0.03
05/24/09	JP-200	-1.4%	-3.13	0.02	-2.32	0.02

05/25/09	JP-201	-1.8%	-3.45	0.01	-2.57	0.01
05/25/09	JP-202	-2.2%	-3.29	0.01	-2.39	0.03
05/25/09	JP-203	-2.0%	-3.23	0.01	-2.27	0.02
05/25/09	JP-204	-1.7%	-3.41	0.02	-2.28	0.03
05/25/09	JP-205	-1.9%	-3.38	0.01	-2.32	0.02
05/25/09	JP-206	-85.5%				
05/25/09	JP-207	-3.9%	-3.91	0.03	-2.76	0.06
05/25/09	JP-208	-0.9%	-3.87	0.02	-2.52	0.03
05/25/09	JP-209	-1.9%	-3.71	0.01	-1.89	0.01
05/25/09	JP-210	-1.7%	-3.78	0.04	-2.48	0.01
05/25/09	JP-211	-12.4%				
05/25/09	JP-212	-95.0%				
05/25/09	JP-213	-0.8%	-4.39	0.03	-2.91	0.04
05/25/09	JP-214	-7.8%	-4.23	0.02	-2.29	0.05
05/25/09	JP-215	-1.7%	-4.30	0.03	-2.88	0.03
05/25/09	JP-216	-5.8%	-4.29	0.02	-2.83	0.02
05/25/09	JP-217	#DIV/0!				
05/26/09	JP-218	-1.4%	-4.32	0.02	-2.81	0.03
05/26/09	JP-219	-1.2%	-4.33	0.03	-2.87	0.04
05/26/09	JP-220	-1.6%	-4.30	0.02	-2.68	0.03
05/26/09	JP-221	-1.6%	-4.33	0.03	-2.77	0.03
05/26/09	JP-222	-0.6%	-4.17	0.01	-2.74	0.03
05/26/09	JP-223	-2.0%	-4.35	0.01	-2.87	0.03
05/26/09	JP-224	-2.1%	-4.40	0.02	-2.92	0.03
05/26/09	JP-225	-2.1%	-4.41	0.02	-2.78	0.01
05/26/09	JP-226	0.8%	-4.38	0.02	-2.63	0.04
05/26/09	JP-227	#DIV/0!				
05/26/09	JP-228	-0.1%	-4.12	0.02	-2.43	0.03
05/26/09	JP-229	-15.8%				
05/26/09	JP-230	-2.8%	-4.11	0.02	-2.39	0.02
05/26/09	JP-231	-1.0%	-4.01	0.00	-2.46	0.03
05/26/09	JP-232	-1.9%	-3.93	0.02	-2.49	0.03
05/26/09	JP-233	-2.0%	-3.87	0.02	-2.61	0.03
05/27/09	JP-234	-1.9%	-3.89	0.01	-2.55	0.02
05/27/09	JP-235	-32.1%				
05/27/09	JP-236	-1.0%	-3.94	0.02	-2.52	0.03
05/27/09	JP-237	-2.0%	-3.84	0.02	-2.62	0.05
05/27/09	JP-238	-8.2%	-3.98	0.04	-2.57	0.06
05/27/09	JP-239	-2.1%	-3.64	0.01	-2.30	0.01
05/27/09	JP-240	-1.4%	-3.65	0.01	-2.27	0.01
05/28/09	JP-241	-6.5%	-3.16	0.03	-2.01	0.04
05/28/09	JP-242	-5.6%	-3.17	0.04	-1.90	0.04
05/28/09	JP-243	-8.5%	-3.21	0.02	-2.13	0.03
05/28/09	JP-244	-2.1%	-3.27	0.02	-2.14	0.02
05/28/09	JP-245	-1.3%	-3.46	0.02	-2.52	0.02
05/28/09	JP-246	-2.3%	-3.40	0.02	-2.42	0.02
05/28/09	JP-247	-1.0%	-3.60	0.03	-2.61	0.04
05/28/09	JP-248	-2.0%	-3.84	0.02	-2.67	0.05
05/28/09	JP-249	-13.1%	-3.77	0.03	-2.71	0.05
05/28/09	JP-250	-24.0%	-3.89	0.03	-2.68	0.05

05/28/09	JP-251	#DIV/0!				
05/28/09	JP-252	-2.1%	-3.93	0.01	-2.48	0.02
05/28/09	JP-253	#DIV/0!				
05/28/09	JP-254	-30.9%	-4.16	0.02	-2.46	0.05
05/28/09	JP-255	-2.2%	-4.23	0.02	-2.55	0.02
05/28/09	JP-256	-1.9%	-4.27	0.03	-2.44	0.03
05/28/09	JP-257	-2.0%	-4.17	0.02	-2.45	0.03
05/28/09	JP-258	-5.9%	-4.06	0.01	-2.35	0.04
05/28/09	JP-259	-1.9%	-3.94	0.02	-2.41	0.04
05/28/09	JP-260	-5.5%	-3.78	0.02	-2.25	0.02
05/29/09	JP-261	-2.0%	-3.78	0.01	-2.36	0.02
05/29/09	JP-262	-1.8%	-3.78	0.02	-2.30	0.04
05/29/09	JP-263	#DIV/0!				
05/29/09	JP-264	-1.8%	-4.01	0.01	-2.40	0.04
05/29/09	JP-265	-0.7%	-4.04	0.02	-2.44	0.04
05/29/09	JP-266	-2.4%	-4.17	0.02	-2.39	0.03
05/29/09	JP-267	-0.7%	-4.04	0.02	-2.46	0.05
05/29/09	JP-268	#DIV/0!				
05/31/09	JP-269	-1.7%	-3.95	0.02	-2.42	0.05
05/31/09	JP-270	-0.8%	-4.04	0.01	-2.18	0.04
05/31/09	JP-271	-1.9%	-4.11	0.03	-2.12	0.02
05/31/09	JP-272	-0.8%	-4.14	0.02	-2.09	0.01
05/31/09	JP-273	-2.0%	-4.40	0.02	-2.23	0.04
05/31/09	JP-274	-1.8%	-4.53	0.02	-2.20	0.04
05/31/09	JP-275	-9.5%	-4.69	0.02	-2.38	0.02
05/31/09	JP-276	-0.7%	-4.71	0.02	-2.43	0.02
05/31/09	JP-277	-2.9%	-4.91	0.01	-2.61	0.05
05/31/09	JP-278	-24.7%	-4.73	0.05	-2.67	0.04
05/31/09	JP-279	-1.1%	-4.99	0.01	-2.93	0.01
06/01/09	JP-280	-0.7%	-4.90	0.01	-2.79	0.04
06/01/09	JP-281	-1.4%	-4.71	0.02	-2.71	0.07
06/01/09	JP-282	-2.4%	-4.67	0.01	-2.59	0.02
06/01/09	JP-283	-2.0%	-4.85	0.01	-2.89	0.03
06/01/09	JP-284	-2.2%	-4.77	0.03	-2.79	0.02
06/01/09	JP-285	-2.4%	-4.81	0.02	-2.88	0.01
06/01/09	JP-286	-1.3%	-4.66	0.01	-2.79	0.02
06/01/09	JP-287	-1.0%	-4.62	0.01	-2.99	0.03
06/01/09	JP-288	-0.6%	-4.41	0.02	-2.94	0.03
06/01/09	JP-289	0.3%	-4.28	0.03	-2.94	0.03
06/01/09	JP-290	-0.5%	-4.02	0.01	-2.85	0.02
06/01/09	JP-291	-1.8%	-3.95	0.01	-2.82	0.03
06/01/09	JP-292	-0.6%	-3.91	0.02	-2.80	0.04
06/01/09	JP-293	-53.8%				
06/01/09	JP-294	-4.5%	-4.06	0.03	-2.91	0.03
06/01/09	JP-295	-4.0%	-4.16	0.03	-2.98	0.06
06/01/09	JP-296	-55.0%				
06/01/09	JP-297	-1.3%	-4.25	0.02	-3.19	0.03
06/01/09	JP-298	-2.5%	-4.21	0.01	-3.15	0.05
06/01/09	JP-299	-60.2%				
06/01/09	JP-300	-2.2%	-4.00	0.01	-3.09	0.02

06/01/09	JP-301	-40.0%				
06/02/09	JP-302	-1.5%	-3.90	0.01	-2.95	0.03
06/02/09	JP-303	-6.4%	-3.84	0.02	-2.54	0.04
06/02/09	JP-304	-2.1%	-4.10	0.01	-3.21	0.04
06/02/09	JP-305	-0.8%	-4.11	0.04	-3.06	0.05
06/02/09	JP-306	-1.7%	-4.04	0.02	-2.87	0.04
06/02/09	JP-307	-1.4%	-4.13	0.04	-2.81	0.04
06/02/09	JP-308	-2.6%	-4.12	0.02	-2.81	0.02
06/02/09	JP-309	-2.1%	-4.16	0.01	-2.72	0.02
06/02/09	JP-310	-1.8%	-4.26	0.01	-2.63	0.02
06/02/09	JP-311	-2.1%	-4.31	0.02	-2.66	0.01
06/02/09	JP-312	-2.6%	-4.33	0.01	-2.53	0.02
06/02/09	JP-313	-0.6%	-4.42	0.02	-2.58	0.02
06/02/09	JP-314	-2.0%	-4.37	0.02	-2.53	0.03
06/02/09	JP-315	-0.6%	-4.23	0.01	-2.31	0.02
06/02/09	JP-316	-2.2%	-4.31	0.03	-2.66	0.04
06/02/09	JP-317	-1.0%	-4.03	0.00	-2.54	0.02
06/02/09	JP-318	-43.6%				
06/02/09	JP-319	-2.3%	-3.71	0.02	-2.36	0.03
06/02/09	JP-320	-42.7%				
06/02/09	JP-321	-2.6%	-3.79	0.03	-2.34	0.02
06/02/09	JP-322	-1.0%	-3.81	0.01	-2.29	0.02
06/02/09	JP-323	-2.7%	-3.82	0.01	-2.43	0.02
06/02/09	JP-324	-2.1%	-3.93	0.02	-2.39	0.03
06/02/09	JP-325	-21.3%				
06/02/09	JP-326	-2.3%	-4.00	0.01	-2.39	0.01
06/02/09	JP-327	-4.4%	-3.98	0.03	-2.56	0.03
06/02/09	JP-328	-2.3%	-4.19	0.02	-2.43	0.03
06/02/09	JP-329	-2.0%	-4.23	0.03	-2.66	0.03
06/02/09	JP-330	-3.3%	-4.24	0.02	-2.61	0.03
06/02/09	JP-331	-1.6%	-4.36	0.03	-2.78	0.05
06/02/09	JP-332	-1.9%	-4.09	0.02	-2.44	0.03
06/02/09	JP-333	-2.2%	-4.14	0.02	-2.79	0.04
06/02/09	JP-334	-1.9%	-3.90	0.02	-2.60	0.02
06/02/09	JP-335	-1.8%	-3.76	0.03	-2.61	0.01
06/02/09	JP-336	-7.5%	-3.79	0.01	-2.48	0.02
06/02/09	JP-337	-0.9%	-3.59	0.01	-2.48	0.01
06/02/09	JP-338	-2.5%	-3.50	0.02	-2.30	0.03
06/02/09	JP-339	-2.2%	-3.45	0.01	-2.36	0.03
06/02/09	JP-340	-1.2%	-3.40	0.02	-2.29	0.01
06/02/09	JP-341	-0.4%	-3.57	0.02	-2.49	0.02
06/02/09	JP-342	-2.4%	-3.57	0.01	-2.44	0.02
06/02/09	JP-343	-1.5%	-3.67	0.04	-2.54	0.04
06/02/09	JP-344	-4.1%	-3.70	0.01	-2.61	0.01
06/03/09	JP-345	-2.0%	-3.79	0.01	-2.78	0.02
06/03/09	JP-346	-1.8%	-3.96	0.00	-2.91	0.02
06/03/09	JP-347	-2.3%	-4.22	0.01	-3.16	0.01
06/03/09	JP-348	-1.8%	-4.38	0.01	-3.24	0.02
06/03/09	JP-349	-2.1%	-4.48	0.03	-3.46	0.01
06/03/09	JP-350	-5.7%	-4.33	0.01	-2.95	0.04

06/03/09	JP-351	-2.6%	-4.31	0.01	-3.29	0.02
06/03/09	JP-352	-0.8%	-4.39	0.02	-3.22	0.03
06/03/09	JP-353	-5.7%	-3.64	0.01	-1.34	0.02
06/03/09	JP-354	-1.9%	-4.20	0.01	-3.20	0.04
06/03/09	JP-355	-2.8%	-4.33	0.01	-3.32	0.03
06/03/09	JP-356	-99.6%				
06/03/09	JP-357	-2.0%	-4.15	0.02	-3.30	0.03
06/03/09	JP-358	-2.2%	-4.12	0.02	-3.21	0.02
06/03/09	JP-359	-2.1%	-4.22	0.01	-3.23	0.04
06/03/09	JP-360	-1.1%	-4.30	0.01	-3.18	0.04
06/03/09	JP-361	-3.0%	-4.43	0.01	-3.11	0.02
06/03/09	JP-362	-3.1%	-4.54	0.03	-3.26	0.01
06/03/09	JP-363	-1.9%	-4.58	0.01	-3.26	0.02
06/03/09	JP-364	-2.2%	-4.68	0.01	-3.27	0.01
06/03/09	JP-365	-47.1%				
06/03/09	JP-366	-2.2%	-4.65	0.02	-3.33	0.03
06/03/09	JP-367	-5.4%	-4.49	0.03	-2.27	0.04
06/03/09	JP-368	-42.6%				
06/03/09	JP-369	-2.4%	-4.57	0.02	-3.45	0.04
06/03/09	JP-370	-2.3%	-4.46	0.03	-3.29	0.04
06/03/09	JP-371	-63.7%				
06/03/09	JP-372	-2.3%	-4.27	0.01	-3.35	0.01
06/03/09	JP-373	-2.1%	-4.12	0.03	-3.23	0.02
06/03/09	JP-374	-2.7%	-4.08	0.01	-3.19	0.02
06/03/09	JP-375	-2.1%	-4.01	0.01	-3.16	0.04
06/03/09	JP-376	-2.5%	-4.17	0.02	-3.21	0.01
06/03/09	JP-377	-17.0%				
06/04/09	JP-378	-2.4%	-4.70	0.02	-3.62	0.02
06/04/09	JP-379	-1.8%	-4.96	0.02	-3.94	0.03
06/04/09	JP-380	-2.1%	-5.07	0.01	-3.97	0.03
06/04/09	JP-381	-2.0%	-4.95	0.02	-4.23	0.01
06/04/09	JP-382	-2.5%	-5.08	0.02	-4.31	0.01
06/04/09	JP-383	-2.6%	-4.86	0.02	-4.36	0.02
06/04/09	JP-384	-3.5%	-4.73	0.02	-4.46	0.03
06/04/09	JP-385	-1.9%	-4.66	0.01	-4.51	0.03
06/04/09	JP-386	-2.1%	-4.44	0.03	-4.16	0.01
06/04/09	JP-387	-2.5%	-4.37	0.02	-4.31	0.02
06/04/09	JP-388	-2.2%	-4.19	0.01	-3.78	0.04
06/04/09	JP-389	-2.1%	-4.13	0.02	-3.72	0.04
06/04/09	JP-390	-6.4%	-3.87	0.01	-3.18	0.03
06/04/09	JP-391	-99.6%				
06/04/09	JP-392	-2.5%	-3.58	0.01	-2.55	0.03
06/04/09	JP-393	-2.0%	-3.49	0.01	-2.35	0.05
06/04/09	JP-394	-3.6%	-3.71	0.01	-2.05	0.02
06/04/09	JP-395	-2.3%	-3.99	0.02	-2.05	0.02
06/04/09	JP-396	-99.6%				
06/04/09	JP-397	-2.4%	-4.42	0.01	-2.26	0.02
06/04/09	JP-398	-1.3%	-4.28	0.02	-2.12	0.03
06/04/09	JP-399	-90.5%				
06/04/09	JP-400	-21.5%				

06/07/09	JP-441	#DIV/0!				
06/07/09	JP-442	-3.9%	-3.94	0.02	-2.72	0.03
06/07/09	JP-443	-0.9%	-3.85	0.01	-2.71	0.02
06/07/09	JP-444	-2.5%	-4.03	0.01	-2.75	0.04
06/07/09	JP-445	-3.1%	-4.23	0.02	-2.96	0.02
06/07/09	JP-446	-5.2%	-4.48	0.01	-2.96	0.03
06/07/09	JP-447	-3.4%	-4.78	0.01	-3.29	0.01
06/08/09	JP-448	-2.7%	-4.93	0.01	-3.32	0.02
06/08/09	JP-449	-3.8%	-4.84	0.01	-3.31	0.03
06/08/09	JP-450	-5.0%	-4.73	0.02	-3.19	0.02
06/08/09	JP-451	-3.8%	-4.89	0.01	-3.28	0.01
06/08/09	JP-452	-5.4%	-5.14	0.01	-3.20	0.02
06/08/09	JP-453	-3.5%	-5.23	0.02	-3.31	0.03
06/08/09	JP-454	-2.8%	-5.23	0.01	-3.08	0.02
06/08/09	JP-455	-3.3%	-5.22	0.03	-3.08	0.02
06/08/09	JP-456	-2.3%	-5.16	0.02	-2.96	0.02
06/08/09	JP-457	-3.9%	-5.03	0.01	-2.95	0.03
06/08/09	JP-458	-4.7%	-4.72	0.00	-2.61	0.02
06/08/09	JP-459	-3.5%	-4.47	0.01	-2.45	0.03
06/08/09	JP-460	-4.4%	-4.33	0.01	-2.32	0.02
06/08/09	JP-461	-2.5%	-4.17	0.01	-2.34	0.02
06/08/09	JP-462	-4.4%	-4.12	0.01	-2.30	0.01
06/08/09	JP-463	-4.3%	-3.94	0.01	-2.24	0.02
06/08/09	JP-464	1.0%	-3.84	0.01	-2.09	0.01
06/08/09	JP-465	-3.6%	-3.80	0.01	-2.16	0.02
06/08/09	JP-466	-3.8%	-3.74	0.03	-2.08	0.05
06/08/09	JP-467	-4.0%	-3.86	0.00	-2.16	0.02
06/08/09	JP-468	-4.6%	-4.09	0.01	-2.32	0.02
06/08/09	JP-469	-2.1%	-4.18	0.01	-2.47	0.02
06/08/09	JP-470	-3.2%	-4.21	0.01	-2.43	0.02
06/08/09	JP-471	-1.8%	-4.30	0.02	-2.58	0.03
06/08/09	JP-472	-3.2%	-4.40	0.02	-2.65	0.03
06/08/09	JP-473	-2.4%	-4.71	0.01	-3.09	0.02
06/08/09	JP-474	-2.4%	-5.05	0.01	-3.34	0.03
06/08/09	JP-475	-3.4%	-4.88	0.01	-3.43	0.02
06/08/09	JP-476	-4.3%	-4.84	0.01	-3.37	0.02
06/08/09	JP-477	-2.3%	-4.83	0.01	-3.53	0.02
06/08/09	JP-478	-2.9%	-4.74	0.02	-3.47	0.01
06/08/09	JP-479	-1.3%	-4.75	0.01	-3.56	0.01
06/08/09	JP-480	-4.4%	-4.81	0.01	-3.62	0.02
06/08/09	JP-401	-2.5%	-3.87	0.02	-2.15	0.01
06/08/09	JP-402	-40.2%				
06/08/09	JP-403	-2.0%	-4.72	0.02	-2.42	0.02
06/08/09	JP-404	-2.2%	-5.13	0.01	-2.60	0.03
06/08/09	JP-405	-2.7%	-5.26	0.01	-2.81	0.03
06/08/09	JP-406	-3.9%	-5.28	0.02	-2.75	0.03
06/08/09	JP-407	1.2%	-5.41	0.02	-2.94	0.02
06/08/09	JP-408	-99.6%				
	JP-409	#DIV/0!				
06/08/09	JP-410	-4.1%	-5.50	0.01	-3.35	0.02

06/09/09	JP-411	-1.6%	-5.36	0.02	-3.24	0.01
06/09/09	JP-412	-0.6%	-4.98	0.01	-3.00	0.02
06/09/09	JP-413	-3.1%	-4.71	0.01	-2.79	0.03
06/09/09	JP-414	-2.2%	-4.66	0.02	-2.63	0.02
06/09/09	JP-415	-4.4%	-4.84	0.01	-2.93	0.02
06/09/09	JP-416	-1.2%	-4.84	0.01	-2.86	0.02
06/09/09	JP-417	-3.3%	-4.73	0.01	-2.77	0.01
06/09/09	JP-418	-3.4%	-4.72	0.02	-2.85	0.02
06/09/09	JP-419	-5.7%	-4.81	0.01	-2.88	0.01
06/09/09	JP-420	-2.5%	-4.90	0.01	-3.04	0.02
06/09/09	JP-421	-3.3%	-4.98	0.01	-3.03	0.03
06/09/09	JP-422	-2.5%	-5.16	0.02	-3.17	0.02
06/09/09	JP-423	-5.9%	-5.35	0.03	-3.39	0.06
06/09/09	JP-424	-3.8%	-5.52	0.02	-3.55	0.02
06/09/09	JP-425	-4.8%	-5.58	0.02	-3.58	0.01
06/09/09	JP-426	-3.3%	-5.37	0.01	-3.17	0.03
06/09/09	JP-427	-5.1%	-5.39	0.01	-3.41	0.01
06/09/09	JP-428	-0.9%	-5.06	0.01	-2.94	0.02
06/09/09	JP-429	-2.2%	-5.01	0.02	-3.32	0.03
06/09/09	JP-430	-39.0%				
06/09/09	JP-431	-2.3%	-4.54	0.01	-3.01	0.02
06/09/09	JP-432	-4.0%	-4.24	0.01	-2.75	0.01
06/09/09	JP-433	-3.7%	-3.99	0.02	-2.69	0.02
06/09/09	JP-434	-4.6%	-3.69	0.01	-2.54	0.02
06/09/09	JP-435	-7.1%	-3.71	0.02	-2.50	0.03
06/09/09	JP-436	-3.4%	-3.98	0.02	-2.68	0.02
06/09/09	JP-437	-3.2%	-4.17	0.02	-2.75	0.02
06/09/09	JP-438	-2.2%	-4.28	0.01	-2.86	0.01
06/09/09	JP-439	-6.7%	-4.28	0.03	-2.90	0.04
06/09/09	JP-440	-7.3%	-4.13	0.03	-2.91	0.04
06/11/09	JP-481	-0.4%	-4.98	0.01	-3.78	0.02
06/11/09	JP-482	-2.5%	-5.25	0.02	-4.26	0.04
06/11/09	JP-483	-2.4%	-4.96	0.01	-3.75	0.03
06/11/09	JP-484	-1.7%	-5.11	0.01	-3.69	0.03
06/11/09	JP-485	-94.4%				
06/11/09	JP-486	-2.9%	-5.34	0.01	-3.56	0.03
06/11/09	JP-487	-2.2%	-5.39	0.01	-3.47	0.01
06/11/09	JP-488	-4.7%	-5.44	0.01	-3.33	0.02
06/11/09	JP-489	-2.8%	-5.39	0.01	-3.22	0.03
06/11/09	JP-490	-2.2%	-5.35	0.01	-3.10	0.03
06/11/09	JP-491	-3.1%	-5.29	0.02	-3.11	0.02
06/11/09	JP-492	-3.5%	-5.24	0.02	-2.95	0.02
06/11/09	JP-493	-3.6%	-5.18	0.01	-2.97	0.02
06/11/09	JP-494	-3.5%	-5.04	0.01	-2.77	0.03
06/11/09	JP-495	-3.1%	-4.96	0.02	-2.84	0.03
06/11/09	JP-496	-2.2%	-4.91	0.01	-2.27	0.02
06/11/09	JP-497	-1.0%	-4.95	0.01	-2.74	0.03
06/11/09	JP-498	-2.2%	-4.96	0.03	-2.73	0.04
06/11/09	JP-499	-1.3%	-4.96	0.01	-2.78	0.03
06/11/09	JP-500	-1.1%	-5.00	0.01	-2.72	0.02

06/11/09	JP-501	-2.8%	-4.99	0.01	-2.91	0.01
06/11/09	JP-502	-3.3%	-4.99	0.01	-2.86	0.03
06/11/09	JP-503	-3.5%	-4.94	0.02	-2.85	0.02
06/12/09	JP-504	-4.0%	-4.84	0.01	-2.79	0.02
06/12/09	JP-505	-3.6%	-4.87	0.01	-2.79	0.01
06/12/09	JP-506	-3.2%	-4.93	0.01	-2.81	0.02
06/12/09	JP-507	-1.2%	-4.98	0.01	-2.95	0.02
06/12/09	JP-508	-4.3%	-5.02	0.01	-2.77	0.02
06/12/09	JP-509	-2.8%	-5.05	0.01	-2.87	0.04
06/12/09	JP-510	-2.8%	-5.12	0.02	-2.88	0.02
06/12/09	JP-511	-2.5%	-5.08	0.03	-2.90	0.02
06/12/09	JP-512	-0.5%	-5.07	0.02	-2.84	0.04
06/12/09	JP-513	-2.4%	-5.00	0.02	-2.89	0.03
06/12/09	JP-514	-3.6%	-4.94	0.02	-2.79	0.01
06/12/09	JP-515	-2.6%	-4.83	0.02	-2.84	0.01
06/12/09	JP-516	-0.8%	-4.62	0.01	-2.31	0.01
06/12/09	JP-517	-3.4%	-4.67	0.01	-2.74	0.02
06/12/09	JP-518	-4.4%	-4.64	0.02	-2.70	0.03
06/12/09	JP-519	-2.8%	-4.71	0.01	-2.84	0.02
06/12/09	JP-520	-3.2%	-4.76	0.01	-2.78	0.02
06/15/09	JP-521	-9.7%				
06/15/09	JP-522	-1.6%	-4.76	0.01	-2.83	0.02
06/15/09	JP-523	-0.5%	-4.78	0.02	-2.96	0.02
06/15/09	JP-524	-0.5%	-4.72	0.01	-2.52	0.03
06/15/09	JP-525	-0.9%	-4.84	0.01	-2.98	0.01
06/15/09	JP-526	-0.8%	-4.93	0.01	-2.99	0.04
06/15/09	JP-527	-2.7%	-4.83	0.02	-2.47	0.04
06/15/09	JP-528	-3.4%	-5.15	0.02	-3.12	0.01
06/15/09	JP-529	-0.8%	-5.31	0.01	-3.29	0.03
06/15/09	JP-530	-1.0%	-5.35	0.01	-3.31	0.04
06/15/09	JP-531	-3.0%	-5.30	0.02	-3.41	0.02
06/15/09	JP-532	-4.3%	-5.22	0.02	-3.36	0.03
06/15/09	JP-533	-3.5%	-5.12	0.01	-3.42	0.01
06/15/09	JP-534	-1.7%	-4.87	0.01	-3.24	0.02
06/15/09	JP-535	-1.5%	-4.76	0.02	-3.24	0.03
06/15/09	JP-536	-3.8%	-4.68	0.01	-3.23	0.02
06/15/09	JP-537	-3.4%	-4.64	0.01	-3.12	0.02
06/16/09	JP-538	-4.0%	-4.73	0.01	-3.35	0.03
06/16/09	JP-539	-2.2%	-4.82	0.01	-3.43	0.02
06/16/09	JP-540	-3.3%	-4.89	0.01	-3.36	0.02
06/16/09	JP-541	-1.7%	-4.97	0.02	-3.52	0.01
06/16/09	JP-542	-1.6%	-4.94	0.01	-3.28	0.03
06/16/09	JP-543	-2.1%	-5.02	0.01	-3.66	0.02
06/16/09	JP-544	-3.2%	-4.74	0.01	-3.35	0.03
06/16/09	JP-545	-3.0%	-4.15	0.01	-2.50	0.03
06/16/09	JP-546	-3.4%	-3.99	0.02	-2.73	0.03
06/16/09	JP-547	-1.9%	-3.90	0.01	-2.74	0.02
06/16/09	JP-548	-5.1%	-3.75	0.01	-2.58	0.01
06/16/09	JP-549	-3.7%	-3.64	0.01	-2.55	0.01
06/16/09	JP-550	-4.2%	-3.56	0.02	-2.53	0.01

06/16/09	JP-551	-1.0%	-3.77	0.02	-2.73	0.05
06/16/09	JP-552	-1.0%	-3.93	0.01	-2.68	0.02
06/16/09	JP-553	-2.2%	-4.21	0.03	-2.79	0.01
06/16/09	JP-554	-2.9%	-4.41	0.00	-2.73	0.02
06/16/09	JP-555	-1.9%	-4.76	0.03	-2.95	0.03
06/16/09	JP-556	-2.4%	-5.02	0.02	-2.96	0.02
06/16/09	JP-557	-3.4%	-5.31	0.01	-3.13	0.02
06/16/09	JP-558	-2.9%	-5.37	0.01	-3.08	0.03
06/16/09	JP-559	-1.0%	-5.17	0.02	-2.87	0.02
06/16/09	JP-560	-0.8%	-4.92	0.01	-2.63	0.02
06/16/09	JP-561	-1.0%				
06/16/09	JP-562	-2.8%	-4.58	0.01	-2.44	0.03
06/16/09	JP-563	-1.1%	-4.75	0.02	-2.59	0.02
06/16/09	JP-564	-2.1%	-4.74	0.01	-2.49	0.01
06/16/09	JP-565	-2.5%	-4.79	0.02	-2.57	0.04
06/16/09	JP-566	-2.9%	-4.85	0.02	-2.66	0.01
06/16/09	JP-567	-1.6%	-4.93	0.01	-2.63	0.03
06/16/09	JP-568	-4.5%	-4.88	0.02	-2.44	0.01
06/16/09	JP-569	-3.2%	-4.75	0.02	-2.42	0.02
06/16/09	JP-570	-5.2%	-4.73	0.01	-2.45	0.02
06/16/09	JP-571	-5.1%	-4.69	0.01	-2.48	0.01
06/16/09	JP-572	-7.5%	-4.66	0.01	-2.38	0.02
06/16/09	JP-573	0.2%	-4.73	0.02	-2.49	0.02
06/16/09	JP-574	-2.2%	-4.74	0.03	-2.11	0.02
06/16/09	JP-575	-2.9%	-4.75	0.01	-2.51	0.03
06/16/09	JP-576	-3.6%	-4.56	0.01	-2.27	0.01
06/16/09	JP-577	-1.3%	-4.34	0.01	-1.94	0.03
06/16/09	JP-578	-5.7%	-4.37	0.01	-2.17	0.03
06/17/09	JP-579	-1.1%	-4.27	0.01	-2.15	0.01
06/17/09	JP-580	-4.2%	-4.33	0.00	-2.06	0.01
06/17/09	JP-581	-5.5%	-4.45	0.01	-2.20	0.02
06/17/09	JP-582	-3.0%	-4.52	0.01	-1.92	0.01
06/17/09	JP-583	-1.7%	-4.74	0.01	-2.33	0.03
06/17/09	JP-584	-2.8%	-4.63	0.02	-1.59	0.04
06/17/09	JP-585	-2.8%	-4.71	0.02	-2.37	0.02
06/17/09	JP-586	-4.1%	-4.48	0.01	-2.22	0.02
06/17/09	JP-587	-2.9%	-4.30	0.01	-2.24	0.03
06/17/09	JP-588	-4.6%	-4.14	0.01	-2.08	0.02
06/17/09	JP-589	-3.4%	-3.97	0.02	-2.04	0.02
06/17/09	JP-590	-4.6%	-3.70	0.02	-1.17	0.02
06/17/09	JP-591	-3.7%	-3.81	0.02	-1.91	0.03
06/17/09	JP-592	-4.0%	-3.77	0.02	-1.86	0.05
06/17/09	JP-593	-3.8%	-3.65	0.01	-1.84	0.02
06/17/09	JP-594	#DIV/0!				
06/17/09	JP-595	-2.4%	-3.69	0.01	-1.81	0.02
06/17/09	JP-596	-3.2%	-3.77	0.01	-1.67	0.05
06/17/09	JP-597	-4.1%	-3.92	0.01	-1.79	0.02
06/17/09	JP-598	-2.6%	-4.02	0.01	-1.81	0.02
06/17/09	JP-599	-1.6%	-4.21	0.01	-1.98	0.02
06/17/09	JP-600	-1.8%	-4.31	0.01	-2.04	0.02

06/19/09	JP-601	-23.7%	-4.27	0.02	-2.16	0.05
06/19/09	JP-602	#DIV/0!				
06/19/09	JP-603	-1.5%	-4.36	0.01	-2.19	0.02
06/19/09	JP-604	-1.8%	-4.38	0.02	-2.06	0.03
06/19/09	JP-605	-2.6%	-4.37	0.02	-2.06	0.02
06/19/09	JP-606	-3.2%	-4.46	0.02	-2.03	0.02
06/19/09	JP-607	-4.2%	-4.50	0.01	-2.11	0.03
06/19/09	JP-608	-4.6%	-4.60	0.02	-2.11	0.02
06/19/09	JP-609	-2.6%	-4.76	0.02	-2.30	0.02
06/19/09	JP-610	-3.6%	-5.00	0.02	-2.27	0.02
06/19/09	JP-611	-3.5%	-5.02	0.01	-2.36	0.02
06/19/09	JP-612	-5.1%	-5.27	0.02	-2.43	0.02
06/19/09	JP-613	-4.6%	-5.34	0.01	-2.51	0.03
06/19/09	JP-614	-3.9%	-5.44	0.01	-2.47	0.01
06/19/09	JP-615	-3.4%	-5.54	0.02	-2.66	0.04
06/19/09	JP-616	-4.9%	-5.59	0.02	-2.59	0.03
06/19/09	JP-617	-3.2%	-5.55	0.02	-2.68	0.03
06/21/09	JP-618	-3.7%	-5.57	0.01	-2.66	0.02
06/21/09	JP-619	-3.6%	-5.44	0.01	-2.65	0.03
06/21/09	JP-620	-4.9%	-5.38	0.01	-2.66	0.03
06/21/09	JP-621	-4.2%	-5.20	0.01	-2.61	0.02
06/21/09	JP-622	-3.7%	-5.04	0.01	-2.54	0.02
06/21/09	JP-623	-6.2%	-4.94	0.01	-2.47	0.03
06/22/09	JP-624	-4.5%	-4.85	0.01	-2.45	0.02
06/21/09	JP-625	-5.1%	-4.84	0.01	-2.48	0.04
06/22/09	JP-626	-4.6%	-4.85	0.01	-2.40	0.04
06/21/09	JP-627	-3.1%	-4.96	0.01	-2.42	0.01
06/22/09	JP-628	-4.9%	-5.06	0.01	-2.40	0.01
06/21/09	JP-629	-3.4%	-5.14	0.01	-2.47	0.01
06/22/09	JP-630	-5.2%	-5.31	0.01	-2.56	0.02
06/21/09	JP-631	-3.3%	-5.39	0.02	-2.63	0.02
06/22/09	JP-632	-2.8%	-5.44	0.01	-2.67	0.03
06/21/09	JP-633	-3.4%	-5.35	0.03	-2.71	0.02
06/22/09	JP-634	-3.6%	-5.20	0.01	-2.67	0.05
06/21/09	JP-635	-6.1%	-5.08	0.01	-2.60	0.03
06/22/09	JP-636	-4.4%	-4.80	0.01	-2.48	0.01
06/21/09	JP-637	-4.0%	-4.56	0.01	-2.31	0.01
06/22/09	JP-638	-3.7%	-4.37	0.01	-2.29	0.03
06/21/09	JP-639	-3.6%	-4.34	0.01	-2.29	0.03
06/22/09	JP-640	-4.8%	-4.42	0.02	-2.34	0.03
06/22/09	JP-641	-3.0%	-4.60	0.02	-2.36	0.02
06/22/09	JP-642	-3.0%	-4.76	0.01	-2.52	0.01
06/22/09	JP-643	-5.8%	-4.67	0.01	-2.53	0.01
06/22/09	JP-644	-99.8%				
06/22/09	JP-645	0.8%	-4.63	0.01	-2.60	0.01
06/22/09	JP-646	-9.7%	-4.68	0.01	-2.62	0.02
06/22/09	JP-647	-2.7%	-4.76	0.02	-2.80	0.02
06/22/09	JP-648	-1.2%	-4.99	0.01	-2.92	0.02
06/22/09	JP-649	-7.0%	-4.92	0.04	-2.47	0.06
06/22/09	JP-650	-1.4%	-5.12	0.02	-3.04	0.02

06/22/09	JP-651	-6.2%	-5.29	0.01	-2.99	0.01
06/22/09	JP-652	-0.3%	-5.29	0.01	-2.93	0.01
06/22/09	JP-653	-3.8%	-5.39	0.01	-3.01	0.03
06/22/09	JP-654	-5.9%	-5.32	0.01	-2.98	0.01
06/22/09	JP-655	-3.9%	-5.35	0.01	-2.97	0.03
06/22/09	JP-656	-0.4%	-5.27	0.01	-2.99	0.02
06/22/09	JP-657	-99.6%				
06/22/09	JP-658	-5.1%	-5.19	0.01	-2.94	0.02
06/22/09	JP-659	-4.4%	-5.16	0.01	-2.97	0.02
06/22/09	JP-660	-5.8%	-5.19	0.01	-3.01	0.02
06/23/09	JP-661	-3.7%	-5.27	0.01	-3.09	0.02
06/23/09	JP-662	-5.2%	-5.44	0.01	-3.21	0.01
06/23/09	JP-663	-3.4%	-5.61	0.02	-3.37	0.03
06/23/09	JP-664	-4.3%	-5.80	0.02	-3.47	0.02
06/23/09	JP-665	-3.8%	-5.94	0.01	-3.59	0.02
06/23/09	JP-666	-5.5%	-6.09	0.02	-3.79	0.01
06/23/09	JP-667	-3.6%	-5.99	0.02	-3.71	0.01
06/23/09	JP-668	-5.3%	-5.76	0.01	-3.55	0.01
06/23/09	JP-669	-5.9%	-5.54	0.01	-3.45	0.01
06/23/09	JP-670	-4.3%	-5.22	0.01	-3.26	0.02
06/23/09	JP-671	-3.7%	-5.05	0.01	-3.13	0.02
06/23/09	JP-672	-4.0%	-5.04	0.01	-3.09	0.02
06/23/09	JP-673	-4.6%	-5.10	0.00	-3.19	0.01
06/23/09	JP-674	-2.4%	-5.06	0.01	-3.16	0.02
06/23/09	JP-675	-4.7%	-5.04	0.02	-3.16	0.02
06/23/09	JP-676	-0.3%	-4.85	0.01	-3.12	0.01
06/23/09	JP-677	-1.2%	-4.76	0.01	-3.02	0.04
06/23/09	JP-678	-3.6%	-4.97	0.01	-3.22	0.02
06/23/09	JP-679	-3.7%	-5.09	0.03	-3.22	0.05
06/23/09	JP-680	-2.5%	-5.12	0.02	-3.32	0.04
06/23/09	JP-681	-1.6%	-5.08	0.01	-3.23	0.02
06/23/09	JP-682	-0.9%	-5.20	0.01	-3.29	0.03
06/23/09	JP-683	-5.0%	-5.33	0.01	-3.31	0.01
06/23/09	JP-684	-3.0%	-5.40	0.02	-3.32	0.03
06/23/09	JP-685	-1.9%	-5.41	0.02	-3.27	0.03
06/23/09	JP-686	-4.0%	-5.40	0.02	-3.34	0.03
06/23/09	JP-687	-1.3%	-5.29	0.01	-3.10	0.02
06/23/09	JP-688	-4.9%	-5.21	0.02	-3.11	0.03
06/23/09	JP-689	-5.8%	-5.11	0.01	-3.05	0.01
06/23/09	JP-690	-5.0%	-4.94	0.01	-2.91	0.01
06/23/09	JP-691	0.3%	-4.68	0.03	-2.75	0.03
06/23/09	JP-692	-1.6%	-4.54	0.01	-2.61	0.01
06/23/09	JP-693	-0.6%	-4.54	0.01	-2.42	0.01
06/23/09	JP-694	-2.2%	-4.52	0.01	-2.42	0.03
06/23/09	JP-695	0.6%	-4.60	0.02	-2.41	0.04
06/23/09	JP-696	0.2%	-4.62	0.01	-2.37	0.03
06/23/09	JP-697	1.0%	-4.86	0.01	-2.43	0.01
06/23/09	JP-698	-1.8%	-4.96	0.02	-2.40	0.01
06/24/09	JP-699	-5.1%	-5.02	0.01	-2.49	0.02
06/24/09	JP-700	-5.2%	-5.01	0.01	-2.47	0.01

Mud layer	Depth to top of mud (mm)	Calander year
1	0.09	2005
2	0.38	2001
3	0.54	1997
4	0.67	1992
5	1.57	1968
6	1.72	1964
7	1.86	1962
8	2.12	1954
9	2.41	1947
10	2.7	1940
11	3.07	1930
12	3.25	1928
13	3.82	1915
14	4.3	1905
15	4.52	1897
16	4.67	1892
17	4.8	1889
18	5.1	1882
19	5.82	1868
20	6.23	1861
21	6.99	1844
22	7.12	1840
23	7.65	1825
24	8.52	1804
25	9.05	1792
26	9.44	1783
27	9.64	1778
28	10.23	1760
29	10.66	1748
30	11.15	1737
31	11.34	1730
32	12.43	1705
33	13.53	1677
34	14.53	1653
35	15.03	1641
36	15.6	1625
37	17.25	1578
38	17.66	1566
39	18.8	1536
40	19.26	1522
41	19.55	1515
42	20.45	1491
43	20.71	1485
44	21.72	1457

45	22.12	1447
46	23.27	1412
47	23.89	1398
48	24.5	1381
49	25.27	1362
50	25.77	1344
51	26.1	1335
52	26.45	1324
53	27.4	1299
54	28.49	1271
55	29.24	1249
56	29.7	1233
57	30.11	1222
58	30.98	1213
59	31.8	1205
60	32.51	1198
61	33.05	1192
62	33.57	1187
63	33.83	1185
64	34.23	1181
65	34.6	1177
66	35.52	1168
67	35.99	1163
68	36.44	1158
69	36.79	1155
70	37.24	1150
71	38.25	1140
72	38.46	1138
73	39.59	1127
74	40.11	1121
75	40.77	1115
76	41.54	1107
77	42.51	1097
78	43.8	1084
79	44.42	1078
80	45.05	1072
81	45.97	1062
82	47.03	1052
83	47.43	1048
84	47.83	1044
85	48.2	1040
86	48.91	1033
87	49.31	1029
88	50.09	1021
89	50.56	1016
90	51.03	1011
91	51.78	1004

92	52.3	999
93	52.96	992
94	53.66	985
95	54.46	977
96	55.47	967
97	55.76	964
98	56.2	959
99	56.65	955
100	56.89	952
101	57.24	949
102	57.78	943
103	58.06	941
104	58.42	937
105	60.01	921
106	60.77	913
107	61.05	910
108	61.71	904
109	62.23	899
110	62.53	896
111	63.1	890
112	63.73	883
113	64.25	878
114	65.12	869
115	65.52	865
116	66.16	859
117	67.03	850
118	68.04	840
119	68.46	836
120	69.07	830
121	69.76	823
122	71.29	807
123	71.57	804
124	72.44	796
125	72.94	791
126	73.55	785
127	74.35	776
128	75.34	767
129	76.3	757
130	76.7	753
131	77.64	743
132	78.42	735
133	79.24	727
134	79.81	721
135	81.1	709
136	81.64	703
137	82.23	697
138	82.7	692

139	83.36	686
140	83.97	680
141	84.75	672
142	85.48	664
143	86.07	658
144	86.28	656
145	86.91	650
146	87.69	642
147	88.44	635
148	89.01	629
149	89.74	621
150	90.72	612
151	91.31	606
152	92.4	595
153	92.98	589
154	93.55	583
155	94.3	576
156	95.01	568
157	95.78	561
158	96.68	552
159	97.55	543
160	98.14	537
161	98.51	533
162	99.27	526
163	99.55	523
164	100.25	516
165	100.82	510
166	101.48	503
167	101.81	500
168	102.35	495
169	103.62	482
170	104.84	469
171	105.99	458
172	107.12	446
173	107.81	440
174	108.3	435
175	108.89	429
176	109.48	423
177	109.9	418
178	110.39	414
179	111.05	407
180	111.59	401
181	111.92	398
182	112.32	394
183	112.75	390
184	113.5	382
185	114.04	377

186	114.49	372
187	115.36	363
188	115.76	359
189	116.44	353
190	117.08	346
191	117.69	340
192	118.68	330
193	119.17	325
194	119.88	318
195	120.44	312
196	120.94	307
197	121.64	300
198	122.42	292
199	122.98	287
200	123.95	277
201	124.86	268
202	125.59	260
203	126.06	256
204	127	246
205	127.66	240
206	128.27	233
207	128.6	230
208	129.5	221
209	130.44	212
210	130.98	206
211	131.4	202
212	131.71	199
213	132.2	194
214	132.91	187
215	133.24	183
216	133.64	179
217	134.2	174
218	134.55	170
219	135.05	165
220	135.8	158
221	139.35	122
222	139.73	118
223	140.06	115
224	140.28	113
225	140.56	110
226	140.79	107
227	141.01	103
228	141.27	98
229	141.53	93
230	141.74	89
231	142.37	78
232	142.6	73

233	142.86	68
234	143.1	64
235	143.52	56
236	143.78	51
237	144.07	46
238	144.4	39
239	145.04	27
240	146.72	-4
241	147.03	-10
242	147.28	-15
243	148.4	-36
244	149.08	-49
245	149.44	-56
246	149.58	-58
247	149.87	-64
248	150.1	-68
249	150.25	-71
250	150.74	-80
251	151.05	-86
252	151.31	-91
253	151.63	-97
254	152.18	-108
255	152.4	-112
256	152.87	-121
257	153.1	-125
258	153.39	-130
259	154.03	-142
260	154.79	-157
261	155.1	-163
262	155.5	-170
263	155.95	-179
264	156.18	-183
265	156.97	-198